uc3m | Universidad Carlos III de Madrid

Bachelor Degree in Aerospace Engineering
Academic Year: 2018-2019

Bachelor Thesis

"Cross-Section Database Generation for Hybrid PIC/Fluid Plasma Codes"

Antonio Castillo Sauca

Mario Merino Martínez

Madrid, June 2019

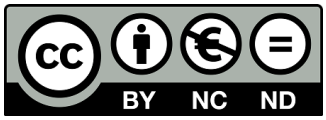

SUMMARY

Plasma volumes are characterized by a certain degree of ionization and a density of charged particles. Both of them are strongly determined by the numerous collision interactions taking place between the different particles inside the plasma system. At the same time, the resulting motion of the charged particles generate electromagnetic fields that interact with the inner particles of the system and the external fields.

Numerous studies aim to predict the behaviour of plasma for its applications in aerospace propulsion systems and actuators. For such purpose it is essential to have a deep understanding of the reaction processes that occur at atomic scale and their effect at macroscopic level.

All these collision processes at atomic levels with influence of quantum effects are measured in terms of a collision cross section, which suggests the probability of a certain collision to occur at a specific relative velocity between the colliding partners. These parameters are used by hybrid codes to estimate the collisions occurring inside a mesh volume and track the results to obtain accurate flow trajectories and properties. This codes, then, require an easy access to the cross sections and an optimization of the amount of interactions to simulate to reduce time and computational costs.

A database is designed to contain specific collision cross sections of the most relevant interactions to provide the hybrid codes with the needed parameters: collision cross sections for reactions between heavy particles, and collision rate coefficients for collisions involving electrons, modelled as a magnetized fluid by the hybrid codes.

The database generated in this thesis is simple and efficient. Created through simple directory folders, sorted in elements and energy levels; and easy readable “YAML" .txt files, the database is able to handle the cross sections stored in it quickly to deliver them to the main hybrid codes in the required standard. To be compatible with the programming language used in the modelling codes, all this “hybrid codes-database" connections are designed in the environment of the former: Python.

Through comparisons between the different potential collision inside the control plasma system, it has been concluded that charge exchange collisions are highly relevant for the simulations between heavy particles. In the modelling of collision with electron flows, it is demonstrated that elastic collision and ionization reactions of the neutral species are frequent within noble gases (Xe, Ar and Kr). In addition, ionization of pre-ionized states of the mentioned propellants become more important for the simulations than double ionization collisions of the neutral species. Finally, it is also concluded that if the studied plasma system achieves high densities of electrons and excited particles, stepwise ionization processes are highly recommended to be implemented inside the hybrid codes.

Keywords: Plasma, Collision-cross section, Collision rate coefficient, Database, Velocity distribution function, Maxwellian distribution, Bi-Maxwellian distribution, Ionization collisions, Charge exchange collisions, Elastic collisions, Stepwise ionization.

CONTENTS

LIST OF FIGURES

LIST OF TABLES

1. INTRODUCTION

1.1. What is Plasma?

Before commenting any aspect of the purpose of this work, it is essential to have a solid understanding of what a plasma is. The "fourth state of matter", as it is sometimes called, is basically an ionized gas.

As temperature increases, molecules become more energetic and change of phases occur [1], [2]. In a solid body, the crystal lattice structure is broken apart transforming into a liquid volume. If this is further heated, until the point where the rate of atoms vaporizing off the surface is greater than the re-condensation rate, a gas is formed. A plasma appears when the increase in the thermal energy of a gas is such that the collisions between the gas atoms lead to a scatter of electrons. Thus, a plasma may be regarded as a mixture of electrons, ions, and neutral particles with random movement which, on average, is electrically neutral.

This ionized gas has unique properties of practical utility. The dynamics of motion of common materials are usually governed by the influence of near-neighbor regions, such as forces arriving from the interaction with walls or electrodes. However, in plasma systems the free charged particles interact with external fields and the motion of the entire matter is affected by this property. Such effect has derived in a variety of interesting applications as it allows a degree of control over the plasma volume through the use of electromagnetic fields. Moreover, the charge difference between the ions and electrons of the plasma leads to the appearance of additional electric fields, which provoke successive flows of charged particles and, consequently, more magnetic fields rise.

From this simple analysis it is clear that this state of matter is of a startling complexity and its properties are of potential utility for numerous applications.

1.2. The importance of collisions

The inherent properties of a plasma are a consequence of the ionized state, itself, of the gas. The variation of the degree of ionization of the plasma is directly related with the strengthening or weakening of the the electric and magnetic character of the matter and, thus, directly varies its behaviour in the current application.

The degree of ionization of a plasma is strongly governed by the numerous collisions that take place among the different particles present in the mixture, which lead to generation and recombination of free charges. However, these are not the only effects under the influence of collision processes. The various interactions between the particles are also responsible for the excitation of atoms, charge and momentum exchanges, and the

thermal equilibrium of the species, among others.

Due to the high number of properties that are conditioned by all the particle interactions, the accounting for collision processes becomes a key factor in the determination of the transport coefficients for the fluid models of plasma species.

An entire field of study is built around the understanding and modelling of all the collision processes. Additionally, the fact that statistical analysis is required to handle the amount of interactions taking place in a volume of plasma makes the researches in these area of an outstanding complexity.

1.3. Classification of collisions

Prior to a complete analysis of the particle interactions that may occur, it is useful to state a first general classification of the different types of collisions and introduce some handling definitions and properties. These are repeatedly present in deeper analysis and treatment methods of the plasma in further chapters, so it is important to have a clear understanding of these basic concepts.

Concerning a general classification of the different colliding processes, the most direct grouping can be performed in terms of the conservation of momentum and mechanical energy of the particles involved, which clearly depicts two types of interactions [2]:

- **Elastic collisions:** These interactions are characterized by a change in direction of the movement of the particles involved, while its internal energy remains unchanged. Thus, there exist a conservation of the total mechanical energy through the collision process.

  As it is further developed in Chapter 2, elastic collisions include pure elastic interactions and the so called *Coulomb collisions*, resulting from the close encounter of two charged particles.

- **Inelastic collisions:** In these interactions the kinetic energy of the particles is totally or partially transferred into internal energy, leading to atomic processes of the particles involved.

  This type of collisions, as it is later introduced in Chapter 3, include processes of relevant importance such as excitation, dissociation, ionization and charge exchange among others.

While the just mentioned classification provides a general view, other classifications are possible and even preferred from different standpoints. For example, collisions can be grouped accounting for the charge exchange, where an electron is transferred between the colliding partners; momentum exchange, where the momentum of one particle is partially or completely transferred to another, or by their combination. However, for hybrid/PIC

codes like the one this thesis is aimed for, an appropriate classification distinguishes between collisions with and without electrons being involved.

The reason behind this later approach lays in the way in which these codes simulate the plasma flow. As explained at the end of this introductory chapter, these codes consider electrons as magnetized fluids and the rest of particles like solids, being required different treatments for each case.

For the purpose of this thesis, the first classification will be provided as represents a clearer structure from the physics standpoint. Nevertheless, it will be shown that in the final database the collisions organization makes perfectly identifiable those with electrons involved, being then the database customized for hybrid/PIC codes.

1.4. Introduction to collision modelling: Cross sections and collision rates

Now that the importance of collisions and their classification have been introduced, it is possible to comment the measuring quantities that are used to treat these interactions. The most important one, and first to be introduced, is the so called *collision cross section*, denoted as "σ".

The common standard of the meaning of a collision cross section between two objects is the total area inside which, if the two object are simultaneously and entirely located, they will touch each other and collide, with a resulting transfer of momentum and possible change of direction. For example, the collision cross section area of two solid spheres corresponds to the sum of the individual cross section areas: $\sigma = \pi(r_1 + r_2)^2$.

However, real collision processes occurring inside a plasma volume are not as simple as the ideal example just presented, where the cross section was directly proportional to the length scale of the spheres. This approach becomes unrealistic when the length scale reduces to atomic levels and new effects must be accounted rising from the relative velocity between the colliding particles and their charge state. As a matter of fact, at such length scales quantum effects become relevant and intervene in collision processes. For this new complex system, the definition of the collision cross section becomes "a measure of the probability of a collision to take place" (or the probability of momentum loss of the particles).

For this new approach, referring to the elastic interactions among plasma particles, the collision cross section may be defined in terms of an equivalent cross section provided if the particles absorb perfectly the momentum. Likewise, in inelastic collisions, the probability of occurring such interaction is given in terms of the equivalent cross section that a particle would have if it was idealized as a solid sphere (it can be noticed in further chapters how some of the models used to simulate the collision cross section make use of the area of a sphere with the Bohr radius).

It is interesting to point out the strong dependence that cross sections have on the

relative velocity between the colliding species. Very large speeds may be translated in a reduction of the cross section due to the fact that the interaction time is much lower [2]. This characteristic behaviour is visible in Figure 1.1(a), which specifically shows the case of the hydrogen ionization by electron collision. As the speed of the striking electron increases to high values, the rate of the reaction increases too, lowering the collision cross section. This figure also introduces another property that characterizes many atomic collisions. There exists a threshold energy below which the collision will not occur (in the figure it example corresponds to the minimum required energy to ionize hydrogen), and after which the cross section rapidly increases to its maximum and then gradually decreases as the energy of the striking particle raises.

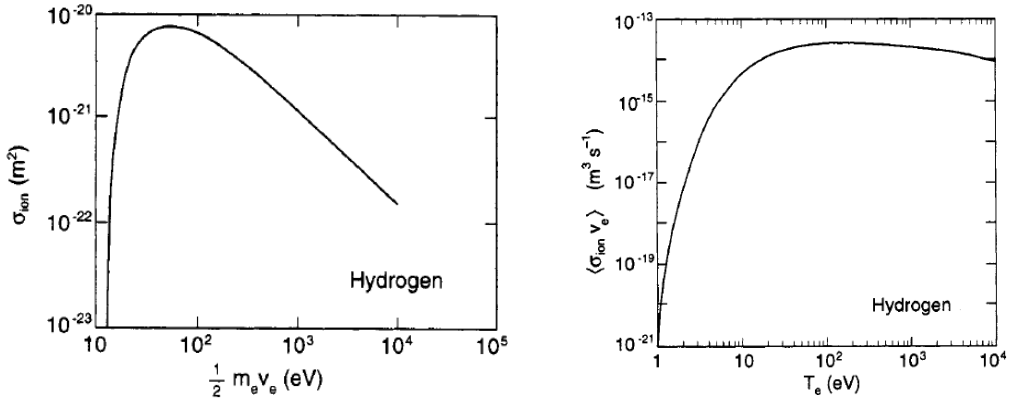

(a) Ionization cross section

(b) Ionization collision rate

Fig. 1.1. Hydrogen ionization by electron impact: collision cross section and rate coefficient [1]

Before commenting Figure 1.1(b), whose meaning is actually much more relevant for hybrid/PIC codes, two other basic parameters must be introduced: the *mean free path (λ)* and the *interaction/collision frequency (ν)* [1], [2]. The simplest interpretation of the former is the distance λ that the striking particle travels before there is a reasonable probability of colliding with another particle. In a binary collision process such as $A + B$, being A the striking particle through a volume of particles B with density "n_B", the mean free path is defined as

$$\lambda = \frac{1}{n_B \sigma} \tag{1.1}$$

where σ represents the previously introduced cross section of the collision. For a particle moving with velocity "v_A", the mean time between collisions is given by $\tau = \lambda / v_A$. Applying the definition of frequency as the inverse of the period, the collision frequency is obtained:

$$\nu = n_B \sigma v_A \tag{1.2}$$

As it is further explained in Chapter 5, the flow of some plasma particles, such as electrons, is modelled following a probability distribution function (usually a Maxwellian distribution). This means that in a flow of electrons with global known velocity, each electron has a specific probability of having a specific amount of energy and move with a determined velocity. So, depending of this energy level, the collision cross section varies (i.e $\sigma = \sigma(v_A)$). With this modelling of plasma particles as a fluid, the just introduced collision frequency is better expressed as

$$\nu = n_B \langle \sigma(v_A) v_A \rangle \tag{1.3}$$

where the terms $\langle \sigma(v_A) v_A \rangle$ results form averaging the product $\sigma(v_A) v_A$ over the entire energy distribution function at a given flow energy. This averaged parameter is the one depicted in Figure1.1(b) (for Hydrogen ionization) and is termed as *rate coefficient*, being commonly preferred to be used over the collision cross section [2]. The importance of this parameter is that it dictates the rate at which the products of reactions are being formed. So, for plasma the rate at which ions are being formed is directly related with the rate coefficient of ionization collisions. Consequently, this parameter is also a measure of the rate of change of the mass of dominant species [3], such as neutrals in cold plasma ; and a reference of the time that a specie in a given energy state survives in the system. A deeper comprehension of this parameter is later developed in Chapter 5.

1.5. Plasma in Aerospace Engineering

Plasma has multiple applications in the aerospace field. One of them is the electric space propulsion. The rise of the electric propulsion came with the appearance of highly efficient electric thrusters during the sixties decade, (such as the Hall-Effect thruster and the Ion thruster [4]) and, since then, large developments and innovations have taken place.

However, the origin of the electric propulsion goes back to the early twentieth century [5]. The first referenced concepts of electric propulsion where conceived by Robert Goddard [6] in 1906 in the USA, and by Tsiolkovskiy [7] in Russia in 1911. During the first half of the century several concept applications for different electric propulsion ideas where collected by Hermann Oberth in Germany in 1929 and Shepherd and Cleaver in Britain in 1949 [8]. But it wasn't until 1964 when the first systematic analysis of an electric propulsion system was performed in the book *Ion Propulsion for Space Flight*, by Ernst Stuhlinger [9]; and Robert Jahn [10] performed a comprehensive description of the physics behind these systems in 1968. The decade of 1960 is a mark on the history of the development of electric propulsion. Significant research programs with the aim of improving this technology were established at several laboratories of the National Aeronautics and Space Administration (NASA) (such as the Glenn Research Center, Hughes Research Center and NASA's Jet Propulsion Laboratory [5]) and at several institutes of

Russia. During this decade the first experimental ion thrusters, making use of cesium and mercury propellants, where launched into orbit.

By the end of the century, electric thrusters had been implemented in station keeping manoeuvres of communication satellites by Russia, the USA and Japan, the USA had performed the first deep-space mission using a solar electric ion thruster and it had begun the commercial use of ion thrusters propelled by Xenon. Not much later, in 2003, the European Space Agency performed a lunar mission with a Hall-effect thruster [4], and during the last decade serious researches have been established to improve this technology as a future potential substitute for chemical rockets.

The reason behind all this interest is that electric propulsion systems require less amount of propellant for a specific mission. This property may result in one of the following advantages: the lower amount of propellant mass allows for an increase of the available payload mass, or the total mass of the device may be reduce, which might imply a reduction in the launch cost of thousands or millions of dollars (comparison made in dollar being assumed as the international currency for space projects).

During all this evolution, all the different types of propulsion systems developed can be grouped in terms of the acceleration method used to provide the thrust force: *electrothermal thruster*, which heated the propellant through a resistively heated chamber or element upstream the nozzle entrance; *electrostatic thrusters*, which accelerate the plasma ions by means of a differential in electrostatic potential; and *electromagnetic thrusters*, that accelerate the charged propellant making use of electromagnetic forces.

Among the mentioned classification, plasma effects in electrothermal thrusters (like "Resistojets" and "Arcjets") are low due to their low ionization level, producing low thrusts and efficiency. Electromagnetic thrusters, such as the "Magnetoplasmadynamic Thruster", are able to produce high thrusts, however they need to operate at very high powers to achieve so. The most succesful thrusters are the electrostatic thrusters, like the "Ion Thruster" and the Hall-Effect Thruster".

Both of the aforementioned motors make use of highly ionized plasma to generate thrust, however, their actuation methods are different. In a concise way, ion thrusters make use of several ionization techniques to dissociate a large fraction of the propellant into plasma. The plasma ions are then accelerated to high velocities through a biased grid by means of an electrostatic potential. In addition, to overcome the charging effect of the spacecraft, which is a main concern in electric propulsion as it may lead to potential hazards, a cathode located outside the ion exit emits electrons to keep the spacecraft neutral [5], [11]. A simplified sketch of this propulsion system is provided in Figure 1.2

The Hall-effect thruster makes use of the so called Hall-effect to dissociate the propellant into plasma in a annular chamber. This effect results from the cross-field of an electron discharge by a cathode and a transverse magnetic field in the annular chamber. The plasma ions are then accelerated to high exit velocities by the difference in electric

potential between the anode and the cathode, while the magnetic field of the chamber prevents the electrons from shorting out the electric field. Alike the ion thruster, the electrons provided by the cathode also neutralize the spacecraft charge, as depicted in Figure 1.3. [5], [11].

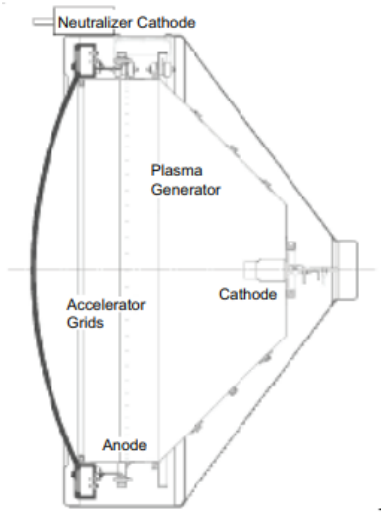

(a) Ion thruster sketch [5]

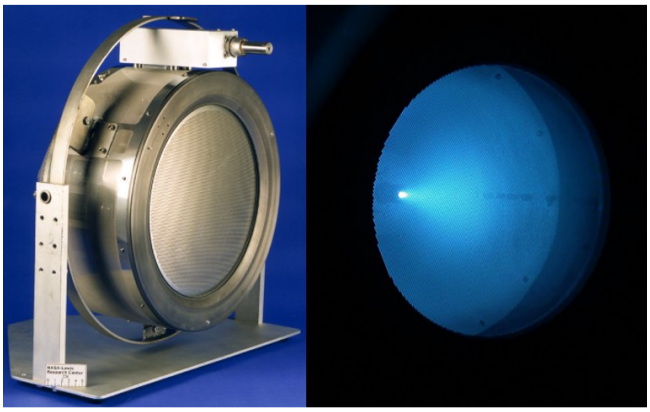

(b) Ion thruster with visible grid and external cathode [12] [13]

Fig. 1.2. Simple layout and exit view of an Ion thruster

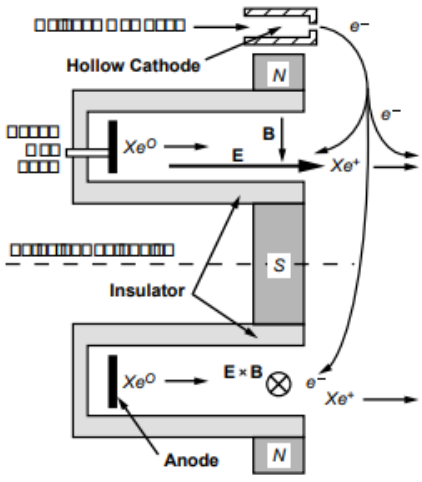

(a) Hall effect thruster sketch[5]

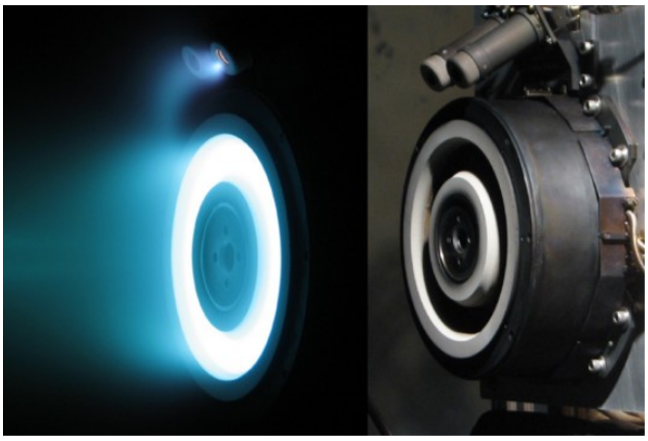

(b) Hall effect thruster nozzle exit and actuation of the external cathode [12]

Fig. 1.3. Hall-effect thruster layout and actuation.

The outstanding characteristic of these electric propulsion systems is its high specific impulse compared to chemical thrusters of solid and liquid propellant. The specific impulse of a propulsive system, I_{sp}, is a direct measure of its efficiency, as it directly relates the achievable thrust force and the propellant mass spent to generate it:

$$I_{sp} = \frac{c}{g_0} = \frac{T}{g_0 \cdot \dot{m}} \ [s] \tag{1.4}$$

Where: c =“effective” escape velocity of the propellant

g_0 =gravity acceleration at sea level

T =thrust force generated by the propulsive system

$\dot{m}$ =propellant mass flow spent to generate the thrust force

While typical chemical thrusters have I_{sp} values of hundreds of seconds, as depicted in Figure 1.4, electric propulsion systems achieve much higher efficiency. Hall-Effect thrusters usually have specific impulses in the range $I_{sp} \simeq 1000 - 3000\ s$, being surpassed by the efficiency of the ion thrusters: $I_{sp} \simeq 2000 - 6000\ s$ [11]. The high values of the former makes it a suitable propulsion system for station keeping manoeuvres and even lunar missions, as it is the mentioned example of the SMART-1 mission carried out by the European Space Agency in 2003 [4]. However, for interplanetary missions higher I_{sp} values are required, being ion thrusters more suitable.

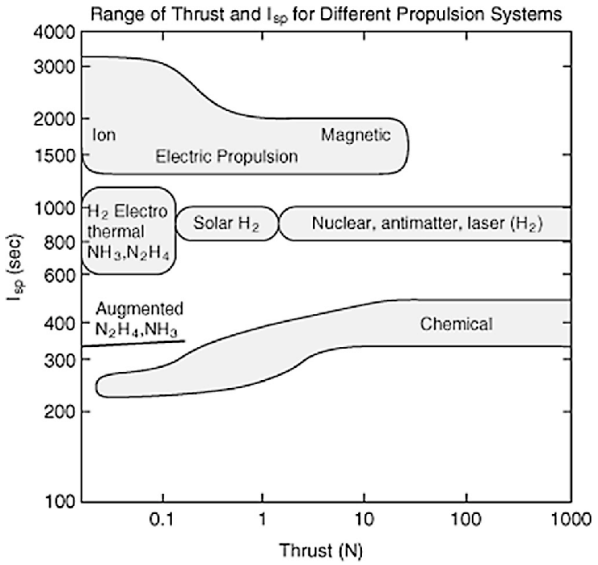

Fig. 1.4. Range of thrust and Isp for different propulsion systems [14]

Unfortunately, despite the advantages shown by electric propulsion systems, nowadays these cannot be implemented as launching propulsion systems. The high efficiency represented by the high specific impulse of these thrusters is translated in a low propellant exit mass flow, that is, low acceleration, which implies that the thrust forces generated by these systems are low. Current researches are centered, among other aims, in increasing the generated thrust force, which can be achieved by increasing the difference in electrostatic potential, to obtain a wider number of applications for these thrusters.

Despite not being as related with the purpose of this thesis as the previous application, some other areas where plasma is highly present are:

- Materials treatment: A common issue around the construction of aerospace structures concerns the long-term bonding of composite materials with metallic components, which weakens after being exposed to hot and wet conditions, aerospace fluids and solvents. It is found that a plasma surface treatment of such materials prior their bonding enhances the long-term durability of the bonding as it is strengthened [15]. While surface bonding represent the most important application on this area, other advantages of performing a surface treatment to polymer and composite materials include surface cleaning and substitutes for surface abrasion techniques [16].

- Flow control actuators: As a general concept, plasma actuators are small electronic devices that generate a weakly ionized plasma around their electrodes and accelerate it by means of an electromagnetic field, leading to a small jet with multiple applications in flow control areas. The two most outstanding applications of these devices are:

  - Flow control inside combustion chambers with *serpentine plasma actuators*. These enhance re-circulation flow and turbulence to obtain a faster homogeneous mixing of fuel and air inside the chamber and, thus, obtain a more homogeneous and stable combustion [17].
  - Enhancement of the flow over an airfoil with *Dielectric Barrier Discharge (DBD) actuators*. The small jet produced by these devices adds momentum to the airflow over the airfoil, usually at the leading edge, to delay the flow separation and enhance the generation of lift [18].

1.6. Introduction to Hybrid/PIC codes and Thesis Objective

The flow inside all these types of electric thrusters are incredibly complex, with multitude of changes on flow properties such as density, charge, ionization degree, energy...All these variations occur through time and depending on the location of the matter. For example, the ionization state of the plasma may change as ions are accelerated from the chamber through the nozzle to the exit. Thus, it is essential to perform an accurate simulation of all the effects, fluxes, interaction...that may occur throughout the entire process to allow a viable prediction of the behaviour of the entire system and make improvements or modifications.

To this end, several simulation methods have been developed with the aim of analyzing the macroscopic behaviour of the overall systems being modeled as fluid motions. However, such is the complexity of the problem, that these methods still need to consider the basic interactions that take place at microscopic scales in order to obtain accurate

solutions for transport and thermodynamic equations, as well as modelling the possible instabilities [3].

In its basis, all the developed methods can be classified as *kinetic methods*, *fluid methods*, and *hybrid methods* (which, as may be thought, brings together the first two methods).

Without entering in in complex physics and math formulation, the former method aims to obtain different distribution functions for each of the species present in the plasma. At a given time, the number of particles that are in a specific place and with a determined velocity is predicted by these functions. At the same time, due to the transient character of the flow, these distribution functions change with time. The evolution of this functions is determined by the well known Boltzmann equation, which will not be provided to keep this introduction theoretical.

Among the different kinetic methods, the Particle-In-Cell (PIC) method has become one of the most standard simulation procedures to study the plasma physics. In this modelling, ions, electrons and neutral are treated as a group inside a mesh cell and collisions are usually modelled through *Monte-Carlo* methodologies. Through these, which require a dominant specie in terms of density, the probability of collisions taking place is evaluated and the macroscopic effects over the species (mass, charge,...changes) are evaluated in the situation where the interaction occurs. It is then vital to have a previous knowledge off all the potential collisions and their outputs to obtain the most accurate tracking of the macroscopic properties of the different species involved. With the new estimation of the volume characteristics, trajectories of the particles are followed and the Maxwell equations are solved to predict the further behaviour of the plasma. Recall that the Maxwell equations model the electromagnetism through differential equations for the electric field intensity ($\vec{E}$) and the magnetic field induction ($\vec{B}$) [19]. A summarized step structure of the previous simulation method may have the following form [3].

1. Setting of the mesh cells: regions where collisions will take place.
2. Computation of the probability of a collision taking place in each cell AND generation of series of random numbers ($\in [0, 1]$) determined by the population algorithm of each specie.
3. If the generated random numbers lay below the collision probabilities, the collision takes place.
4. Study of the new properties of the particles, mass, charge, density ... in case a collision occured.

On the other hand, the fluid methods make use of classical mechanic techniques designed to study magnetized fluids to solve the different conservation equations of charge, momentum and energy of the plasma. This method usually provide a more accurate

plasma behaviour than the previous one. However, this technique suffers from a very high computational cost.

Hybrid methods provide a mid point approach between the kinetic and fluid methods. Hybrid procedures model part of the plasma species (usually electrons) as a fluid, while the rest of species are modelled by a PIC technique. Obviously, all these methods perform several assumption that simplify the problem to be solve. Nevertheless, the hybrid methods allow to obtain a reasonable accurate description of the mentioned flow properties variation with a much lower computational cost than fluid methods. An sketch of the simulation loop characteristic of hybrid codes is presented in Figure 1.5.

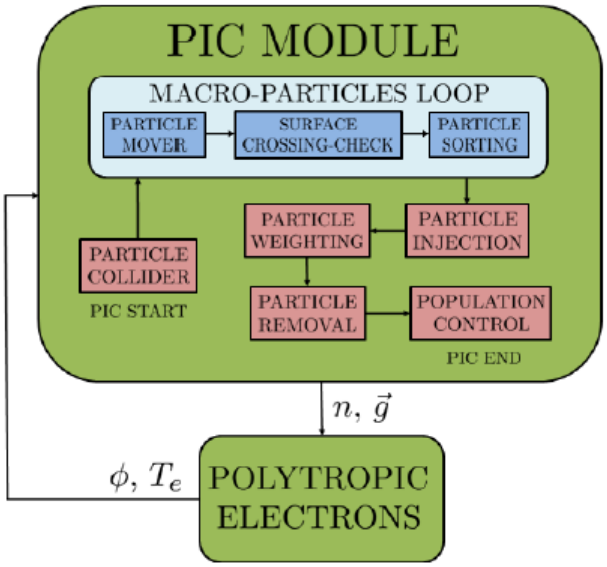

Fig. 1.5. Simulation loop of an hybrid code including PIC and electron fluid models [20]

The objectives of this thesis are to provide relevant information of the particle collisions that should be accounted in the hybrid/PIC codes, with different methods of cross section measurements and comparisons between them; and elaborate a database of collision cross sections between different species of the plasma to be implemented in the presented codes. This data is a representation of the interactions taking place at a microscopic scale and so is crucial for the proper simulation and determination of the distribution functions and flow properties. The information provided by a good database will be also helpful in the prediction of potential new propellants for electric thrusters. Moreover, this database must be designed in a way that it can be easily called by the simulating codes and the data must be extracted as fast as possible to minimize to computational cost of the overall process.

A contextualization of this database in the technical field is presented in the following section and the socioeconomic environment of this project is exposed in Chapter 9.

1.7. Regulatory Framework

Although initially electric propulsion systems made use of mercury and cesium as propellants, since the 1980s Xenon has been widely introduced as propellant, becoming the current one in every electric thruster, due to the advantages that it presents [21]. As an inert gas, no hazards are present when handling it around the testing facilities. It shows a low ionization potential compared to other inert gases, so less energy is required to ionize it. Additionally, it is easily pumped into vacuum spaces by means of condensation on cryopumps.

However, it presents two main drawbacks [21]:

- Its extraction is expensive, and so is its selling price (4-5 €/g). With current mission loads requirements, such as the approximated 160 kg for geostationary satellites and 80 kg for exploratory missions, propellant costs represent a high percentage of the total investment for space missions.

- As a substance to be expelled to the space, it becomes a limited source. The availability of Xenon has become a real issue due to the growing number of spacecrafts using electric propulsion systems, the increasing ambition capabilities of these, and the appearance of multiple different applications that make use of Xenon, such as the mentioned actuators.

A primary focus of multiple researches is centered in the search on new cheaper propellants to substitute Xenon. Krypton and Argon are currently in the spotlight of a number of studies for such purpose, as well as some Alkali metals (Li, Na, K, ...) and other neutral gases (He and Ne).

This project aims then to facilitate essential information for the simulation of propellants in the hybrid codes, whose results will lead in a future to improvements of current systems and propellants.

Other databases already exist with information regarding collision interactions between different species, such as those to be introduced in Chapter 3. However, these databases are directed towards other implementations of plasma, such as atomic fusion reactions, so the information stored is not exactly the needed for electric propulsion; or do not have a direct connection system with hybrid codes. This thesis is, then, centered in generating a database of collisions specifically for the purpose of electric propulsion and with efficient working links between the hybrid/PIC codes and the database information.

Consequently, all the data stored in this database must be referenced when the parameters are obtained from an external public database, and the linking system between the codes and the system is designed to follow the same environment as that one in which the hybrid/PIC codes are developed, as it will be further developed in Chapters 3 and 4.

2. ELASTIC COLLISIONS

Elastic collisions (or elastic scatterings) may be defined as *those where the inner nature and energy state of the colliding particles remains unchanged through the whole processes.*

Several types of elastic interactions are identified, being each of such types more present in plasma of different ionization degrees and making use of different measuring models.

2.1. Elastic collisions with neutrals

Low and partially ionized plasma, cold plasma, is characterized by a high presence of elastic scattering with neutral particles (i.e. neutral-neutral, electron-neutral or ion-neutral elastic collisions). As these collisions may be understood as a simple bouncing of the involved particles, it may be deducted that their results will be dependent on the approaching relative velocity, the distance, and the angle between the initial trajectories of the particles, as sketched below in Figure 2.1.

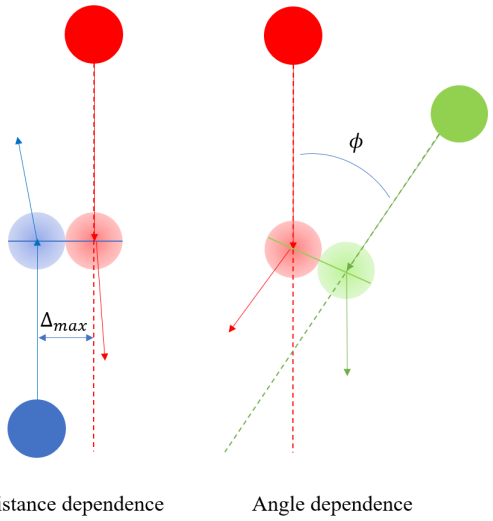

Fig. 2.1. Representation of the dependence of the cross section of a pure elastic collision with the distance and angle between the colliding particles

However, considering the atomic length scale, a rough estimation of the cross section of this type of elastic collisions can be geometrically obtain through the cross section area of an atom with the Bohr radius:

$$\sigma_n \sim \pi {a_0}^2 \sim 10^{-20}\ [m^2] \tag{2.1}$$

Even though this rough approach completely neglects the relative velocity and angle between the colliding particles, the results provided do not move much away from average values derived from empirical results retrieved from external databases [22], [23]. Figure 2.2 represents the collision cross sections for elastic electron impact with four common plasma species. In this image it is clearly observable how the average values for these interactions lay in the order of $\sim O(10^{-20})m^2$. The result obtained then by Equation 2.1 is a good approximation for the average cross section.

In addition, it is appreciable in this image a low peak value for low energies in the majority of noble gas species. This effect corresponds to a quantum mechanical effect denominated *Ramssauer effect* [24], which takes place when the characteristic size of the atom and the electron wavelength are of the same order of magnitude ($O(10^{-12})m$). At those energies, the electron and the external shell electrons of the atoms approximately have the same wave function and the collision cross section decreases. However, this effect is usually neglected due to the low energy range were it appears($(0, 1)ev$).

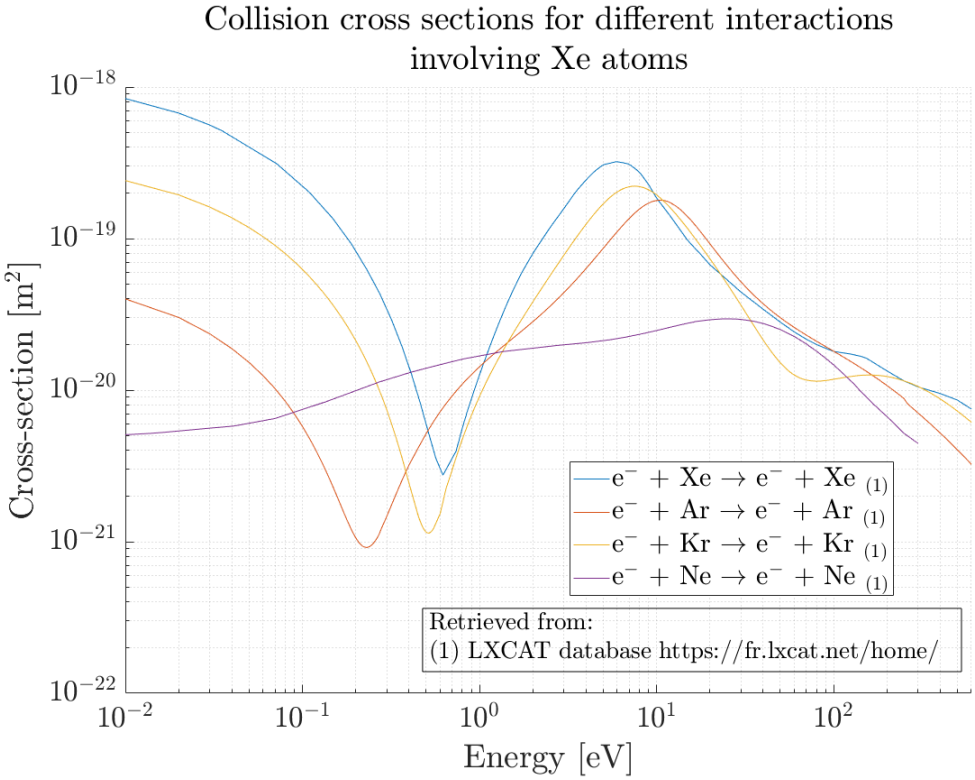

Fig. 2.2. Collision cross section for elastic collisions of electron with neutral: Xe, Ar, Kr, Ne

2.2. Elastic collisions between charged particles: Coulomb collisions

When the charge of all the particles involved is not null, different effect rise from the interaction of these charged particles with and electric fields. Among the possible situations in which the charged particles may be involved, only short-range interactions occurring within close distances between particles are tackled in this thesis. The interactions with

the macroscopic electric fields generated by the moving charges of the plasma itself is not covered as they do not model the interactions between particles and so, do not govern over the momentum evolution of the particles at atomic scale.

Close range interactions start to become dominant when the temperature and ionization degree of the plasma increases (electron-electron, electron-ion, and ion-ion collisions collisions). The are the so called *Coulomb collisions*.The basic physics of this type of interaction is the force felt by the charged particles in relative motion, the *Coulomb force*. This force is directly proportional to the product of the charge of the particles involved and inversely proportional to the distance between them:

$$F_{coulomb} = \frac{Z_1 Z_2}{4\pi\epsilon_0 r^2} \tag{2.2}$$

where: Z_i = charge of the particle $[C], i \in [1, 2]$

ϵ = permittivity of free space $\simeq 8.8542 \cdot 10^{-12} \left[\frac{C}{N \cdot m^2}\right]$

r = distance between the particles $[m]$

Notice, from the previous expression, that the resultant Coulomb force will be attractive between the two particles when these have opposite charge sign, while particles will mutually repel if their charges have the same sign. This force results in a deflection of the initial trajectories of the particles proportional to the mass of each particle, the product of their charges and the *impact parameter*. The *impact parameter* (denoted as "b'' in Figure 2.3), is the minimum distance between the unperturbed rectilinear trajectories that the charged particles would follow.

If the previous deflection is as much as 90°, the electron losses most of its initial momentum, thus this interaction has the same momentum standpoint than elastic collisions with neutrals, allowing the term "collision" to be used with Coulomb interactions. Moreover, this deflection gets larger when the kinetic energy of the colliding electron and the potential energy of the Coulomb force coincide. That is:

$$\frac{Z_1 Z_2}{4\pi\epsilon_0 b} \sim \frac{mv^2}{2} \sim T_e \tag{2.3}$$

This condition allows to estimate an effective cross section of Coulomb collisions similar to that one of elastic collisions with neutrals. Taking as reference the Coulomb collision of an electron with an hydrogen ion [1]:

$$\sigma_i \sim \pi b^2 \sim \frac{\pi e^4}{(4\pi\epsilon_0)^2 T_e^2} \sim \frac{10^{-17}}{T_e^2}\ [m^2] \tag{2.4}$$

where: T_e = electron temperature $[eV]$

Comparing both cross section expressions, Equations 2.1 and 2.4, it is proved that Coulomb collisions are dominant in plasma once it is just a few percent ionized, supporting the spotlight on Coulomb collisions rather than elastic collisions with neutrals. However, this followed approach is only an estimation to obtain the order of magnitude of the process cross section, a deeper analysis of this interaction is performed in the following sections.

Although this thesis is aimed for cold plasma simulations, an analysis of this type of interaction is provided as it not only describes interactions with electron, but also interactions between other charged species. Thus, coulomb alike interaction will be latter identified in recombination processes (like ion-ion recombination) and charge exchange interactions.

2.2.1. Singular Coulomb Collision

Back to the deflection effect, particles of equal charge and mass experience the same deflective angle and both particles exit the collision with the same velocity magnitude. That is, there is a null energy transfer. However, if there exist a high difference in mass and charge between the particles (i.e. electron-ion collision), as the same amount of momentum is transferred between the particles, the lightest particle (electron) experiences a deflection much larger than the heavy particle (ion). This latter situation is used to study the general behaviour of Coulomb collisions.

At the same temperature (same energy), electrons move with a velocity much higher than the ions due to their infinitely lower mass. Then, to perform this study, the ion particle (the biggest mass) is defined as the point of reference to which the electron approaches. Figure 2.3 represent a Coulomb collision with such reference frame.

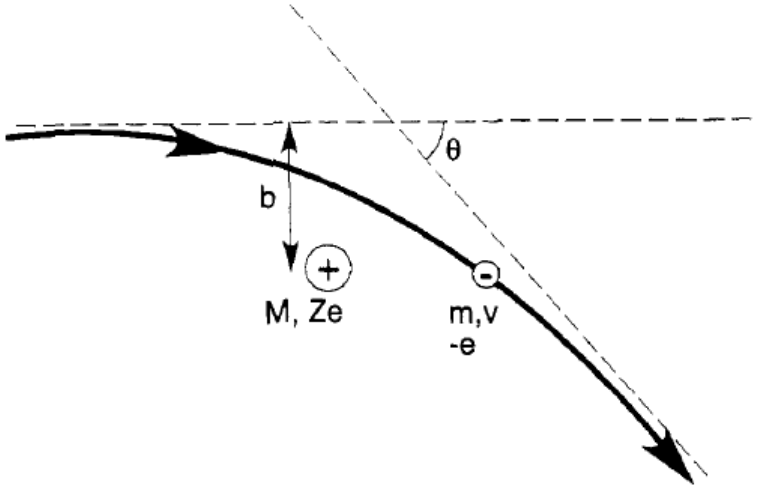

Fig. 2.3. Deflection θ of the orbit of an electron through a Coulomb collision with a fixed ion of charge Ze.[1]

As depicted, the result of the inverse-square-law Coulomb force of Equation 2.2 is a hyperbolic orbit followed by the electron (being θ the limiting angle of the hyperbole). Moreover, classical mechanics prove that the deflection angle resulting from this interaction follows the form:

$$\tan\left(\frac{\theta}{2}\right) = \frac{Ze^2}{4\pi\epsilon_0 m v^2 b} \tag{2.5}$$

where: Z = charge of the ion $[C]$

e = charge of the electron $\simeq 1.602177 \cdot 10^{-19}[C]$

ϵ_0 = permittivity of free space $\simeq 8.8542 \cdot 10^{-12}\left[\frac{C}{N \cdot m^2}\right]$

m = mass of the electron $[Kg]$

v = velocity of the electron $\left[\frac{m}{s}\right]$

b = impact parameter $[m]$

This hyperbolic limit angle demonstrates the previous estimated effective coss section of Equation 2.4. If the electron is deflected 90°, $tan(\theta/2) = 1$, meaning that the impact parameter b_0 is

$$b_0 = \frac{Ze^2}{4\pi\epsilon_0 m v^2} \Rightarrow tan\left(\frac{\theta}{2}\right) = \frac{b_0}{b} \tag{2.6}$$

Resulting in the cross section: $\sigma_i = \pi b_0^2 = \frac{\pi Z^2 e^4}{(4\pi\epsilon_0)^2 m^2 v^4} = \pi b_0^2 = \frac{Z^2 e^4}{16\pi\epsilon_0^2 m^2 v^4}$ (2.7)

2.2.2. Cumulative Coulomb Collision

The derivation for the effective cross section of Equation 2.7 was obtained for a singular large-angle electron-ion Coulomb collision. Nevertheless, in a highly ionized environment, due to the long-range nature of the Coulomb attraction, there is a much higher frequency of small angle collisions than large angle collisions. Indeed, many cumulative small angle deflections produce an effect larger than the relative fewer large angle deflections. Thus, to obtain a more realistic standpoint, a derivation of the cross section is performed accounting for cumulative small angle scatterings with a large number of ions and impact parameters.

For the ease of this derivation, it is considered a situation such as the one depicted in Figure 2.4, with the initial velocity in the z direction.

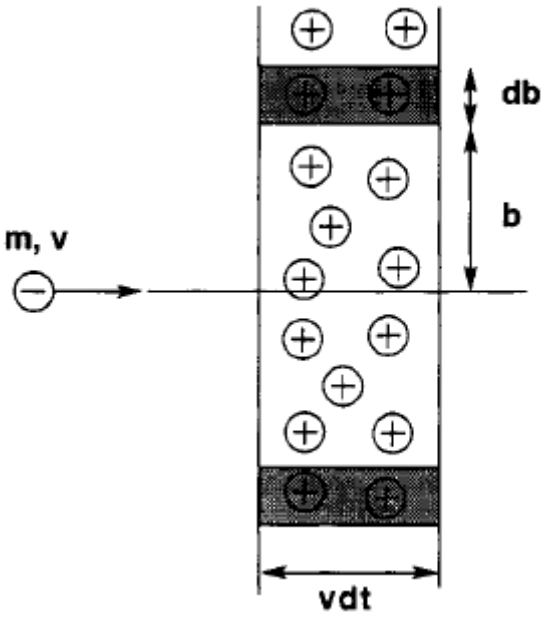

Fig. 2.4. Electron Coulomb scattering by ions through an annular volume with impact parameter b and $b + db$ as the electron moves a distance vdt[1]

Through the multiple small-angle scatterings that the electron will suffer, it will be given an incremental velocity in the normal directions $\Delta v_\perp = v\sin(\theta) = \Delta v_x$ and Δv_y. While the averages of these increments must vanish due to the fact that the direction is independent of the scattering ($\langle \Delta v_x \rangle = \left\langle \Delta v_y \right\rangle = 0$), the mean square deflections do not vanish ($\left\langle (\Delta v_x)^2 \right\rangle = \left\langle (\Delta v_y)^2 \right\rangle = \frac{1}{2}\left\langle (\Delta v_\perp)^2 \right\rangle \neq 0$).

From the hyperbolic deflection angle stated in the previous section, $\sin(\theta)$ can be inferred as follows:

$$\begin{aligned} sin(\theta) &= 2\sin\left(\frac{\theta}{2}\right)\cos\left(\frac{\theta}{2}\right) = 2\tan\left(\frac{\theta}{2}\right)\cos^2\left(\frac{\theta}{2}\right) \\ &= \frac{2\tan\left(\frac{\theta}{2}\right)}{1+\tan^2\left(\frac{\theta}{2}\right)} = \frac{2\left(\frac{b}{b_0}\right)}{1+\left(\frac{b}{b_0}\right)} \end{aligned} \tag{2.8}$$

Leading to the normal velocity deflection of one collision:

$$(\Delta v_\perp)^2 = v^2\sin^2(\theta) = \frac{4v^2\left(\frac{b}{b_0}\right)^2}{\left[\right]1+\left(\frac{b}{b_0}\right)\Big]^2} \tag{2.9}$$

The rate at which this normal velocity varies as the electron crosses the volume element can be found knowing the ion density n_i in the scattering volume:

Ion density: n_i

Scattering volume: $2\pi b \cdot db \cdot vdt$

So:

$$\frac{d\left\langle(\Delta v_\perp)^2\right\rangle}{dt} = 2\pi n_i v \int_{b_0}^{b_{max}} (\Delta v_\perp)^2 b db = 8\pi n_i v^3 \int_{b_0}^{b_{max}} \frac{\left(\frac{b}{b_0}\right)^2 b db}{\left[\right]1 + \left(\frac{b}{b_0}\right)\Big]^2} =$$

$$= 4\pi n_i v^3 b_0^2 \left\{ \ln\left[1 + \left(\frac{b_{max}}{b_o}\right)^2\right] + \frac{1}{1 + \left(\frac{b_{max}}{b_0}\right)^2} - 1 \right\} \tag{2.10}$$

where b_0 was defined for a singular coulomb collision in Equation 2.6 and b_{max} corresponds to the impact parameter where the coulomb forces stop being relevant. As the latter parameter is more difficult to obtain, the ratio $\Lambda = b_{max}/b_0$ will be temporarily considered, with some estimation of the values that it may acquire provided in Table 2.1.

$$\text{If } \Lambda \equiv \frac{b_{max}}{b_0} \gg 1, \text{ then: } \frac{d\left\langle(\Delta v_\perp)^2\right\rangle}{dt} = 8\pi n_i v^3 b_0^2 \ln\Lambda = \frac{n_i Z^2 e^4 \ln\Lambda}{2\pi\epsilon_0^2 m^2 v} \tag{2.11}$$

Regarding the velocity parallel to the original direction, a reduction in this one ($\Delta v_\parallel$) is appreciable. This is reasoned with the fact that the electron scattering off the heavy ion loses all its momentum but its energy is nearly conserved. So, an expression for the rate of change of this reduction is obtained by means of energy conservation:

$$(v + \Delta v_\parallel)^2 + (\Delta v_\perp)^2 = v_\parallel^2 \tag{2.12}$$

As: $O(\Delta v_\parallel) \ll O(\Delta v_\perp)$ and$v = v_{initial} = v_\parallel$, then

$$v(\Delta v_\parallel) + \frac{1}{2}(\Delta v_\perp)^2 = 0 \Rightarrow (\Delta v_\parallel) = -\frac{1}{2}\frac{(\Delta v_\perp)^2}{v} \tag{2.13}$$

So the rate of change of $\langle\Delta v_\parallel\rangle$ is:

$$\frac{d\langle\Delta v_\parallel\rangle}{dt} = -4\pi n_i v^2 b_0^2 \ln\Lambda = \frac{n_i Z^2 e^4 \ln\Lambda}{4\pi\epsilon_0^2 m^2 v^2} \tag{2.14}$$

This last relation allows to obtain the definition of a collision rate (v_{ei}) for loss of electron momentum:

$$\frac{d\langle \Delta v_{\parallel} \rangle}{dt} = -\nu_{ei} v \Rightarrow \nu_{ei} = -\frac{d\langle \Delta v_{\parallel} \rangle}{v dt} \tag{2.15}$$

$$\nu_{ei} = 4\pi n_i v b_0^2 \ln \Lambda = \frac{n_i Z^2 e^4 \ln \Lambda}{4\pi \epsilon_0^2 m^2 v^3} \tag{2.16}$$

As developed in Equation 2.16, the rate at which the electron loses its momentum is inversely proportional to the cube of its initial velocity and directly proportional to $\ln \Lambda$. It is, then, a reasonable moment to estimate the values of this parameter Λ. However, in order to do so, two new concepts must be introduced and understood: the *Boltzmann factor* and the *Debye length*, λ_D.

The *Boltzmann factor* defines the relative probability "P_r" of a particle to have energy E_r as:

$$\text{Boltzmann factor: } P_r = \exp\left(-\frac{E_r}{kT}\right) = \exp\left(-\frac{E_r}{T}\right) = \exp\left(-\frac{\frac{mv^2}{2} + q\phi}{T}\right) \tag{2.17}$$

Where the Boltzmann constant, K, converts the temperature from Kelvin to energy units: $K = 1.38 \cdot 10^{-23}[J/K] = 1.6 \cdot 10^{-19}[J/eV]$.

Notice the physical dependence through the potential term $p\phi$. The reason behind is that charged particles in the volume tend to gather around a particle with the opposite sign charge and distance from particles with the same sign charge. This means that, recalling the initial study, when an electron enters a highly ionized volume, the ions tend to gather around such electron, shielding out the electron electric field further away of a given distance from the electron. This shielding length is the so called *Debye length* (λ_D). The statistical treatment of the Debye shielding is valid if there exist a high number of particles within the Debye sphere, with volume $(4/3)\pi\lambda_D^3$, which is implicit in the definition itself of Debye shielding.

$$\text{Debye length: } \lambda_D = \left(\frac{\epsilon_0 T_e}{n e^2}\right)^{\frac{1}{2}} \tag{2.18}$$

Returning to the initial derivation of the cross section, the just introduced Debye length provides the maximum impact parameter ($b_{max} = \lambda_D$) as the Coulomb field at larger distances is suppressed by the Debye shielding. This also allows the computation of the order of the minimum impact parameter b_0. To do so, b_0 is evaluated as an average over a Maxwellian distribution considering $mv^2 \sim 3T$, and in accordance with the definition of b_0 stated in Equation 2.6

$$b_0 = \frac{Ze^2}{4\pi\epsilon_0 m v^2} \Rightarrow b_0 \sim \frac{Ze^2}{12\pi\epsilon_0 T} \sim \frac{\frac{Z}{12\pi}}{n\lambda_D^2} \tag{2.19}$$

$$\text{Meaning that } \Lambda \equiv \frac{b_{max}}{b_0} \equiv \frac{\lambda_D}{b_0} \sim \left(\frac{Z}{12\pi}\right) n\lambda_D^3 \tag{2.20}$$

Even though the parameter Λ is a function of n and T, the resulting logarithm present in the different expressions is fairly insensitive to the variations of such variables (even when the variations are of orders of magnitude). This property enables to obtain an estimation of this parameter Λ from tables such as the one below [2], which shows that typical values of $ln\Lambda$ vary no more than a factor of two for a large range of n and T parameters.

Table 2.1. SCOPE OF $LN(\Lambda)$FOR SEVERAL TYPES OF PLASMA

Plasma source	**n(m^{-3})**	**T(eV)**	**ln(Λ)**
Solar Wind	10^7	10	26
Van Allen Belts	10^9	10^2	26
Earth's ionosphere	10^{11}	10^{-1}	14
Solar corona	10^{13}	10^2	21
Gas discharge	10^{16}	10^0	12
Process plasma	10^{18}	10^2	15
Fusion experiment	10^{19}	10^3	17
Fusion reactor	10^{20}	10^4	18

Now that all the needed parameters have been defined, it is possible to derive an expression for the cross section of cumulative small-angle Coulomb collisions from the relation of collision frequency (v_{ei}) and the cross section (σ_{ei}):

$$v_{ei} = n_i \sigma_{ei} v \Rightarrow \sigma_{ei} = \frac{Z^2 e^4 \ln\Lambda}{4\pi\epsilon_0^2 m^2 v^4} \tag{2.21}$$

Comparing this result with the cross section for a singular Coulomb collision stated in Equation 2.7, it is realized that the size of the cross section for cumulative small-angle Coulomb collisions is "$4\ln\Lambda$" times larger than that one of an isolated Coulomb interaction. This larger size is the result of many cumulative small-angle scatterings.

As a final remark, to allow an easier analysis of the Coulomb cross section, it is possible to transform Equation 2.21 in terms of the total energy of the electron, that is, the parameter T[eV][1]:

$$\sigma = \frac{Z^2 e^4 \ln \Lambda}{4\pi\epsilon_0^2 m^2 v^4} \simeq \frac{Z^2 e^4 \ln \Lambda}{4\pi\epsilon_0^2} \left(\frac{1.602177 \cdot 10^{-19}}{T_e} \right)^2 \tag{2.22}$$

Being $Z =$ ion charge

$e =$ electron charge $\simeq 1.602177 \cdot 10^{-19}$ $[C]$

$\epsilon_0 =$ permittivity of free space $\simeq 8.8542 \cdot 10^{-12} \left[\frac{C}{N \cdot m^2} \right]$

$\Lambda \sim \left(\frac{Z}{12\pi} \right) n\lambda_D^3$

$T_e =$ electron energy $[eV]$ (2.23)

This analysis to obtain the cross section of the elastic collisions in terms of the flow energy, which are most probably the simplest interactions to analyze, is a good indicator of the complexity of the problem to be simulated to obtain the performance of a plasma flow. These not only require large computation costs, but also deep analysis and approaches to introduce the effects of the particle collisions in the overall behaviour.

3. INELASTIC COLLISIONS

As previously introduced in Chapter 1, through inelastic collisions, transfers between the kinetic energy of a particle and its internal energy take place. The analysis and efforts to simulate this interaction are, then, much more complex that those just derived in Chapter 2.

Inelastic collisions, which have special relevance for highly energized plasma, might be classified in terms of the resulting states of the different particles involved in the process:

- **Ionization processes:** This type of processes are the most relevant ones as they are responsible for the plasma generation, that is, they are responsible of the generation of new electrons and positive ions in the environment.
- **Mechanisms of recombination:** Oppositely to ionization processes, the mechanisms of free electron "losses" are relevant for plasma studies as they are responsible for the loss of free charged particles. The final density of charged particles in the plasma is the result of the balance between the ionization processes and the recombination mechanisms.
- **Charge exchange interactions:** Through this type of interaction an electric charge is transferred between two colliding atoms. This type of process shows high orders of cross section and, so, are of special importance in the modelling process of cold plasma.
- **Excitation collisions:** Against the rest of the inelastic interactions, excitation interactions do not show any movement of charges between atoms, just their excitation to a higher energy level. The collision cross sections of this type of processes are expected to be several orders of magnitude lower than the previous interactions. Consequently this reactions will not be further explained, although may be mentioned and present in further explanations or comparisons.

3.1. IONIZATION INTERACTIONS: PLASMA GENERATION

Inelastic ionization collisions result in the ionization of one of the species involved in the interaction. Some of the most relevant plasma ionization processes are [1] [2]:

- **Direct Electron Impact Ionization:** Ionization of atoms struck by an electron with sufficient large energy to free one of the particle's valence electrons in just one collision. If the striking electron initially has enough energy, the process may lead

to double ionization. Triple ionization may also be possible, however their effect is negligible against the previous cases.

- **Stepwise Ionization by Electron Impact:** Ionization of preliminary excited neutrals by means of an electron impact, leading to an spontaneous exothermic de-excitation of the atom whose energy frees one electron and the atom becomes ionized .

- **Indirect Ionization or Autoionization:** The collision of an electron with a neutral results in an intermediate highly excited state which subsequently decays as a form of ionization. This type is of ionization is quite important in high dense and hot plasma and just in rare situations may be present in cold plasma with low ion density like our case of study [25].

- **Ionization by Collision with Heavy Particles:** Ionization process that takes place during ion-molecular or ion-atomic collisions, and in collisions between electronically or vibrationally excited species when the total collision energy exceeds the ionization potential.

- **Radiative Ionization or Photoionization:** The ionization of a neutral resulting from the collision with photons.

- **Surface Ionization:** This type of ionization takes place in the boundary between the plasma and its container, so it may be conditioning for the designed material of the container. However, it will not be further explained in this thesis as it is primary directed towards the study of the collisions in a complete plasma environment.

3.1.1. Direct Electron Impact Ionization

As introduced, in this process the common involved particles are electron and neutrals and, specifically, the collision takes place between the striking electron and the valence electron of the neutral. During this interaction, the ionization of the neutral (represented in Figure 3.1) takes place when the energy transfer $\Delta\varepsilon$ between the incident electron with energy ε and the valence electron exceeds the ionization potential I of the neutral. This type of ionization is the most important in cold or non-thermal discharges where the electric fields (and so the electron energies) are high, but the level of excitation of neutrals is relatively moderate.

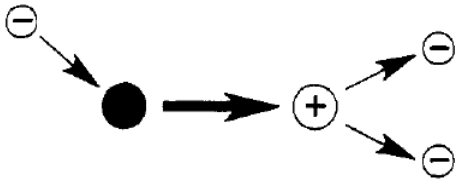

Fig. 3.1. Direct electron impact ionization process [1]

As this type of collision is present in all plasma configurations, regardless of the degree of ionization, it is the process around which most models have been developed. Each of these models, which are presented below, was designed, or resulted more accurate, for a specific type of ionization. Thus, when performing the simulation, it is important to apply the appropriate method for the studied situation.

3.1.1.1 Thomson Model

[2]The most basic Thomson formulation simplifies the problem by assuming that the valence electron is at rest and neglecting the interaction of the colliding electrons with the rest of the neutral particle. It derives an expression for the cross section starting from its differential expression, in terms of the energy transfer $\Delta\varepsilon$, defined by the Rutherford formula

$$d\sigma_i = \frac{1}{(4\pi\epsilon_0)^2}\frac{\pi e^4}{\varepsilon(\Delta\varepsilon)^2}d(\Delta\varepsilon) \tag{3.1}$$

Integrating Rutherford formula and accounting for the condition $\Delta\varepsilon \geq I$ which indicates that the ionization process takes place (being I the ionization energy required by the atom), the most basic "Thomson formula" is obtained:

$$\sigma_i = \frac{1}{(4\pi\epsilon_0)^2}\frac{\pi e^4}{\varepsilon}\left(\frac{1}{I} - \frac{1}{\varepsilon}\right) \tag{3.2}$$

In general, the previous equation should be multiplied by the number of valence electron Z_v. Additionally, it is interesting to point that, following Thomson formula, the maximum collision cross section takes place when the electron energy equals $\varepsilon_{\sigma^{max}} = 2I$, leading to the value

$$\sigma_i^{max} = \frac{1}{(4\pi\epsilon_0)^2}\frac{\pi e^4}{4I^2} \tag{3.3}$$

However, to obtain more accurate results it is attractive to introduce the effect of the kinetic energy of the valence electron, ε_v, for which Equation 3.2 me be adjusted as

$$\sigma_i = \frac{1}{(4\pi\epsilon_0)^2}\frac{\pi e^4}{\varepsilon}\left(\frac{1}{\varepsilon} - \frac{1}{I} + \frac{2\varepsilon_v}{3}\left(\frac{1}{I^2} - \frac{1}{\varepsilon^2}\right)\right) \tag{3.4}$$

Next improvements introduce the neglected interaction of the valence electron with the rest of the neutral. A common approach to do so models such interaction as a Coulomb interaction. Then, classical mechanics state that $\varepsilon_v = I$ and the cross section takes the form

$$\sigma_i = \frac{1}{(4\pi\epsilon_0)^2}\frac{\pi e^4}{\varepsilon}\left(\frac{5}{3I} - \frac{1}{\varepsilon} - \frac{2I}{3\varepsilon^2}\right) \tag{3.5}$$

As it can be derived, the electron energy for which the updated cross section is maximum is lower than the previous one, $\varepsilon_{\sigma^{max}} = 1.85I$, which leads to a maximum cross section value twice as much as the previous one:

$$\sigma_i^{max} = \frac{1}{(4\pi\epsilon_0)^2}\frac{\pi e^4}{2I^2} \tag{3.6}$$

Nevertheless, the resemblance of all the previous expressions enables the formulation of a general expression for the cross section as

$$\sigma_i^{max} = \frac{1}{(4\pi\epsilon_0)^2}\frac{\pi e^4}{I^2} Z_v \cdot f\left(\frac{\varepsilon}{I}\right), \tag{3.7}$$

and the results of experimental data agree with the results provided by that the Thomson formula of Equation 3.2 when the function f remains between two limits. So, it may be stated that Thomson formula

$$\sigma_i = \frac{1}{(4\pi\epsilon_0)}\frac{\pi e^2}{I^2} Z_v f(x) \tag{3.8}$$

with $f(x) = \frac{1}{x} - \frac{1}{x^2}, \quad x = \frac{\varepsilon}{I}$, is valid for the range [2]

$$\frac{10(x-1)}{\pi(x+0.5)(x+8)} < f(x) < \frac{10(x-1)}{\pi x(x+8)} \tag{3.9}$$

3.1.1.2 Gryzinski Model

Alike Thomson model, Gryzinski approach also predicts the cross section as a function of the loss of energy in the interaction. It states that the cross section $Q_G(\varepsilon, \varepsilon_{k\lambda}, \Delta\varepsilon)$ for an energy loss greater or equal than $\Delta\varepsilon$ by an incoming electron with energy ε colliding with one of the ξ_k bound electrons in the k^{th} level is defined as [26]

$$Q_G(\varepsilon, \varepsilon_{k\lambda}, \Delta\varepsilon) = 4\pi a_0^2 \left(\frac{\varepsilon_{1\lambda}^H}{\Delta\varepsilon}\right)^2 \xi_k g(u, v) \tag{3.10}$$

where

$$g(u,v) = \frac{u-1}{u^2}\left(\frac{u}{u+v}\right)^{3/2}\left(1-\frac{1}{u}\right)^{v/(v+1)}\left\{1+\frac{2v}{3}\left(1-\frac{1}{2u}\right)ln\left[e+\left(\frac{u-1}{v}\right)^{1/2}\right]\right\} \tag{3.11}$$

being $u = \frac{\varepsilon}{\Delta\varepsilon}$ and $v = \frac{\varepsilon_{l\lambda}}{\Delta\varepsilon}$.

Through this approach, it is seen that the the equation is applicable for a wide range of energy transfers, which, in theory, allows it to study ionization processes as well as excitation ones. For the current interested ionization process, it is deducted that its cross section takes place when the condition $\Delta\varepsilon = \varepsilon_{k\lambda}$ is satisfied, so that the parameter v equals the unity and the previous expressions become

$$\sigma_G^{(k\to\lambda)}(\varepsilon) = 4\pi a_0^2 \left(\frac{\epsilon_{1\lambda}^H}{\epsilon_{k\lambda}}\right)^2 \xi_k g(u,1) \tag{3.12}$$

being

$$g(u,v) = \frac{u-1}{u^2}\left(\frac{u}{u+1}\right)^{3/2}\left(1-\frac{1}{u}\right)^{1/2}\left\{1+\frac{2}{3}\left(1-\frac{1}{2u}\right)ln\left[e+(u-1)^{1/2}\right]\right\} \tag{3.13}$$

and $u = \frac{\varepsilon}{\Delta\varepsilon} = \frac{\varepsilon}{\varepsilon:k\lambda}$.

The derivation followed to obtain the Gryzinski equation, although based in classical mechanics, performed some *ad hoc* assumptions to adjust the final results with experimental values. For this reason this model may be conceived as a semi-empirical approach.

Nevertheless, several comparison between this model and experimental results have been made and these equations do not differ too much from the measured values. A wide number of comparisons were made by Ochkur and Petrun'kin [26] in 1963 both around the threshold ionization energy and away from that region and computed results differed no more than a factor of two from the measurements. However, better agreement with empirical results, of less than an order of magnitude, were presented when the comparison was made with excitation cross section.

3.1.1.3 Drawing Model

The Drawin Ionization Model introduced in 1961 was experimentally demonstrated by Mathus and Badrinathan to predict the cross-section for the first double ionization due to electron-neutral inelastic collision [3], [27], specifically for the following ionization process:

$$Xe + e^- \longrightarrow Xe^{++} + 3e^-$$

The Drawin model may be seen as an modification of the Gryzinski model to fit the computed cross section with empirical results. For such purpose, a "universal" equations is expressed in terms of the electron energies (as the Gryzinski model) as well as in terms of two constants, β_1 and β_2. These constants are the parameters to be determined

through empirical measurement to fit the equation to the results, making this model to be conceived as an empirical model.

The just mentioned “universal" formula suggested by the Drawin Ionization Model is

$$\sigma_{i++} = 2.66\pi a_0^2 \beta_1 \left(\frac{\varepsilon_i^H}{\varepsilon_i}\right)^2 \xi_k g(u) \quad \text{with} \quad g(u) = \frac{u-1}{u^2} \ln(1.25\beta_2 u) \tag{3.14}$$

In this case ε_i = threshold energy for the double ionization, as it is expressed for the above reaction as an example of how it would be adjusted to double ionization reactions, although this formula also works well for first ionization reactions.

As this approach was derived from the Gryzinski model, most of the times there is not much difference between choosing either of these models for the study case. However, despite the accuracy of this particular method, the necessity of performing and empirical fitting to obtain the constants makes this model to be available for vary few species. Some of the constants that have been measured for some propellants are presented in the next table.

Table 3.1. DRAWIN MODEL CONSTANTS FOR ARGON AND XENON

Specie	β_1	β_2
Argon	0.82	1.00
Xenon	1.00	0.80

3.1.1.4 Bell Model

When considering the second single ionization (for example the reaction $Xe^+ + e^- \rightarrow Xe^{+2} + 2e^-$) it is preferred to manage the ionization data in the form of rate coefficients instead of using the cross section approach (notice that this preference was advanced in the introductory chapter)[28]. The rate coefficients are often computed from the ionization data by means of an averaging of the ionization cross section over the electron velocity/energy distribution function. Some of the mathematical procedures to perform this integration is proposed by Crandall et al. [29]. As it has already been commented, the distribution function for the electron velocity is considered in this procedure to follow a Maxwellian distribution [28].

Bell Ionization Model, then, makes use of rate coefficients to model the inelastic electron-atom collision. Together with the Clenshaw’s algorithm [30], Bell provides the following analytic expression for the rate coefficient [28]:

$$\alpha(T) = \frac{1}{2}\sqrt{T_e}\exp\left(-\frac{I}{kT_e}\right)(b_0 - b_2) \tag{3.15}$$

where: I = Ionization energy of the sample to study $[eV]$

k = Boltzmann constant $\simeq 8,6173324(78) \cdot 10^{-}5$ $[eV/K]$

T_e = Electron energy expressed as a temperature $[K]$

b_0 and $b_2 = f(T_e)$ parameters obtained using Clenshaw's algorithm [30] $[cm^3/s]$

In order to adjust Bell model to simulate the collisions such as that previously shown, two parameters of $O(1)$, f_1 and f_2, are introduced into the Bell model[3]:

$$\alpha(T) = \frac{1}{2}\sqrt{T_e}f_1\exp\left(-f_2\frac{I}{kT_e}\right)(b_0 - b_2) \tag{3.16}$$

In a similar way to the Drawin model, to set the values of the constants f_1 and f_2 empirical measurements must be performed to assign them the values that lead to most accurate predictions. Moreover, naturally this constants adopt different values for different plasma species, and the equation is adjusted to the particular study case. This becomes a disadvantage of this model, as numerous researches must be carried over a large scope of species to allow this method to be widely used.

In addition, this model has a drawback: the hypothesis of considering the electron velocity as a Maxwellian distribution is not accurate at all because the released electrons in the collision make this distribution to be more complex[3].

3.1.1.5 Theoretical comparison and comments on the proposed models

As remarked during the previous presentation of the diverse models, some of them were specifically developed to model a particular type of direct ionization process.

Concerning the most basic ionization reaction ($Xe + e^- \rightarrow Xe^+ + 2e^-$), the Thomson model stands over the rest. However, it must be taken into account that it is restricted to the energy ratio range described in the expression 3.9. The Gryzinski model provides less accurate, but valid enough, results for this reaction, being also able to be evaluated at different energy ranges with a somewhat acceptable estimation of the cross section.

Derived from the Grazinski model, the empirical Drawin model is appropriate for the study of single and double ionization reactions ($Xe + e^- \rightarrow Xe^{+2} + 3e^-$). Unfortunately, the empirical character of this model makes it unavailable until the respective constants are fitted for different species.

The same problem is presented in the Bell Model, which best fits reactions concerning the second ionization of an element ($Xe^+ + e^- \rightarrow Xe^{+2} + 2e^-$).

Higher order ionization process are not worthy to consider in the simulation of plasma codes as they account for a very little fraction of the total process. For example, the cross section ratio between triple ionization and single ionization of Xenon is of the order $O(0.01)$. This means that the cross section for single ionization is two orders of magnitude higher than for triple ionization [31]. Taking this fact into account, triple ionization is not a primary interest for the study of plasma generation. Figure 3.2 provides support to the previous claim as it shows how the cross section values decrease with increasing ionization degree.

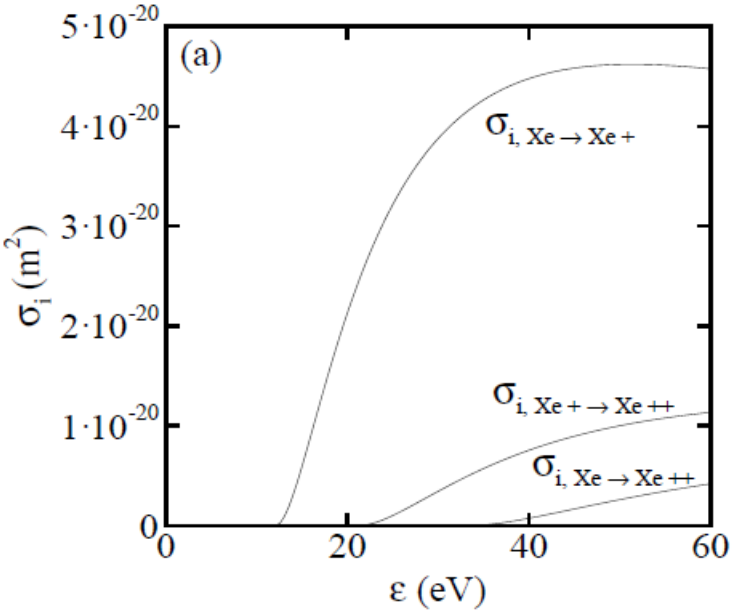

Fig. 3.2. Ionization cross section by electron impact for different ionization degrees [4]

3.1.1.6 Databases sources and Experimental Measurements:

It is noticeable that the current modeling of direct ionization reactions is restricted to a limited number of species due to empirical fitting requirements. So, at the time of selecting cross section values to be further used, it is preferable to retrieve information from databases or empirical measurements, as the validity of their values is usually supported by different sources. Some of the databases consulted during the elaboration of this project are:

- LXCat database [22]: resulting from the *Plasma Data Exchange Project* to make freely available to the community interaction data including cross sections, swarm parameters, reaction rate...not only of ionization reactions, but also elastic and excitation interactions.
- NIFS database [23]. This database belongs to the National Institute of Fusion Science of Sokendai, Japan. It provides free access to ionization cross section and rates, as well as data for excitation, recombination and charge exchange processes

among other. Even though this database is oriented to fusion physics applications, some interactions for the purpose of this thesis can be found in it.

– NIST database [32]: From Physics Measurement Laboratory of the National Institute of Standards and Technology (U:S), provides collision data from a more chemist standpoint. However, this database is more restrictive for the public than the previous ones and specific species for the interest of this project were not available.

Concerning the empirical methodologies, the most reliable way to measure cross-sections is *(Multi-)Crossed-beam method*. In this method, parallel primary and secondary beams (for example electron and Xe beams) are crossed at right angles to keep the scattering region as small as possible [33]. Then, a moving detector measures the differential cross section of the process. While the accuracy of this method is undeniable, it suffers from two disadvantages/issues: Due to space charge particles repulsion, the energy of the ion beams cannot be lowered too much without losing ion current, and the motion of the detector inside the vacuum chamber is quite complicated.

The Multi-crossed-beam method tackles this issues making use of multi-slotted masks in the beam source and in the detector [34], as sketched in Figure 3.3. The resulting encoded beams generate a square pattern of scattering areas that, measured through the specific mask' slot pattern of a fix detector, highly accurate cross sections are measured.

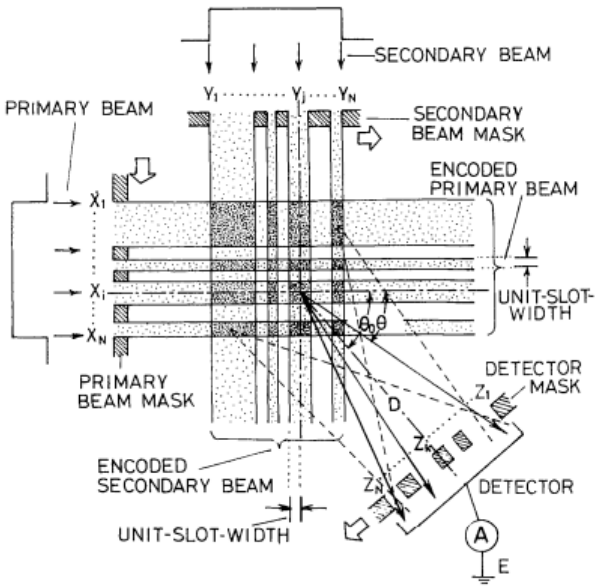

Fig. 3.3. Conceptual design of the multi-crossed-beam method [34]

In general, all the experimental procedures to measure a collision cross section are composed of at least one beam of particles, an area where reactions take place (by collision with a crossed beam or a gas volume), and a detector device to measure the cross section from the received data (charge densities, waves lengths, amount of radiation,...).

However, empirical measurements require a monetary investment in the equipment and the beam species. For this reason, there are not experimental data for all the possible interactions. For these unmeasured collisions, the mentioned databases commonly retrieve their values from a highly supported and accurate program that solves the Boltzmann equations of transport for electrons under the influence of electromagnetic fields: the *Magboltz* program[35], [36].

3.1.2. Stepwise Ionization by Electron Impact

In the situation where the concentration of electrons, and thus the concentration of excited neutrals, is relatively high, the necessary ionization energy I may be provided in two different ways:

1. A direct ionization process, where the energy can be provided by the interaction of the excited neutrals with the plasma electrons.
2. The ionization energy required may be obtained from the high energy preliminary electronic excitation. This process is the so called Stepwise Ionization.

Oppositely to direct ionization, stepwise ionization requires of several electron impacts. First, an excited specie results from an electron-neutral collision. The actual ionization act is provided by the collision of this excited neutral with a relatively low energy electron.

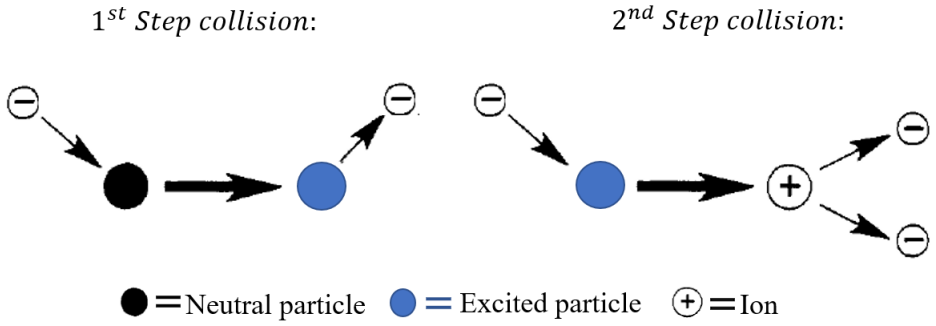

Fig. 3.4. Stepwise ionization by electron impact

While both processes (direct and stepwise ionization) provide the same amount of energy, stepwise ionization contributes the most in the total ionization rate. Due to the fact that the statistical weight of electronically excited neutrals exceeds that one of free plasma electrons, the stepwise ionization is much faster than direct ionization if the level of electronic excitation is high enough. Explained in terms of energy, if $T_e << I$ (electron energy much lower than ionization potential), the free plasma electrons have much less probabilities of reaching the ionization energy than the excited particles.

As it has been briefly explained, the stepwise ionization is an interaction with high importance in the prediction of the behaviour of plasma with high density of electrons and excited neutrals. In this case, the contribution of this collision can be easily implemented as it is easily compared with that one of direct electron impact ionization. Specifically, when modelling such interactions with rate coefficients (which is preferable for the hybrid/PIC code), the ratio between both rates follows the approximated formula [2]:

$$\frac{k_i^s(T_e)}{k_i(T_e)} \approx \left(\frac{I}{T_e}\right)^{\frac{7}{2}} \tag{3.17}$$

where $k_i^s(T_e)$ and $k_i(T_e)$ are the rate coefficient functions of the stepwise and direct ionization by electron impact respectively, I is the ionization energy of the specie, and T_e the velocity (expressed as energy) of the electrons flow.

3.1.3. Indirect Ionization or Autoionization

Autoinization processes result from the excitation of a particles' core electron into an intermediate high energy state which subsequently decays and an electron or electrons are released. Even though this type of collisions is highly relevant in hot dense plasma, in rare occasions it may be present in cold plasma with a low density of ions [25]. Then, just a brief introduction for this type of collisions will be provided to transmit the basic knowledge for a case that, although extremely improbable, may be possible.

This type of indirect ionization can be classified as "non-resonant" and "resonant"[37] depending on the result of the first interaction. Within non-resonant processes, a first collision with an electron provokes the excitation of an inner-shell electron or directly its ionization. In the former situation, *Excitation-autoionizaton* (EA), the exothermic deexcitation will result in the release of an outer electron and, thus, the ionization of the atom. In the latter, *Ionization-autoionization* (IA), the "hole" created by the ionized electron is filled by one of the outer electrons and, thus, the atom becomes ionized.

Oppositely to non-resonant processes, resonant interactions are characterized by the capture of the first striking electron at the same time that an inner-shell electron gets excited. Depending on the decay mechanism to the final ionized atom, the process is defined as: *Resonant-Excitation-Double-Autoionization* (REDA), where the atom experiences two subsequent deexcitation processes; and *Resonant-Excitation-Auto-Double-Ionization* (READI), in which two electrons are simultaneously emitted in the decay process.

This type of indirect autoionization are complex to predict due to the subsequent steps that take place and the inherent properties for each specie that dictate the decay process and rate.

3.1.4. Ionization by Collision between Heavy Particles

Oppositely than with electrons, in ionization processes through collision between heavy particles, ions and neutrals, even if these have the sufficient kinetic energy, they cannot ionize the striking particle due to the fact that their velocities are much lower than those of electrons in electron impact ionization processes [2]. That is, even if the particle has the enough energy, due to its reduced velocity it will not be able to transferred the required energy for the ionization of the partner particle.

Nevertheless, the situation is much different when the heavy particles are electronically excited. If the colliding heavy particles have a total electron excitation energy close to the ionization potential of one of such particles, the resonant energy transfer and effective ionization may occur. Two specific examples are used to illustrate these non-adiabatic ionization processes: the *Penning ionization* effect and the *Associative ionization*.

Penning ionization:

The Penning ionization may result from the collision of a stable excited atom A*, a metastable atom; and another atom B, whenever the electron excitation energy of the metastable A* exceeds the ionization potential of the atom B. Thus, this type of process usually takes place through the intermediate generation of unstable excited quasi molecules.

The ionization cross sections of this type of ionization are very high. For example, its contribution to the total kinetics of plasma generation is significant ($O(10^{-18})m^2$) when the following pair of highly excited metastable species are present (Element("excitation energy")): Ne(16.6eV), He(2^3S, $19.8eV$)[2].

Associative ionization:

This process follows the same principle of the Penning ionization, but in this case, the stability of the intermediate excited quasi molecule is different. Associative ionization occurs when the total electron excitation energy of the colliding particles is lower than the ionization potential of any of the particles. In such case, the heavy species stick together as a molecular ion whose bonding energy contributes to the ionization process. In other words, the sum of the electron excitation energy of both particles is lower than the ionization potential of any of such particles separately, but exceeds the ionization potential of the molecule formed by the particles and, consequently, the collision results in the ionized molecule:

$$A^{\star} + B \rightarrow AB^{+} + e^{-} \tag{3.18}$$

Similar to Penning ionization, associative ionization cross sections might be quite high.

Despite the notorious values that the cross section may adopt for these collisions with heavy particles, this type of interactions are more relevant in plasma isolated from electric

fields [2]. Combining this with the fact that the current hybrid/PIC codes simulate an uniquely element species (combination of different propellant are not being simulated), the cross sections of this type of collisions will not be required to be implemented.

3.1.5. Radiative Ionization or Photoionization

Apart from collisional ionization processes, ionization may also occur through the interaction with high energy photons [2]. In its basis, the photoionization process of a neutral particle A, with ionization potential $I[eV]$,through the interaction with a photon, ω, with wavelength λ may be treated depicted as (the energy of the photon is identified as $\hbar\omega$, and satisfies the relation $\hbar\omega = \hbar\frac{2\pi c}{\lambda}$ [1]):

$$\hbar\omega + A \longrightarrow A^+ + e^-, \quad \lambda < \frac{12,400}{I(eV)}$$

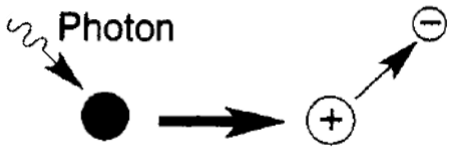

Fig. 3.5. Radiative ionization

To ionize a ground state atom, usually the photon wavelength should belong to the ultraviolet range, that is $\lambda < 1000$Å. However, in the case the photon strikes a previously excited atom or molecule, the effective ionization of such may be obtained with lower photon energies and longer electromagnetic waves.

Despite the high value cross sections shown for photoionization, the photoionization contribution to most of the total ionization process is usually insignificant due to the low concentration of high energy photons. Still, there are a few of situations where this process plays an important role as a source of new seed electrons for further ionization by electron impact. It is the case of the following discharge processes[2]:

- "Streamer propagation in nonthermal discharges, where photoionization supplies seed electrons to start electron avalanches".
- " Propagation of nonthermal and thermal discharges in fast flow (including supersonic flow) where the rest of propagation discharges are too slow".
- "Non-self-sustained discharges where the ultraviolet radiation replaces the relativistic electron beams" to pre-ionize the gas.

These situations, however, are not of special relevance in the simulations performed by hybrid/PIC codes and, thus, the collision cross section do not need to be provided. Nevertheless, as it will be introduced in next section, photon collisions should be also accounted in some plasma in relation with *radiative recombination*, which releases photons that my lead to undesirable or unexpected further ionization reactions.

3.2. PLASMA RECOMBINATION PROCESSES

Together with all the interactions presented in the previous section, which describe the generation of ions and free electrons (plasma generation), there exist a variety of other types of interactions which produce the absorption of the free charged particles the characterize plasma ("loss" of ions). That is, this last type of interactions provoke the recombination of the plasma.

The final degree of ionization of the plasma is a balance between the ionization collisions (source of charged particles) and the charge-loss interactions (sink of charged particles). Then, it is highly important to have a basis of the different types of interactions that may result in the lowering of the ion-density in the plasma. In a general approach, these processes may be classified in terms of the channel through which the charged particle is recombined [1], [2]:

- **Electron-Ion Recombination:** Exothermic collisions between charged particles that result in their mutual neutralization. Three main electron-ion recombination processes are matter of study:
  - Dissociative electron-ion recombination
  - Three-body electron-ion recombination
  - Radiative electron-ion recombination
- **Ion-Ion Recombination:** The decrease of the plasma ionization degree results from the neutralization of a positive ion through the collision with a negative ion. At the same time, the latter type of ions have appeared from the attachment of electrons to a neutral atom. Consequently, the density of free electrons in the flow is also reduced, with the respective influence in the collisions involving free electrons.

  Even though this interaction requires two different species and the destination codes of this study consider just one propellant, a description of this type of collision will be provided to serve as a first contact with a potential step forward in the research: the simulation of mixing propellants.
- **Surface Recombination:** In a similar way than the surface ionization, plasma charged particles may be reduced through the interaction with the walls of the container, usually in the form of diffusion. Alike its ionization partner process, this

thesis focuses on the collisions appearing from an isolated plasma volume, so surface recombination cross sections would be a further expansion of the current study.

3.2.1. Electron-Ion Recombination

As just introduced, electron-ion recombination collisions lead to the neutralization of two charged particles through a highly exothermic process. Indeed, the released energy during the collision corresponds to the ionization potential of the neutralized specie. This is a good estimator of the amount of energy released, as usually the order of magnitude of the ionization energy of common plasma propellants studied is of several electron-volts. The mechanisms through which this energy is absorbed by the systems clearly differentiates three main types of processes: *Dissociative, Three-body* and *Radiative*.

3.2.1.1 Dissociative electron-ion recombination

$$AB^+ + e^- \rightarrow (AB)^\star \rightarrow A + B^\star \tag{3.19}$$

As formulated, the energy is guided into a resonance process that results in the dissociation of the molecular ion and the following excitation of, at least, one of the products. Along the process, and intermediate excitation state of the complete molecule is present. This state is defined as a "repulsive autoionization" level of the molecular ion, The dissociation takes place when this autoionization state is maintained as the neighbour atoms travel apart on the repulsive term.

This reaction is the fastest recombination process within molecular plasma (with relevant presence of molecular ions). with rate coefficients inversely proportional to the electron and gas temperatures (and, thus, energies) as expressed in Equation 3.20[2].

$$k_r^{ei}(T_e, T_0) \propto \frac{1}{T_0 \sqrt{T_e}} \tag{3.20}$$

Then, these collisions are important in the range of energies studied in this thesis (<30 eV) and should be accounted if molecules are present in the system.

3.2.1.2 Three-body electron-ion recombination

$$A^+ + e + e \rightarrow A^\star + e \tag{3.21}$$

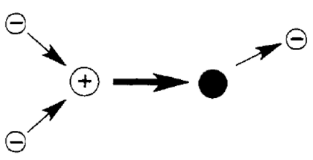

Fig. 3.6. Three body recombination

In this recombination reaction, the released energy is directed towards increasing the kinetic energy of the resulting free electron, the so called “third body”. Concerning the complete description of the process, the collision of two electrons with a positive ion passes through the capture of one of those electrons by the ion, and the released energy being transferred to the remaining electron[2]. Notice that this process behaves as the inverse reaction for the direct electron impact ionization collision.

The three body recombination is the most relevant plasma recombination process in high density equilibrium plasma of total temperature in the order if $1eV$. It is desirable to provide a measurement of the collision as a reaction rate coefficient, accounting for the three-body property of the system, writes

$$k_r^{eei} = \frac{\sigma_0}{I}\left(\frac{I}{T_e}\right)^{4.5} 10^{-}14 \quad \{\frac{cm^6}{s}\} \tag{3.22}$$

Paying attention to the previous formula, the consideration of the involvement of the three particles is present in the units of the coefficient, accounting for the three-dimensional space of each of the two “two-body" problems (2x[Ion-electron]), resulting in a rate units of cm^6/sec.

3.2.1.3 Radiative electron-ion recombination

$$A^+ + e^- \rightarrow A^\star \rightarrow A + \hbar\omega \tag{3.23}$$

Fig. 3.7. Radiative recombination [1]

Being introduced at the end of the ionization collisions, the radiative electron-ion recombination behaves as the inverse reaction to the photoionization. In the recombination interaction, the free electron interacting with the positive ion is absorved by the latter, which gets highly excited. Then, the relaxation of the excited atom release a high amount of energy in the form of a photon. Due to the requirement of a photon emission, this process is relatively slow. Nonetheless, it may be an outstanding role in the balance of charged plasma particles when the plasma density is low and no molecular ions are present.

Even though this interaction leads to moderate cross sections in the aforementioned plasma, of the order of $10^{-21}cm^2$, it has low influence for the plasma being considered by the hybrid codes, in the same way that happened with its ionization conjugate process.

3.2.2. Ion-Ion Recombination

Ion-ion recombination stands as the prime cause of plasma recombination due to electron attachment processes to neutrals becoming negative ions. These negative charges neutralizes the positive ions characteristic of the plasma. The collision rate coefficients associated with these interactions are generally high, independently of the environmental conditions at which the plasma is studied, as shown by Figure 3.8. Indeed, different ion-ion recombination mechanisms are dominant in different pressure ranges [2].

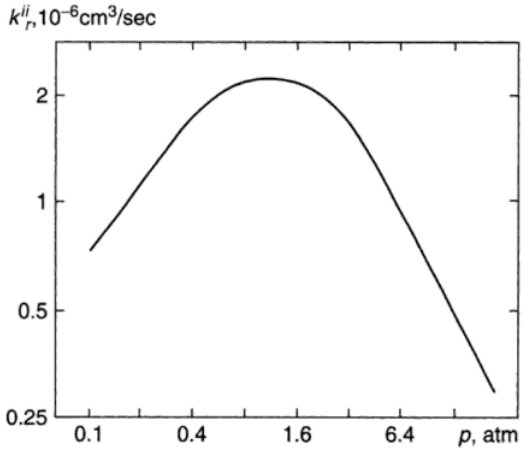

Fig. 3.8. Ion-ion recombination rate dependence with pressure [2]

For the purpose of the hybrid codes for which this thesis is performed, pressure ranges near vacuum will be the ones to be considered . This is coherent, as the real conditions in which the final devices operate in space correspond to vacuum pressure levels, lower than $5 \cdot 10^{-5} mbar$[38]. In these range of pressures, the mechanisms of plasma recombination that predominate correspond to binary ion-ion collisions [2], where the transferred energy lead to electronic excitation of one of the species:

$$A^- + B^+ \rightarrow A + B^\star \tag{3.24}$$

In a first approach, the interaction of the two ions can be treated as a Coulomb attraction, explained in Chapter 2. When the two heavy particles are far away from each other, the Coulomb potential is lower than the difference in potential of the colliding ions ($A^- - B^+$, corresponding to the electron affinity of particle A: EA_A), and greater than the resultant potential difference ($A - B^\star \simeq \frac{I_B}{n}$, where I is the ionization potential of particle B and n its principal quantum number after recombination). So, the Coulomb energy at the approaching phase may be approximated to be in the range

$$\Delta E \approx \frac{I_B}{n^2} - EA_A \tag{3.25}$$

From this expression, it is observed that if the principal quantum number is known

to be low, the electronic terms of the reactants and the products are close during the approaching phase. However, this parameter is usually unknown, so the energy range is usually approximated to the electron affinity: $\Delta E \sim EA_A$

At the same time, the high reaction rates of dominant in ion-ion recombination processes, as provided in Figure 3.8, indicate that the reaction is prompt to take place even when the ions are still at large distances, R_{ii}. Consequently, the Coulomb attraction, even at large distance, is sufficient to compensate for the required ΔE. Then:

$$R_{ii} \approx \frac{e^2}{4\pi\epsilon_0} \frac{1}{\left(\frac{I_B}{n^2} - EA_A\right)} \approx \frac{e^2}{4\pi\epsilon_0 EA_A} \sim \tag{3.26}$$

The cross section can be then computed from the conservation of angular momentum in the hyperbolic Coulomb trajectory and through its impact parameter, b, which is proportional to the kinetic energy ε in the center of mass of the system:

$$b \approx R_{ii} \frac{\sqrt{EA_A}}{\sqrt{\varepsilon}} \tag{3.27}$$

This results in the recombination cross section as:

$$\sigma_{rec}^{ii} = \pi b^2 \approx \pi \frac{e^4}{(4\pi\epsilon_0)^2} \frac{1}{EA_A} \frac{1}{\varepsilon} \tag{3.28}$$

Nonetheless, there is still one effect that must be accounted in the recombination cross section. It is the case of quantum electron tunneling [39], which provide and additional dependence on the kinetic energy in the form

$$\sigma_{rec}^{ii} \propto \frac{1}{\sqrt{\varepsilon}} \tag{3.29}$$

and leads to the final ion-ion recombination cross section:

$$\sigma_{rec}^{ii} \approx \sigma_0 \frac{I}{EA_A} \frac{I}{\varepsilon} \quad \text{where } \sigma_0 = \frac{1}{(4\pi\epsilon_0)^2} \frac{\pi e^4}{I^2} \tag{3.30}$$

3.3. CHARGE EXCHANGE COLLISIONS

In its most basic formulation, during a charge exchange interaction an energetic ion absorbs an electron of a cold (less energetic) neutral, which adopts the energy levels of the previous ion and this one the energy levels of the initial cold neutral.

$$A^+ + B \rightarrow A + B^+ \tag{3.31}$$

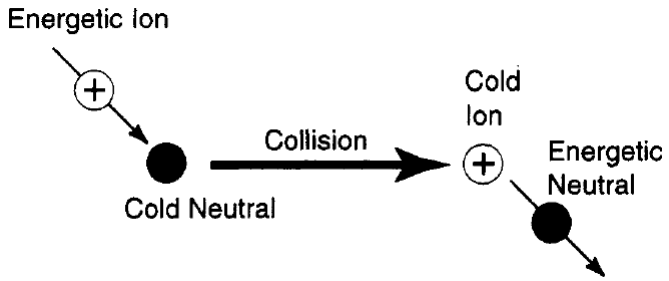

Fig. 3.9. Charge transfer/exchange collision [1]

These interactions are responsible for the presence of any neutral in the center of a dense plasma. Furthermore, the high cross section values ($O(10^{-19})m^2$) [1] indicate a very low probability of having a hot-ion plasma with an appreciable neutral-gas density in its interior. Ions rapidly turn into energetic neutrals, which allows them to travel larger distances into the plasma volume. Chain reactions of consecutive charge exchange interactions may occur, which lead to successively higher energized neutrals that, in the end, are able to escape the plasma volume. Due to this effect, this reactions a highly important in the simulations in near-plume regions as they lead to back-flow of plasma against the satellite [40], as represented in Figure 3.10.

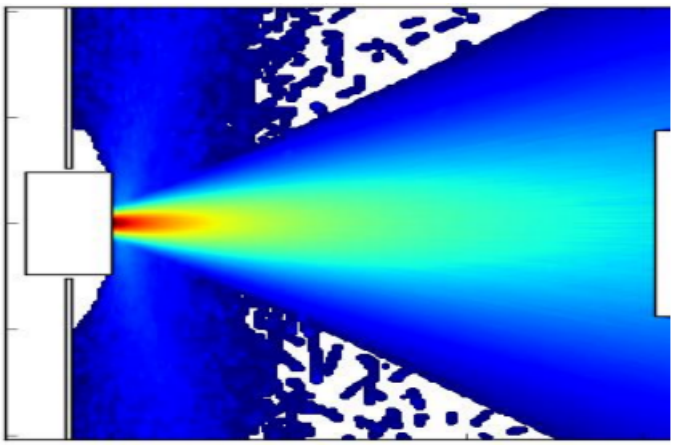

Fig. 3.10. Near-plume region back flow due to charge exchange interactions [40]

Similar to ion-ion recombination, quantum effects are present in charge exchange interactions. These allow to make a subdivision into *resonant* processes, whose initial and final quantum mechanical states have the same energy; and *non resonant* charge transfer processes. However, the interest is primarily set in the former, as they present much higher cross sectional values and, thus, are much more probable to take place.

To obtain a preliminary theoretical value for the cross section, the Coulomb energy potential of the transferred electron is constricted in the the coulomb field of A^+ and B^+

[2]:

$$U(z) = -\frac{e^2}{4\pi\epsilon_0 z} - \frac{e^2}{4\pi\epsilon\,|r_{AB} - z|} \tag{3.32}$$

where z is the electron distance from the center of the coulomb system and r_{AB} the distance between the colliding particles.

In the framework of classical mechanics, Equation 3.32 is constrained with the upper limit of the initial energy E_B required to transfer the electron from the n energetic level. So

$$E_B = -\frac{I_B}{n^2} - \frac{e^2}{4\pi\epsilon_0 r_{AB}} \geq U_{max} = -\frac{e^2}{\pi\epsilon_0 r_{AB}} \tag{3.33}$$

which allows to obtain the maximum distance at with the reaction will take place:

$$r_{AB}^{max} = \frac{3e^2n^2}{4\pi\epsilon_0 I_B} \tag{3.34}$$

Then, the classical reaction cross section is obtain through the idealization [2]

$$\sigma_{ch.ex}^{class} = \pi(r_{AB}^{max})^2 = \frac{9e^4n^4}{16\pi\epsilon^2 I_B^2} \tag{3.35}$$

Nevertheless, quantum effects, specifically electron tunneling, result in a total charge exchange cross section much higher than the results derived from Equation 3.35.

The accounting for electron tunneling [39] requires the analysis of an additional cross section that expresses such effect. The derivation of this added cross section is a function of the relative velocity of the colliding partners (v), the potential barrier height ($\sim I_B$) and width ("d"). Final estimations of this parameter take the form

$$\sigma_{ch.ex}^{tunn} \approx \frac{1}{I_B}\left(\frac{\pi\hbar}{8me}\right)\left(ln\left(\frac{I_B d}{\hbar}\right) - ln(v)\right)^2 \tag{3.36}$$

$$\approx \frac{1}{I_B[eV]}\left(6.5\cdot 10^{-7} - 3\cdot 10^{-8} ln(v)[cm/s]\right)^2 \tag{3.37}$$

Due to the high complexity of the previous derivation, a multitude of different approaches with fitting equations have appeared, resulting in proposed general expression in terms of constants whose value changes for each specie [41]–[44].

4. DATABASE GENERATION

Up to this moment, a simplified background of all the collision reactions has been provided, as well as the identification of those relevant for the objective of this thesis. In addition, several developments and methodologies to measure the cross section of these processes were explained. Now, it is the time to design the storing method that shall be used to gather the collision cross sections of all the process and from which the hybrid/PIC codes will extract the required information for their computations.

4.1. Database Structure

The database to be generate will be storing the different collision information of not just one type of interaction, but as much relevant interactions as possible and the maximum amount of species combinations. The information must contain data of different types of ionization reactions, excitation processes, charge exchange collisions ... between different particles, elements and molecules.

With all the different combinations that must be stored, it is essential to design a simple but efficient organization system. The simplest organization model allowing a quick informative view of the data is a table, in which the data of each box is related to the corresponding column and row header. For the purpose of this database, the simplest way to classify the rows and columns is in terms of the colliding species. Then, each row and each column of the table will correspond to a specific specie, and the intersection cell will collect the information of a collision between such species. Additionally, if the row and column species are set to be equal, the table is simplified to half of it, avoiding cells with redundant information. A preliminary example of this organization is presented for Xenon in Figure 4.1

BINARY	e^-	Xe	Xe*	Xe^+
e^-	$e^- + e^-$	$e^- + Xe$	$e^- + Xe^*$	$e^- + Xe^+$
Xe		Xe + Xe	Xe + Xe*	$Xe + Xe^+$
Xe*			Xe* + Xe*	$Xe^* + Xe^+$
Xe^+				$Xe^+ + Xe^+$

Fig. 4.1. Database preliminary organization model

Once the general style has been set, the next step is to design a sorting system that enables a coherent organization within one specie. This chosen system must work with all the species to be included in the database to make it a simple as possible. The easiest and most understandable way to sort the different states within the same specie is by the increase of energy/charge level. Following this model, the first element to appear

will be the most negatively charged specie and the last one the most positive particle. As the elementary negative charge particle, the electron will remain as the first element, corresponding to the upper left corner in the graphical representation of the database. Notice that if there are multiple excitation or ionization levels within one specie, they will also be sorted in terms of charge. The simple case presented in Figure 4.1 is then expanded as depicted in Figure 4.2

BINARY	e^-	Xe (4d10 5s2 5p6)	Xe* (5p5 5d)	Xe* (5p5 7s)	Xe* (6s 6p)	Xe^+ (4d10 5s2 5p5)	Xe^{++} (4d10 5s2 5p4)
e^-	$e^- + e^-$	$e^- + Xe$	$e^- + Xe^*(...)$	$e^- + Xe^*(...)$	$e^- + Xe^*(...)$	$e^- + Xe^+$	$e^- + Xe^{++}$
Xe (4d10 5s2 5p6)		Xe + Xe	Xe + Xe*(...)	Xe + Xe*(...)	Xe + Xe*(...)	$Xe + Xe^+$	$Xe + Xe^{++}$
Xe* (5p5 5d)			Xe*(...) + Xe*(...)	Xe*(...) + Xe*(...)	Xe*(...) + Xe*(...)	$Xe^*(...) + Xe^+$	$Xe^* + Xe^{++}$
Xe* (5p5 7s)				Xe*(...) + Xe*(...)	Xe*(...) + Xe*(...)	$Xe^*(...) + Xe^+$	$Xe^* + Xe^{++}$
Xe* (6s 6p)					Xe*(...) + Xe*(...)	$Xe^*(...) + Xe^+$	$Xe^* + Xe^{++}$
Xe^+ (4d10 5s2 5p5)						$Xe^+ + Xe^+$	$Xe^+ + Xe^{++}$
Xe^{++} (4d10 5s2 5p4)							$Xe^{++} + Xe^{++}$

Fig. 4.2. Organization model implementing the sorting by energy level

When more species want to be added to the database, another sorting method must be implemented to allow grouping all the collisions of particles belonging to the same specie. The most universal way is to sort the elements in alphabetical order. However, the electron collision shall remain in the first location due to the importance of the collisions involving it. Electron collisions are one of the most common and present interactions in plasma and, maintaining its first location on the database will allow a quick check of the interactions that are already stored in the database. A simple result of this structure is depicted in Figure 4.3, which includes Xenon, Kripton and Argon collisions.

BINARY	e^-	Ar	Ar*	Ar^+	Kr	Kr*	Kr^+	Xe	Xe*	Xe^+
e^-	$e^- + e^-$	$e^- + Ar$	$e^- + Ar^*$	$e^- + Ar^+$	$e^- + Kr$	$e^- + Kr^*$	$e^- + Kr^+$	$e^- + Xe$	$e^- + Xe^*$	$e^- + Xe^+$
Ar		Ar + Ar	Ar + Ar*	$Ar + Ar^+$	Ar + Kr	Ar + Kr*	$Ar + Kr^+$	Ar + Xe	Ar + Xe*	$Ar + Xe^+$
Ar*			Ar* + Ar*	$Ar^* + Ar^+$	Ar* + Kr	Ar* + Kr*	$Ar^* + Kr^+$	Ar* + Xe	Ar* + Xe*	$Ar^* + Xe^+$
Ar^+				$Ar^+ + Ar^+$	$Ar^+ + Kr$	$Ar^+ + Kr^*$	$Ar^+ + Ar^+$	$Ar^+ + Xe$	$Ar^+ + Xe^*$	$Ar^+ + Xe^+$
Kr					Kr + Kr	Kr + Kr*	$Kr + Kr^+$	Kr + Xe	Kr + Xe*	$Kr + Xe^+$
Kr*						Kr* + Kr*	$Kr^* + Kr^+$	Kr* + Xe	Kr* + Xe*	$Kr^* + Xe^+$
Kr^+							$Kr^- + Kr^+$	$Kr^+ + Xe$	$Kr^+ + Xe^*$	$Kr^+ + Xe^+$
Xe								Xe + Xe	Xe + Xe*	$Xe + Xe^+$
Xe*									Xe* + Xe*	$Xe^* + Xe^+$
Xe^+										$Xe^+ + Xe^+$

Fig. 4.3. Organization model for binary collision processes

Each of the cells presented in the database will have an inner division corresponding

to the different collision processes that are being included in the database and the source from where it has been extracted or computed. In the same way as the species division previously commented, this one will be appearing as the database is being filled. An sketch of a suggested resultant divisions after the inclusion of some cross sections is provided in Figure 4.4. It is obvious that, as depicted, there will be a different inner division in different pairs of colliding partners as some collision are more probable between some reactants than others.

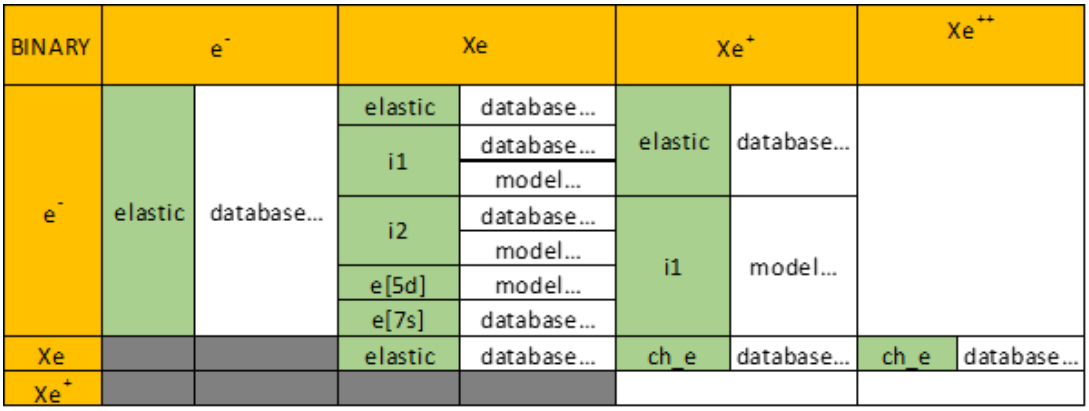

Fig. 4.4. Database structure within different collision partners

In the example just provided, it is regarded that reactive couple for which more collision cross sections have been stored is the electron impact collision "$e^- + Xe$". As it has been explained in previous chapters, each collision cross section is a measure of the probabilities of such outcome to occur and, the more information stored, the more accurate the result will be. On the other hand, no data has been included for the colliding particles "$e^- + Xe^{++}$", "$Xe^+ + Xe^+$" and "$Xe^+ + Xe^{++}$", perhaps due to the negligible effect that their outcome could derive. As remarked, this database is specifically created for hybrid/PIC codes, so it will uniquely gather relevant collisions for such codes. Figure 4.4 also provides the source of the data, which is either a database or a model, such as those introduced in Chapter 3. Furthermore, it is clear that most of the names of each type of collision are shortened (i1, e[...], ch_e...), fact that leads to the next step in the database design: the actual creation of the database.

However, so far only binary collisions have been organized. Unary reactions (such as spontaneous decay of excited atoms) must be also provided, specifically the de-excitation rate of different species. This one is an indispensable parameter in reactions such as stepwise ionization (because it provides an estimation of the survival time of the pre-excited atom) and thus, it should be collected in the database. For this type of reactions, a simpler structure is possible as it is an inherent property of the specie. Then, a simple column table in which each row corresponds to a different specie, as the one suggested in Figure 4.5, will be sufficient to store this information. Ancillary data such as mass, atomic number, ... may be also stored in this file as depicted in the mentioned figure (would correspond to the "specie_info.txt" file). As a final remark, to make this information

easily accessible, the columns must be ordered alphabetically like in the case of binary collisions.

UNARY			
Ar	specie_info.txt	de_ex	database...
Kr	specie_info.txt	de_ex	article...
Ne	specie_info.txt	de_ex	model...
Xe	specie_info.txt	de_ex	database...
...	...	...	...

Fig. 4.5. Database structure for unitary processes

4.2. Database Generation: Folders and Nomenclature

The idea of how the database aims to look has been established. Next step consists in physically generate the database. For such purpose a set of rules and nomenclatures are set to ensure its proper operation.

The database must allow an easy access for the codes. The easiest way to ensure this condition is by simply generating the designed structure in a personal directory. That is, the database itself is developed as a "tree" of folders seeded in a specific directory. This simple built-in allows to have an easy access to any of the information stored. Moreover, the organization established in the previous section has to be built in the folder structure in such a way that allows an easy identification and access to the information. This is achieved in the following way:

1. Concerning a couple of colliding particles, if they belong to the same specie, the specie with more negative charge is located at a higher level than the more positively charged particle. For example, if the information wants to be extracted from a "$Xe[5p5\ 5d] + Xe^{+}$", the directory root will appear as "`...\Xe[5p5_5d]\Xe+\...`". Otherwise, the species are ordered alphabetically as previously commented, resulting in paths such as "`...\Kr+\Xe\...`". However, as stated before, all the collisions by electron impact are of primary relevance and remain in the first location, as showed in Figure 4.3. Then, whenever an electron is one of the colliding particles, its will be located at a higher lever and the root will appear as "`...\e-\anyotherparticle\...`". On the other hand, unary reactions do not involve two particles and, thus, the appearance of the directory root will be alike "`...\Xe\...`".

   Due to the expanding character of the database, it is essential to follow a strict criteria around the label of the various species and states:

   - The electron is labelled as: e-

- The identification of all the species is done in terms of their nomenclature in the periodic table with the first letter in upper case style. Examples: Ar, Kr, Xe, O, I, ...
- Whenever the specie is excited, right after the identification is written between square brackets the electronic configuration of the last valence layer, making use of "_" to separate energy levels. Examples: Xe[5p5_5d], Xe[6s_6p], ...
- Whenever the specie is ionized, right after the identification is provided the sign of the charge and the number of charges. Examples: Xe+1, Xe+2, Kr+1,...
- As stated, if the colliding particles belong to the same specie, the most negatively charged one is first identified. Examples: Xe\Xe+, Xe[5p5_5d]\Xe+2,...
- As stated, if the colliding particles belong to different species, the are called in alphabetic order. Examples: Xe\Kr, Ar\Xe,...
- Whenever the collision is due to electron impact, the electron shall be called first. Examples: e-\Xe, e-\Kr+2,...

Notice that all the root paths provided above as examples follow the just mentioned criteria.

2. Inside the path of folders of the collision couple, the different interactions are identified with the following criteria (regard that the labelling must be exactly as provide, including upper case or lower case letters):

   - **i1** Ionization reaction of one electron. That is, both of the following ionization processes will be identified by "i1": Xe→Xe+1, Xe+1→Xe+2
   - **i2** Ionization reaction of two electrons, as it is the reactions Xe→Xe+2
   - **e[...]** Excitation of the particle. The highest level of the final electronic configuration of the excited electron is described inside the square brackets, making use of "_" to separate energy levels. Examples: e[7s], e[6s_6p],...
   - **elastic** Elastic collision between the colliding particles. No distinction is made between coulomb collisions and pure elastic ones as they are complementary.
   - **ch_e** Charge exchange.
   - **de_ex** De-excitation rate.

3. To identify the source of the information, the files stored in the folder identified with the just mentioned criteria must follow as well a label structure. Again, special attention must be paid to upper and lower case characters:

   - **source_NAMEOFTHESOURCE** The data source can be a database or a mathematical model. Some examples of data file names are:
     - **database_NIFS**

  - **database_LXCAT**
  - **model_DRAWIN**
  - **model_GRYZINSKI**
  - **article_TITLEOFARTICLEWITHOUTSPACES**
- The file containing the ancillary data shall be named **specie_info**, as represented in Figure 4.6

The properties composing the file itself are discussed in the following section as do not influence the structure of the database.

4. In the previous points it was fixed the nomenclature and structure of the lower levels, which identified the pair of colliding species (or the isolated specie in case of unitary processes), the type of reaction for which the data is introduced, and the labeling of the file containing the data. However it is still needed to provide a differentiation between binary and unary processes, as the number of involved particles has required different amount of structure requisites:

   - The folder **UNARY** will contain all the unary processes gathered. Inside this folder, the secondary folders are sorted alphabetically to provide an easy and helpful organization. For example, the final root path of a file containing the de-excitation rate of the Kripton element will be

     `...\DATABASE\UNARY\Kr\de_ex\database_LXCAT.txt`

     Moreover, the file "specie_info" will be stored at the same level as folders like "de_ex" to avoid confusion in the roots of files that actually contain primary information. This is clearly exemplified in Figure 4.6.
   - The folder **BINARY** will contain all the cross sections related to binary collision processes. Inside this folder, the first sub-folder must be the one containing electron impact collisions, **e-**. The rest of the sub-folders are in alphabetic order. Then, the root path of a file containing the first ionization cross section by electron impact for Argon may be similar to

     `...\DATABASE\BINARY\e-\Ar\i1\model_DRAWIN.txt`

As it is shown in the previous paths, the entire database is stored in one file, called **DATABASE**. A sample sketch of the appearance of this "tree" is depicted in Figure4.6. Some advantages of storing the database this way is the easiness to be saved, modified and shared from any computer. Even old versions can be shared and used while it is being upgraded elsewhere. This, however, introduces the disadvantage that if it is upgraded, the old version will not automatically update and the most complete version must be forwarded. Nevertheless, the best advantage provided by this storage method is the ability to be open with any code language being used by the user. Only a command line to read the file being stored in a specific path is necessary, without the need of downloading packages or specific software.

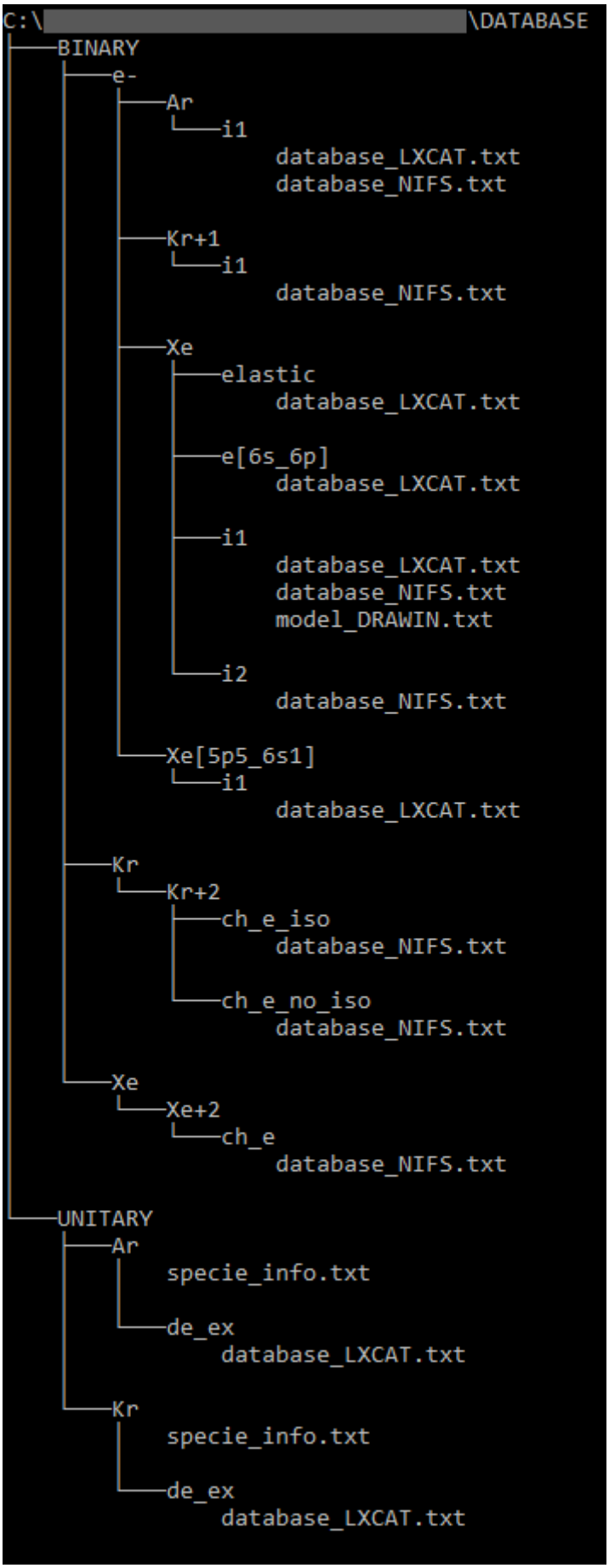

Fig. 4.6. Directories “tree" appearance of the database structure

4.3. Data Document File Format

All the designed work performed until this point has been focused on providing an easy access to the data. A second selection must be carried now concerning the easy reading and understanding of the cross section data. The best approach is to write the cross section data in the most universal format and the most efficient language as possible.

Regarding the file extension in which the parameters will be written, the best option is to use to the worldwide extended ".txt" format. These are the simplest data storage documents and are easily editable with a wide variety of programs, most of which come already installed in any computer or are freely available, such as Notepad and Notepad++. The database can be then expanded by a future user with a simple text editor and following the delivery style and language criteria later explained. Moreover, ".txt" files can be opened and read by any coding language with a simple command, which allows the database to be used by a wide variety of codes regardless of their programming environment.

The content layout and the writing style are chosen taking into account that the file will be opened and read by a variety of codes. For such purpose, the "YAML" writing standard was selected due to the easiness with which it is read by the variety of coding environment (in the study case, Python was used) Additionally, apart from the obvious information like the cross section data and the reference, they must provided some clue parameters to indicated the codes how to handle the data. For example, it is not handled in the same way the information provided by a database, which is a set of energies and corresponding cross sections; than the fitting constants of a Mathematical model, which must be latter transformed into the set of energies and associated cross sections. While the codes will be later explained, the structure and language format are now presented, being exemplified at the end of this section in Figure 4.7

4.3.1. Document content and layout

For the ease and simplicity of further work, all the delivery documents must provide the maximum amount of information in the best reading structure. The organization and contents that must be followed in the ".txt" file are the following:

1. **TYPE**: First and foremost, it must be exposed what type of information is being provided, whether it was downloaded from another database or where computed from a mathematical model. As it is a clue parameter for the proper performance of the codes, the possible options here must be:
    - **Database** indicates the set of data was retrieved from an external database.
    - **model-Nameofthemodel** indicates the model to which the parameters belong. Examples: **model-Drawin**, **model-Grazynski**,...
2. **SOURCE**: The origin of the information must be given if it was downloaded from

another database, indicating the name of such source and its URL. For example: “LXCAT DATABASE: `https://nl.lxcat.net/data/set_type.php`. This point may be skipped when the cross sections are computed from a model.

3. **RETRIEVAL DATE**: Introduced in European style (d/m/y). This will provide an estimation of the level of update of the cross section in the database.

4. **ORIGINAL REFERENCE**: While the “SOURCE" section just provides the name of a the origin, in this section must be indicated the complete original reference and necessary information to go with it. Usually, the data already stored in external databases has been provided by specific companies, institutions, specific software and even other databases. These first providers must be referenced in this section. Some examples:

   «Syage, J.A., Electron-impact cross sections for multiple ionization of Kr and Xe., Phys. Rev. A, vol. 46 pp 5666, 1992»

   «Biagi-v7.1 (Magboltz version 7.1),
   www.lxcat.net/Biagi-v7.1,
   COPYRIGHT 2004 STEPHEN FRANCIS BIAGI, Cross sections extracted from PROGRAM MAGBOLTZ, VERSION 7.1 JUNE 2004»

5. **COMMENTS**: In this section it is gather all the relevant information relative to the collision process that is being treated, such as the description of the reaction, the particles involved, the charge state and electronic configuration of the both, reactant and products, the method used to measure the cross sections, the number of measurements provided, the scope of energies covered by the measurements, ... If the data belongs to a specific mathematical model, as the example provided in Appendix A, the description of such model as well as the meaning of each of its parameters is provided in this section.

6. **DATA**: The last section of the file contains the actual parameters to be used by the codes. Together with the values, the units must be indicated. In the case of data retrieved from a database, the information in divided in two sections, one for energy values and the second one with the associated cross sections, including their units. The cross sections introduced in this file must be “differential cross sections”. These will be later integrated over the energy distribution being considered by the user codes, such as a Maxwellian distribution.

   If the parameters provided belong to a specific model, there is a subsection for each parameter, indicating its value and units as provided by Appendix A

Oppositely to the primary files, that must contained the mentioned sections, ancillary files may contain any type of extra information believed to be useful by the user. However, to maintain the same format and be able to be read by the codes, each new information shall be introduced as a new section and following the required writing standard as explained in next section.

4.3.2. Document standard: YAML

The writing environment and syntax in which these files are developed must comply with to requirements:

1. As previously commented, the codes must be able to read, extract and store all the information in the most efficient way. The aim of this thesis is to provide cross section values for hybrid/PIC codes written in PYTHON. Then, an efficient procedure would be to deliver the content in the form of a Python "dictionary" structure, which allows a clear differentiation between the sections and a quick retrieval of the parameters knowing its classification.

2. For the ease of writing the file, it is preferable to use a writing format allows users with none programming skills to build these documents. That is, the writing syntax should be the closest to the quotidian one.

With this requirements, the best option is to use "YAML" syntax. YAML. "YAML Ain't Markup Language", a "human friendly data serialization standard for all programming languages" [45], [46]. That is, this style is understood by a wide variety of programming languages and has a high resemblance with daily syntax. In addition, this format allows to write its content in such a way that, when opened by programming codes, it is directly organized in the desired dictionary configuration. There is no need to implement special key characters, words or lines that separate content, usually used when the entire file is read line by line searching for a key that tells it when to do a specific action. To do so there are variety of rules to and nuances to consider. Together with the fact that the writing style must ensure the proper compilation of the codes, the following criteria describing the writing procedure must be fulfilled:

- In Python, the dictionary structures are contained between curly bracket "{}"" and contain a key section and a value section, separated by a colon followed by a space. The key is the name of the section, so when a value wants to be extracted, the command makes reference to its key. Value sections can contain strings of characters, number arrays (both described in the following points), and more dictionaries. The, the established sections that contain more specific section must include their information between these characters. Example: 'COMMENTS': {...}

- All the strings are contained between quotes and, if quotes are contained within the string, the string shall be contained between double quotes. Example: 'ORIGINAL REFERENCE': "[...] and V. Guerra 'Electron-neutral scattering cross sections for CO2: a complete and consistent set and an assessment of dissociation' 2016 [...] "

- Isolated numbers do not required to be included between special characters. However, number arrays must be written inside square braces. Examples: '# OF MEASUREMENTS': 32, 'RANGE OF ENERGIES': [12, 200]

- As shown in the previous examples, all the section titles are written in capital letters, including those referring to the units and values of the data (as shown in Figure 4.7). An exception is made for the data obtained through mathematical models. In these, the mathematical model constants shall be identified with the name of the associated letter accounting for upper or lower case characteristics (as depicted in Figure A of Appendix A)

- Different sections are separated by a comma or double newline. Additionally, if a clear "tree" structure wants to be performed, some software do not handle tab commands for dictionaries (it is the case of Notepad++). In this situation, as its is the case of the file provided in Figure 4.7, the lining-up must be done be successive spaces to ensure the proper working of the codes.

- As a final remark, if explanatory notes are required about a specific content, they should not be read by the code. To do so, they are identified with a blank space followed by a number sign # and are located outside quotes. Example: 'RETRIEVAL DATE': '...' #(d/m/y)

A suggested finished ".txt" file for cross section values extracted from an external database is provided below in Figure 4.7. The corresponding file template for cross sections computed from a model is provided in Figure A of Appendix A.

```
'TYPE': 'Database'

'SOURCE': 'NIFS DATABASE: https://dbshino.nifs.ac.jp.'

'RETRIEVAL DATE': '25/03/2019' #(d/m/y)

'ORIGINAL REFERENCE': 'Wetzel, R.C. & Baiocchi, F.A. & Hayes, T.R. & Freund, R.S.
                       1987
                       Absolute cross sections for electron-impact ionization of the rare-gas atoms by the fast-
                            neutral-beam method
                       Phys. Rev. A,
                       vol. and issue 35, page 559'

'COMMENTS': {
             'PROCESS': 'Ionization e- + Xe --> 2e- + Xe+',
             'SPECIES': 'e/Xe',
             'INITIAL STATE': 'Xe +0',
             'INITIAL # e-': 54,
             'INITIAL E.C. ': '[Kr] 4d10 5s2 5p6',
             'FINAL STATE': 'Xe +1',
             'FINAL # e- ': 53,
             'FINAL E.C. ': '[Kr] 4d10 5s2 5p5',
             'METHOD': 'Crossed beam method',
             '# OF MEASUREMENTS': 32,
             'RANGE OF ENERGIES': [12, 200]
             }

'DATA': {
         'ENERGY': {
                    'units': 'eV',
                    'values': [1.200000e+01, 1.300000e+01, 1.400000e+01, 1.600000e+01, 1.800000e+01,
                                       2.000000e+01, 2.200000e+01, 2.400000e+01, 2.600000e+01, 2.800000e+01,
                                       3.000000e+01, 3.200000e+01, 3.400000e+01, 3.600000e+01, 3.800000e+01,
                                       4.000000e+01, 5.000000e+01, 6.000000e+01, 7.000000e+01, 7.500000e+01,
                                       9.000000e+01, 1.000000e+02, 1.100000e+02, 1.200000e+02, 1.300000e+02,
                                       1.400000e+02, 1.500000e+02, 1.600000e+02, 1.700000e+02, 1.800000e+02,
                                       1.900000e+02, 2.000000e+02]
                    },
         'CROSS-SECTION': {
                           'units': 'cm^2',
                           'values': [1.000000e-17, 3.100000e-17, 6.300000e-17, 1.350000e-16, 1.930000e-16,
                                              2.420000e-16, 2.910000e-16, 3.300000e-16, 3.590000e-16, 3.890000e
                                                   -16,
                                              4.130000e-16, 4.330000e-16, 4.510000e-16, 4.620000e-16, 4.720000e
                                                   -16,
                                              4.800000e-16, 4.840000e-16, 4.890000e-16, 4.960000e-16, 4.980000e
                                                   -16,
                                              4.920000e-16, 4.840000e-16, 4.770000e-16, 4.630000e-16, 4.550000e
                                                   -16,
                                              4.460000e-16, 4.380000e-16, 4.300000e-16, 4.240000e-16, 4.160000e
                                                   -16,
                                              4.080000e-16, 4.030000e-16]
                           }
         }
```

Fig. 4.7. Suggested .txt file for data extracted from an external database

5. DATA HANDLING FOR THE HYBRID/PIC CODES

The database of this thesis has now adopted as solid shape and is being filled with a complete scope of differential cross sections ($\sigma(v)$) of low level models. Throughout this chapter it will be studied how the cross sections data are simulated in the hybrid/PIC codes and, thus, how this data is required to be provided.

Hybrid codes obtain reasonable descriptions of a plasma behaviour by combining classical fluid mechanic techniques for magnetized fluids and Particle In Cell (PIC) algorithms. Specifically these codes apply fluid conservation equations to treat electrons as a magnetized fluid and applies the PIC algorithms to the rest of the particles to model them as a big ensemble towards which the electron flow is directed.

5.1. Collisions between heavy particles. PIC requirements: differential cross section

For particles modelled as solid ensembles, that is, any interaction where electrons are not involved; hybrid codes directly use the differential cross section to estimate whether the collision takes place or not (as explained in Chapter 1). The only required parameter to be provided to these codes is directly the differential cross section associated to a specified relative velocity.

Almost no data handling is necessary to provide the required differential cross section, just an interpolation at the specified velocity and a conversion from speed to energy. The latter, if required, is directly given by the relation

$$E = \frac{mv^2}{2} \tag{5.1}$$

where "m" is the mass of the specie involved. If a final conversion is needed for the energy units, the Boltzmann constant is used, recalling its definition from Chapter 2:

$$K = 1.38 \cdot 10^{-23} \frac{J}{K} = 1.6 \cdot 10^{-19} \frac{J}{eV} \tag{5.2}$$

5.2. Collision with electrons. Fluid model requirements: Collision rate coefficient

Concerning all the collisions involving electrons, two approaches must be considered.

On one side, collisions with electrons are responsible for the majority charge generation or recombination. As previously seen in Chapters 1 and 3, the direct measure of the rate at which charge particles are generated or recombined is given by the collision rate coefficient. This parameter is then the handled value by the hybrid codes and the required one to be provided by the database.

On the other side, the hybrid codes models the flow of electrons as a magnetized fluid. As such, a specific relative velocity may be associated with the entire flow volume but the particles inside the fluid volume have a random movement. For this reason, it is not accurate to provide the collision rate coefficient directly computed from a differential cross section associated with a give velocity. Instead, the rate coefficient should be computed through an average over the velocity distribution function ($f(v,T)$, where T is the flow energy and v the velocity for which the probability is computed) at the given flow velocity. This integration is defined as follows:

$$\langle \sigma(v)v \rangle = \frac{\int \sigma(v)vf(v,T)dv^3}{\int f(v,T)dv^3} = \frac{1}{n_e}\int \sigma(v)vf(v,T)dv^3 \tag{5.3}$$

5.2.1. The velocity distribution function: the Maxwellian distribution

A widely spread distribution function $f(v,T)$ is the *Maxwell-Boltzamann distribution*, commonly named as *Maxwellian distribution*. Its name makes reference to James Clerck Maxwell, who derived a distribution function for the molecular speed of gases in 1806 , and Ludwig Boltzmann, who performed strong researches into the physical origin of this distribution later in 1870 [47].

A very clear procedure to understand the physics behind this velocity distribution function is proposed by R. J, Goldston and P. H. Rutherford [1], and it begins in a plasma volume with uniform space distribution and in a near-equilibrium state. That is, the time scale with which the particles in this plasma volume collide with each other is much lower than the characteristic time scale over which the particles and energy are replaced.From this volume, any individual specific particle "A" is a distinguishable micro-system. For the ease of this derivation, only the particles that behave following the classical laws are considered, so the quantum-mechanical laws are ignored. The thermal distribution of velocities in plasma aims to define the probability P_A of finding such particle in a particular state of energy W_A.

If the total thermal energy of the volume is W_{total}, and the particle "A" must have obtained its energy state W_A through collisions with other particles, the remaining thermal "bath" of particles must have an energy state equal to "$W_{total} - W_A$". It is further assumed that the amount of collisions taking place is sufficiently high for the *fundamental theorem of statistical mechanics* to hold [48]. This theorems states that for an isolated system with a determine known composition and energy, the probabilities of finding the system in any of the possible accessible micro-states of the total system are the same. Thus, the probability P_A of a given state of the particle A is obtained by evaluating the amount of accessible micro-states of energy $W_{total} - W_A = W$.

If the number of all possible micro-states in the bath of total energy W is identified as Ω, statistical mechanics states the following relation between the temperature T of any

thermal system, the number of possible micro-states Ω and their energy W:

$$\frac{1}{T} \equiv \frac{kd\ln(\Omega)}{dW} \equiv \frac{dS}{dW} \tag{5.4}$$

where: k = Boltzmann constant

S = Entropy of the systems, defined as: $S \equiv k \ln \Omega$

Since the energy of the particle in the specific micro-state is smaller than the total volume energy, $W_A << W_{total}$, the amount of accessible micro-states may be approximated as follows:

$$\ln(\Omega)|_{(W_{total}-W_r)} \approx \ln(\Omega)|_{(W_{total})} - \frac{W_A}{kT} \Rightarrow \Omega|_{(W_{total}-W_r)} \approx \Omega|_{(W_{total})} \exp\left(-\frac{W_A}{kT}\right) \tag{5.5}$$

Notice that $\Omega|_{(W_{total})}$ does not depend on the micro-state energy W_A, meaning that the probability P_A of the particle having energy W_A must be given by the exponential term "$\exp\left(-\frac{W_A}{kT}\right)$", better known as the *Boltzmann factor*, introduced in Chapter 2.

By neglecting any possible contribution of potential energy due to the position of the particle, the micro-state energy W_A will be given by the kinetic energy of the particle, whose velocity will be found in a range of velocities $dv_x dv_y dv_z$ around a mean velocity $\vec{v} = (v_x, v_y, v_z)$. Thus, the probability P_A of a particle of mass m to be found with a specific energy is better expressed as

$$\exp\left(-\frac{m(v_x^2 + v_y^2 + v_z^2)}{2kT}\right) dv_x dv_y dv_z \tag{5.6}$$

In addition, it is appropriate to define the phase-space density function $f(\vec{x}, \vec{y})$, where $\vec{x}$ stands for the physical space and $\vec{v}$ the velocity space. In this way, this function f describes the number of particles per unit $dxdydzdv_x dv_y dv_Z$. So integrating this function over the velocity space $\vec{v}$ the density of particles per unit volume n is found:

$$n = \int f dv_x dv_y dv_z \tag{5.7}$$

The Maxwell-Boltzmann, or Mawellian, distribution f_M is simply the following normalization of the Boltzmann factor:

$$f_M(v) = \frac{n}{(\sqrt{2\pi} v_t)^3} \exp\left(-\frac{v^2}{2v_t^2}\right) \tag{5.8}$$

In this expression the variable "v_t" is the thermal velocity of the entire system, defined as

$$v_t \equiv \sqrt{\frac{kT}{m}} \tag{5.9}$$

so that Equation 5.8 may be rewritten as

$$f_M(v) = n\left(\frac{m}{2\pi kT}\right)^{3/2} \exp\left(-\frac{mv^2}{2kT}\right) \Rightarrow \text{In S.I.: } f_M(v) = n\left(\frac{m}{2\pi T}\right)^{3/2} \exp\left(-\frac{mv^2}{2T}\right) \tag{5.10}$$

The following two sections expand the distribution just exposed for isotropic and anisotropic flows, which require to integrate over one, two or more directions to obtain an average parameter.

5.2.2. Isotropic Maxwellian distribution

It is usually of interest the study of a one-dimensional velocity distribution. This one is obtained integrating the velocity distribution function over the other two components of the velocity. In the simple case of a velocity distribution expressed in Cartesian coordinates the following results are obtained:

$$f(v_x) = \int_{-\infty}^{+\infty} \int_{-\infty}^{+\infty} f(v_x, v_y, v_z) dv_y dv_z \tag{5.11}$$

$$f_M(v_x) = n\left(\frac{m}{2\pi T}\right)^{1/2} \exp\left(-\frac{mv_x^2}{2T}\right) \tag{5.12}$$

In addition, the usual three-dimensional distribution $f_M(v_x, v_y, v_z)$ is isotropic, that is, the same properties and distribution are found in all directions. This property makes the spherical velocity coordinates (v, θ, ϕ) to be a more appropriate coordinate system to work with. In this new coordinate system the volume element is expressed as: $d^3v = v^2 sin(\theta) d\phi d\theta dv$, where $v \in [0, \infty)$, $\theta \in [0, \pi]$ and $\phi \in [0, 2\pi]$ as presented in Figure 5.1(a)

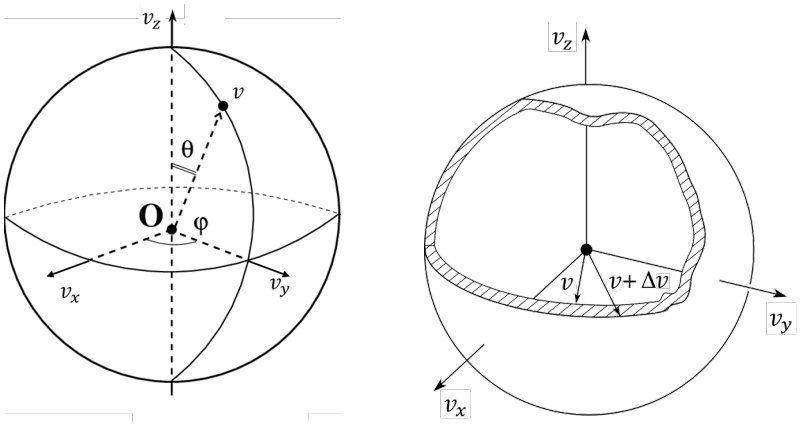

(a) Spherical coordinates in the control volume [49]

(b) Control volume shell [50]

Fig. 5.1. Isotropic control system

It is possible to integrate over the ranges of θ and ϕ since the Maxwellian distribution f_M is independent of these coordinates. As the integral results in $\int sin(\theta)d\phi d\theta = 4\pi$, the differential volume element becomes the differential volume of a thin spherical shell in the velocity space: $d^3v = 4\pi v^2 dv$ (see Figure 5.1(b)). With this simplification, it is possible to write the expression for a uni-directional Maxwellian distribution that provides the density per unit of velocity magnitude of the three-dimensional velocity space ($[f] = m^{-3}(m/s)^{-3} = s^3/m^6$). In other words, all the volume planes parallel to the flow direction have the same energy, which results in the following density distribution function in terms of such energy (T). An example of its graphical representation is provided in Figure 5.2.

$$f_M(v) = 4\pi n \left(\frac{m}{2\pi T}\right)^{3/2} v_x^2 \exp\left(-\frac{mv_x^2}{2T}\right) \tag{5.13}$$

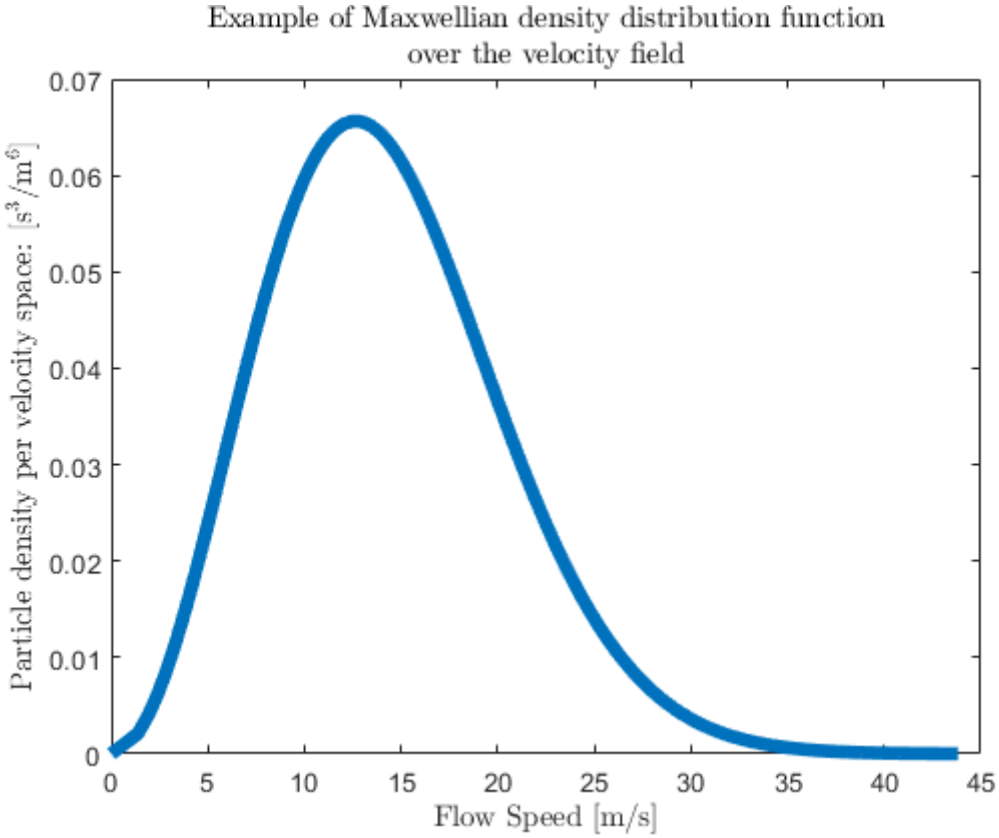

Fig. 5.2. Example of Maxwellian density distribution function

This last equation can be expressed in terms of total energy of the plasma flow, which is a much common data that is known when studying its performance. Neglecting again the potential energy of the particles, it is found that the total energy is the kinetic energy $E = \frac{mv^2}{2}$, so that the simpler expression for the Maxwellian distribution is expressed as below (the mathematical derivation is provided in Appendix B):

$$f_M(E) = n\frac{2}{\sqrt{\pi}}\frac{\sqrt{E}}{T^{3/2}}\exp\left(-\frac{E}{T}\right) \tag{5.14}$$

Regard that the dependence on the mass of the system has disappeared from the equation and that the original density over the velocity space function has now become a density over energy field. This is a tremendous advantage as Equation 5.14 becomes a universal formulation for the isotropic velocity distribution regardless of the volume being studied. Notice also that, due to the probability distribution function, despite its change of meaning (which may be also regarded by comparing Figures 5.2 and 5.3), the integral over the the velocity range provides the particle density of the volume:

$$\int_0^\infty f_M(v)dv = n \tag{5.15}$$

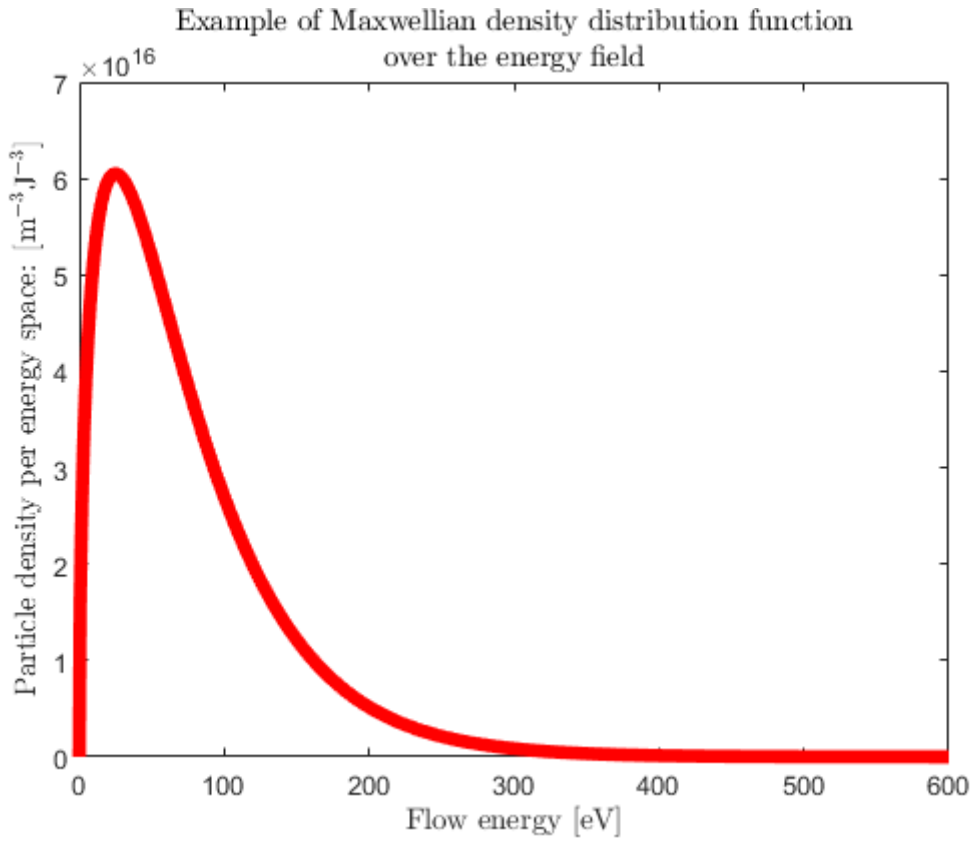

Fig. 5.3. Example of isotropic density distribution function over the energy field

5.2.3. Bi-Maxwellian distribution function

In a lot of cases, such as the hybrid codes this thesis attends, the plasma volume studied has different velocity distributions in different directions (the flow is anisotropic). In the particular case where the flow has two characteristic and perpendicular distribution directions, the plane distribution function with a thermal velocity along the magnetic field ($T_{\parallel}$) and another one across the field ($T_{\perp}$) is approximated by the so called *bi-Maxwellian* distribution.

If Cartesian coordinates are used again, the *z-direction* might be set coincident to the magnetic field. Then the Maxwell-Boltzmann function in its most basic formulation of previous Equation 5.8 is better written as

$$f_{bM}(v) = \frac{n}{(\sqrt{2\pi}v_{t\parallel})(\sqrt{2\pi}v_{t\perp})^2} \exp\left(-\frac{v_z^2}{2v_{t\parallel}^2} - \frac{v_x^2 + v_y^2}{2v_{t\perp}^2}\right) \tag{5.16}$$

where

$$v_{t\parallel} \equiv \sqrt{\frac{T_{\parallel}}{m}} = v_z \qquad\qquad v_{t\perp} \equiv \sqrt{\frac{T_{\perp}}{m}} = \sqrt{v_x^2 + v_y^2} \tag{5.17}$$

being $T_{\parallel}$ and $T_{\perp}$ the thermal energies expressed in S.I. ([J]).

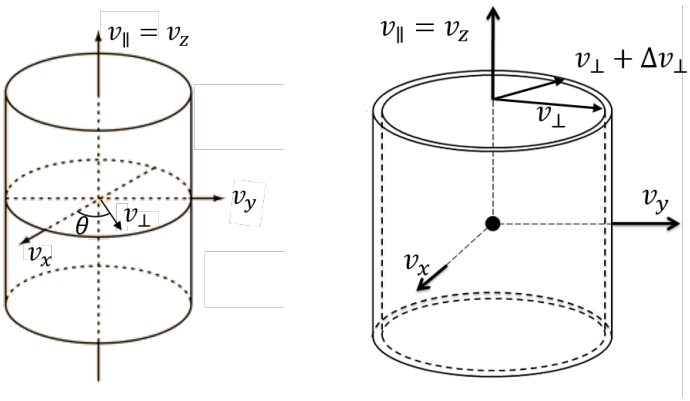

(a) Cylindrical coordinates in the control volume [51]

(b) Cylindrical control volume shell [52]

Fig. 5.4. Anisotropic control system

In this case, it is regarded that the use of cylindrical coordinates are more convenient for this system. A study control volume as the one depicted in Figure 5.4(a) is defined. The differential volume is then $dv^3 = v_\perp dv_\perp dv_\parallel d\theta$, where $v_\parallel \in [-\infty, \infty)$, $v_perp \in [0, \infty)$ and $\theta \in [0, 2\pi]$. Alike the isotropic plasma case, the velocity distribution is independent of the θ parameter and, then, the differential volume becomes $dv^3 = 2\pi v_\perp dv_\perp dv_\parallel$. It is possible to rewrite Equation 5.16 as below, being graphically exemplified in Figure 5.5

$$f_{bM}(v) = n\frac{m^{(3/2)}}{\sqrt{2\pi T_\parallel} T_\perp} v_\perp \exp\left(-\frac{mv_\parallel^2}{2T_\parallel} - \frac{mv_\perp^2}{2T_\perp}\right) \tag{5.18}$$

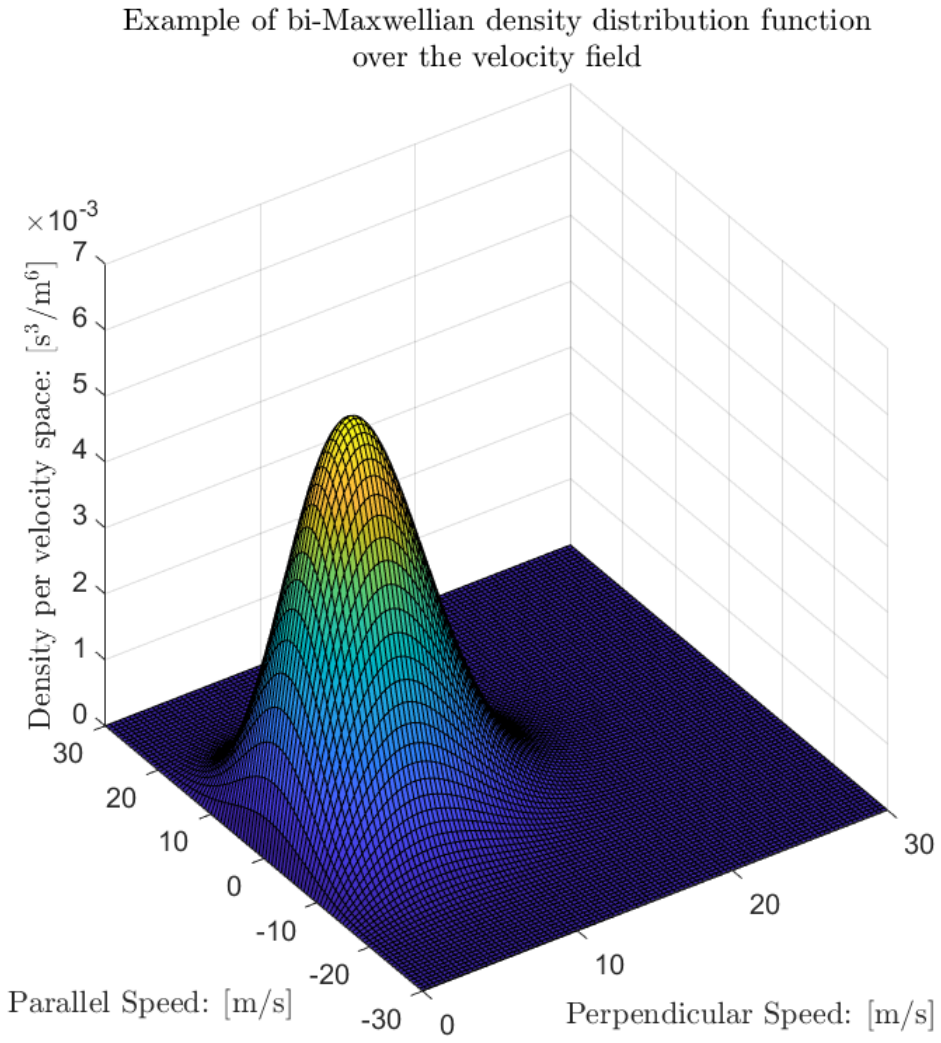

Fig. 5.5. Example of bi-Maxwellian density distribution function

Once again, the distribution expression may be translated in terms of total energy to obtain a more useful expression independent of the mass of the volume and in terms of the energy field. In this case the distinction is made between the parallel and the perpendicular direction and their range of the former. The energy range must account for the double direction that the parallel speed could adopt in the control volume, then $E_{\parallel} \in [0, \infty)$ while $v_{\parallel} \in [-\infty, \infty]$. Figure 5.6 is the translation of the same velocity ranges of the previous image into energy field, showing the clear change of ranges and behaviour. As in the previous case, the procedure followed to arrive to the final expression is provided in Appendix B.

$$f_{bM}(E) = n \frac{1}{\sqrt{\pi T_{\parallel}} T_{\perp}} \frac{1}{\sqrt{E_{\parallel}}} \exp\left(-\frac{E_{\parallel}}{T_{\parallel}} - \frac{E_{\perp}}{T_{\perp}}\right) \tag{5.19}$$

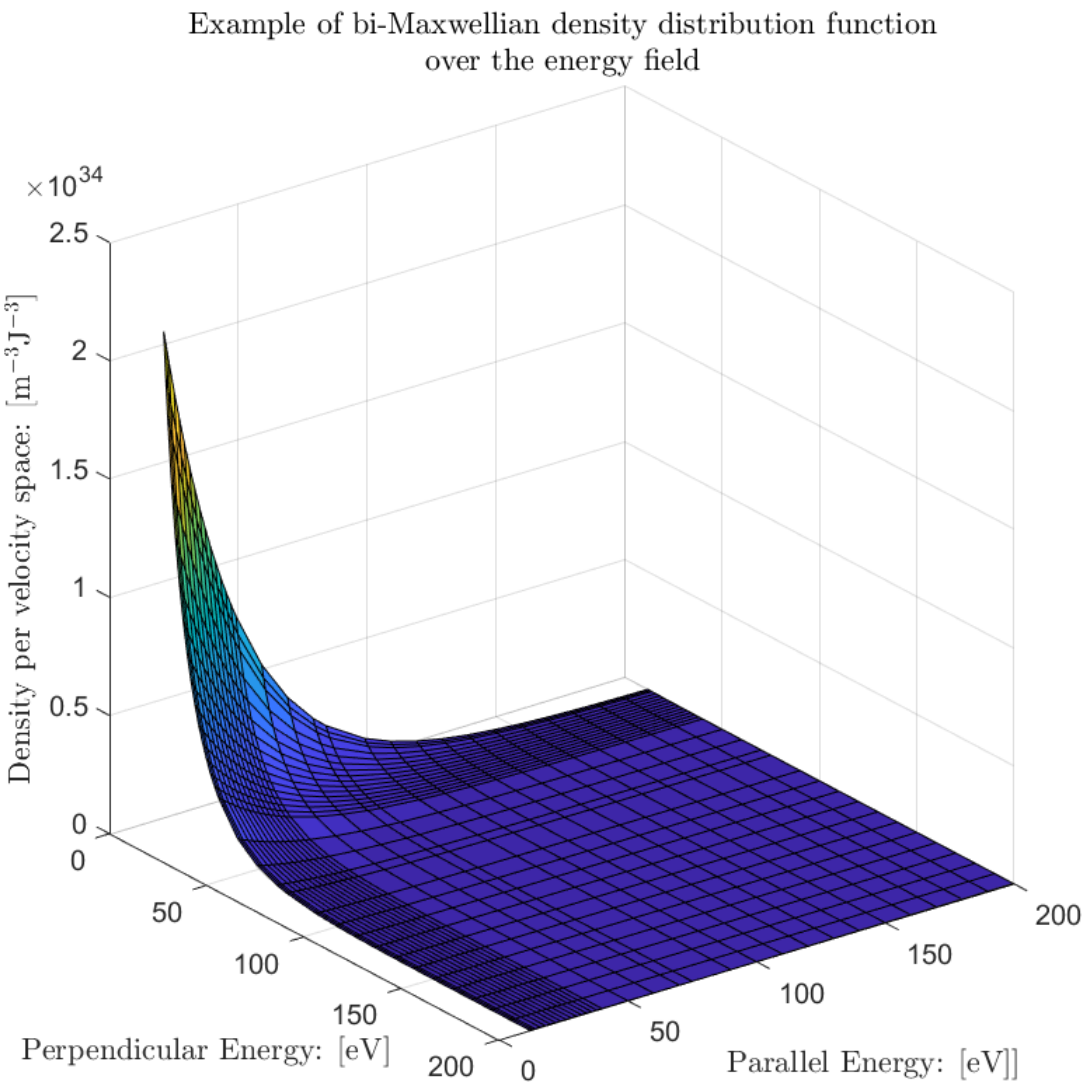

Fig. 5.6. Example of bi-Maxwellian density distribution function over the energy field

Notice that, as in Equation 5.14, the integration of Equation 5.19 over the parallel and perpendicular directions also results in the the density of the volume. Moreover,it is essential to remember that the derivations performed to the final equation of both distribution were carried out in S.I. units. However, energy ranges in researches concerning plasma flow are usually expressed in electron-Volts. Then, special importance must be paid to make sure that the energies introduced in Equations 5.14 and 5.19 are expressed in Joules with the help of the Boltzmann constant previously stated in Equation 5.2.

Nevertheless, this last equation brings up an instability as the energy goes to 0. This is clearly visible in Figure 5.6. Due to this drawback, it is sometimes preferred to keep the dependence on the mass and used Equation 5.18. Notice that this peculiarity only affects the an-isotropic distribution, the isotropic Maxwellian does not present any instability at any of its expressions.

6. DATABASE CODES

In this chapter it will be presented the written codes that work as a the nexus between the hybrid main code and the database generated. The working principle of the use of these codes is simple: the user of the hybrid code, or the code itself, will call one of the following functions when a specific parameter is required and these codes directly provide such value. No more interactions or superfluous deliveries are needed.

To provide the maximum efficiency in the connection between the hybrid code and the database, the database codes have been written in the same coding language used in the hybrid code, Python. This specific coding environment will then required to import the modules and functions used in the linking codes to assure a proper performance.

After several communications with the research group handling the main hybrid code, four specific codes were concluded to be needed, with their respective inputs and outputs, to be explained in the following sections.

All the functions that are presented in the following sections were written inside module called "db_codes". For the main code to connect with the database this module must be imported and, the, the functions inside it may be called, following the example exposed in Appendix C. As commented, four specific functions were designed to directly interact with the user. These are

- *get_collision_info.py*
- *interpolate_at_velocity.py*
- *collision_rate_Maxwellian.py*
- *collision_rate_BiMaxwellian.py*

,the rest of the functions were designed to interact with each other, so there is no need to call them. Nevertheless, all the codes created for this database are publicly available in the GitHub repository:

`https://github.com/100345796/Cross-section-database-for-hybrid-PIC-fluid-plasma-codes`

6.1. Dictionary collision information: *get_collision_info.py*

This is the simplest of the three required functions. This function reads the information stored in the database of a collision reaction specified by the user. Then, this function is not desired to specifically provide data to the hybrid code but to provide the user with the

data stored: energies, differential cross section, reference, method used to compute the cross section ...

- Required inputs (the user must enter the inputs strictly following the standard criteria exposed in Chapter 4):
  - rootdir: root directory where the database is stored in the computer, USB,... Ex: rootdir = 'C:/Users/Antonio/Desktop/DATABASE'.
  - Type: type of desire reaction. It must be: Type: 'BINARY' or 'UNARY'.
  - specie1 = first specie involved in the collision. Ex: specie1 = 'e-' or 'Xe' or 'Xe+1'...
  - specie2: secnod specie involved in the interaction.

    IMPORTANT NOTE 1: the species are introduced with their sign an their electronic state as stated by the structure criteria.Some examples are:
    - 'e-' for electron
    - 'Xe' for neutral Xe
    - 'Xe+2' for double ionized Xenon–> Symbol+Charge+#charges
    - 'Xe[5s2]' for excited Xe –> Symbol[electronic state of the last valence e-]

    IMPORTANT NOTE 2: the species do not necessarily need to be entered in order. The code itself checks the input species and, if required it, sorts them to commit with the database standards.

    IMPORTANT NOTE 3: If the type "UNARY" is introduced, the secondary specie should be left as empty string: specie2: ".
  - process: desired reaction. Following the criteria, some inputs may be
    - 'i1' for one ionization of 1 e-
    - 'elastic' for elastic collision
    - 'e[...]' for excitation to the [...] electronic configuration
  - file_name: name of the file that wants to be read (it must be a .txt). Example: file_name = 'database_LXCAT.txt'

    IMPORTANT NOTE 3: If the name of the .txt is unknown, leave it as empty string (file_name = '') and the code will automatically read the first file associated with a database or, in the case where only one file is stored, it will read that file. This is done calling the secondary function

    _select_fileroot_filename_unknown.py

    which will be introduced in section 6.4 of this chapter.

- Provided output: identified as "info" inside the function, the code returns the information stored at the specified file of the desired reaction between two given particles. Thanks to the used YAML standard, all the information included in the .txt files is returned in an organized Python dictionary.

A step by step description of this function is the following:

1. The species are studied to sort the in the appropriate way to commit with the database structure standards.
2. The directory root of the desired file is obtained.
3. The file at such root is read and translated from the YAML language to a Python dictionary.

6.2. Differential cross section at a specific energy: *interpolate_at_velocity.py*

Oppositely to the previous function, this one is designed to directly interact with the hybrid code. The aim of this function is to provide the specific differential cross section of a determined collision between given particles at the relative energy required by the hybrid code.

- The required inputs in this function are the same as those for the previous function, *get_collision_information.py*, plus the additional term
  - Velocity: relative velocity between the colliding particles. It must be introduced in [m/s].
- The output is the interpolated differential cross section associated with the required collision at the specified relative velocity. It is provided to the hybrid code in [m^2].

This function will be mostly used by for collisions without electrons, as the hybrid code makes use of the differential cross sections without any averaging for these systems. This is relevant as the velocity introduced by the user is in [m/s] and the differential cross section of the collision is a function of energy in [eV]. Then a translation between these to forms must be made as

$$E = \frac{1}{K[J/eV]} \frac{m[Kg] \cdot v[m/s]^2}{2} \tag{6.1}$$

In addition, the mass term in the previous equation must be adequated to the studied collision. In case the collision involves an electron, the term corresponds to the electron mass because the center of the reference system is located at the bigger mass and, so, the relative velocity is given in terms of the electron motion. However, when electrons are not present in the collision, the mass to be accounted is that one of the specie involved. Here, the effects of mass variation due to ionization are neglected, as the electron mass is several orders of magnitude lower than the neutral atoms studied.

The step by step working procedure of this function is as follows:

1. Obtain the dictionary collision information from the specified directory making use of the previous function *get_collision_info.py*

2. Extract the differential cross sections from the dictionary file through the function (which is later explained):

   _get_E_and_CS_arrays_from_info.py

3. The input velocity is translated to relative energy accounting for the proper mass as explained above, for which it reads the "specie_info.txt" files stored in the "UNARY" section of the database.

4. The interpolation is done through a simple linear method. For reactions with threshold energy, below this energy the cross section is null. For the rest of the cases a simple linear interpolation is done.

6.3. Collision rate computation

The idea of this code is to provide the collision rate for those reactions involving electrons. Two different codes are provided for this purpose differentiating between the isotropy of the velocity distribution function.

6.3.1. Isotropic collision rate: *collision_rate_Maxwellian.py*

In this case the hybrid codes considers an isotropic Maxwellian distribution, the collision rate coefficient is computed averaging over this function.

- The inputs if this function are similar to the previous function: The identification of the type of collision and species involved and the file where the data is stored, like in the first explained function, and the following parameter:
  - Velocity: in this case this velocity is the relative velocity of the flow of electrons with respect to the collision target particle. Oppositely to the previous function, this time the velocity is already introduced in [eV].
- The output of this code is the value of the collision rate coefficient averaged over the Maxwellian distribution set by the given velocity.

In this occasion, as the Maxwellian distribution is defined in S.I., the energy needs to be translated from [eV] to [J]. This is simply done making use of the Boltzmann constant.

The step by step description of this code is provided below:

1. Obtain the dictionary collision information from the specified directory making use of the function *get_collision_info.py* and both, the differential cross sections and

the associated energies, are extracted from the dictionary file through the function *_get_E_and_CS_arrays_from_info.py*

2. To increase accuracy, a set of velocities in S.I. (through the electron mass and the Boltzmann constant) is set in the range of those whose cross sections are stored in the database. In this case, this array is set to correspond to the parallel and perpendicular velocities, $v_{\parallel}$ and $v_{\perp}$.

3. A 2D array of Bi-Maxwellian distribution values is obtained for the given flow energy and the set array of velocities, making use of Equation 5.18

$$f_M(v) = 4\pi n \left(\frac{m}{2\pi T}\right)^{3/2} v_x^2 \exp\left(-\frac{m v_x^2}{2T}\right)$$

4. The differential cross sections at each of the terms in the velocity array set are obtained through interpolation.

5. Finally, the collision rate coefficient is computed as explained in Chapter 5:

$$\langle \sigma(v) v \rangle = \frac{\int \sigma(v) v f(v,T) dv^3}{\int f(v,T) dv^3} = \frac{1}{n_e} \int \sigma(v) v f(v,T) dv^3$$

Notice that, ideally, the density term "n_e" corresponding to the integration of the Maxwellian distribution function is equal to the unity. However, this is is not true for the studied case as it is not being integrated over the entire velocity field ($v \in [0, \infty)$. Thus, the values compute for such term are lower, which would lead to a disagreement with the ideal final results. Nevertheless, as both the numerator and denominator of the above equation are integrals over a specific range of the velocity field, the obtained values for $n_e < 1$ compensate for the regions not included in the averaging and the analysis becomes conservative.

6.3.2. Anisotropic collision rate: *collision_rate_BiMaxwellian.py*

Alternatively, if the hybrid code simulates an an-isotropic flow with different parallel and perpendicular velocities, the Bi-Maxwellian distribution function must be used.

- In this case, the inputs include all the mentioned file and collision information plus the following parameters:
  - Velocity_parallel: velocity is the relative velocity of the flow of electrons with respect to the collision target particle in the parallel direction to the approaching motion.This velocity must be introduced in [eV].
  - Velocity_perpendicular: velocity is the relative velocity of the flow of electrons with respect to the collision target particle in the perpendicular direction to the approaching motion.This velocity must be also introduced in [eV].

- The output of this code is the value of the collision rate coefficient averaged over the two directions of the Bi-Maxwellian distribution set by the given velocities.

The step by step procedure of this function is similar to the previous one, expressing as well all the energies in Joules to be implemented in the different equations:

1. Obtain the dictionary collision information from the specified directory making use of the function *get_collision_info.py* and both, the differential cross sections and the associated energies, are extracted from the dictionary file through the function *_get_E_and_CS_arrays_from_info.py*

2. A set of velocities in S.I. (through the electron mass and the Boltzmann constant) is set in the range of those whose cross sections are stored in the database. This is done to decrease the measurement intervals and gain accuracy.

3. The Maxwellian distribution value is obtained for the given flow energy and the set array of velocities previously set in Equation 5.13

$$f_{bM}(v) = n\frac{m^{(3/2)}}{\sqrt{2\pi T_{\parallel}}T_{\perp}}v_{\perp}\exp\left(-\frac{mv_{\parallel}^2}{2T_{\parallel}} - \frac{mv_{\perp}^2}{2T_{\perp}}\right)$$

4. The differential cross sections at each of the “cells" of the 2D matrix is obtained through interpolation with the database data, accountign for the fact that the velocity in each “cell" is defined as

$$V = \sqrt{v_{\parallel}^2 + v_{\perp}^2}. \tag{6.2}$$

5. Finally, the collision rate coefficient is computed as explained in Chapter 5:

$$\langle\sigma(v)v\rangle = \frac{\int\sigma(V)Vf(v_{\parallel},v_{\perp},T_{\parallel},T_{\perp})dv^3}{\int f(v_{\parallel},v_{\perp},T_{\parallel},T_{\perp})dv^3} = \frac{1}{n_e}\int\sigma(V)Vf(v_{\parallel},v_{\perp},T_{\parallel},T_{\perp})dv^3$$

   Again, the values that the parameter n_e acquires in this process are lower than 1. But, in the same way as before, compensate for the regions not included in the averaging and the analysis becomes again conservative.

6.4. Secondary functions

To keep the main codes clean a readable, secondary functions with a specific objectives were implemented. Inside each code, specific tasks are performed by the following functions and even by the already mentioned ones. For example, the first function *get_collision_info.py* is called during the execution of the other functions.

As these functions do not interact with the user, their inputs and outputs will not be deeply explained as they are already linked with the inner structure of the main database codes.

6.4.1. *_get_directory_structure*

This function takes as input the directory root where the database is stored and scans all the folders and files inside that root.

It provides two different outputs:

- A Python dictionary structure with all the folders and files found in the provided directory.
- A tree-like scheme of the previous dictionary to obtain a quick sight of what is included in the database. This figure would be quite similar to the structure represented in Figure 4.6 of Chapter 4

6.4.2. *_select_fileroot_filename_unknown.py*

The objective of this function is to provide the directory root of a .txt file when the user does not know which files are stored in the database for the desired collision process.

With the given indicators of the collision reaction and the species involved, this function goes into the specific folder where the file should be and does one of the following:

- If folder only contain one data file, the function will output the root of such file, independently of the source of the data contained in it.
- If the folder contains more than one file, the function will output the first file corresponding to a database source.

  This process is done for both, binary and unitary reactions.

6.4.3. *_get_E_and_CS_arrays_from_info.py*

This function extracts from the previously obtained dictionary of collision data an array of cross section, in [m^2] and associated energies, in [eV].

For that end, this function reads the .txt file and considers the type of source:

- If the data stored was obtained from an external database, where the values are already given in arrays, this function just returns as output those arrays in the mentioned units.
- If the data stored is composed of constants needed to implement a cross section model, such as Drawin model from Chapter 3, the function will identified which model it is and, if such model is already stored in the code lines, it will be able to provide as output an array of energies and computed cross sections in [eV] and [m^2].

7. RESULTS

This chapter will present all the results achieved throughout the project: Starting from the final state of the database and codes in section 7.1, results arriving from differential cross sections introduced in the database and with potential to be modeled by hybrid codes in part 7.2, and finally, results form collision rate coefficients 7.3.

7.1. Database and Codes Performance

The database was first filled with cross sections of the current most spread propellant, Xenon. The data introduced for this element includes electron impact elastic collisions, single ionization and excitation collision from its neutral state; and ionization reactions of pre-ionized and pre-excited atoms. Between heavy particle, data contains the differential cross-sections corresponding to charge transfer interactions between neutral Xenon and ionized Xenon (Xe^{+1} and Xe^{+2}).

The process of filling the database was complemented with simultaneous analysis of the cross-sections introduced. The results of these analysis, exposed in next section, provided a guide of the appropriate collisions to be next implemented into the database. After the first results of relevant processes with Xenon, collision involving Argon and Krypton were introduced focusing on the reliable interactions found for Xenon. Collision cross sections regarding Argon and Krypton by electron impact include single and double ionization reactions of the neutral state, and single ionization of the single pre-ionized atoms; as well as pure elastic interactions. Concerning collisions with heavy particles, the cross sections for collisions between their neutral and ionized states were implemented. Additionally, the charge transfer collision between both species, "Ar^{+1} + Kr→ Ar +Kr^{+1}", was also stored in the database.

Last cross sections introduced in the database belong to non conventional species that are being suggested to be tested. These include CO_2, N_2 Ne and O_2. Specifically, the data stored for these species is focused on their direct ionization and elastic collisions by electron impact.

In the "UNARY" section of the database, only the information concerning the steady characteristics of the implemented species where introduced. Due to the low electron mass, every ionized state of any specie is considered to have the same mass and properties than the neutral specie. On the other hand, values related to unary reactions relevant for hybrid/PIC codes required further researches to provide definitions of what are really inherent properties of the specie and not consequence of previous interactions. For example, de-excitation reactions in plasma occurring in processes such as autoionization, it must be clarify whether this rate is inherent to the plasma particle or results from the previous collision with an electron.

All together, the final layout of the database is provided below in Figure 7.1.

BINARY	e⁻	Ar	Ar+1	Ar+2	CO2	Kr	Kr+1	Kr+2	N2	Ne	Ne+1	O2	Xe	Xe[5p5_6s1]	Xe+1	Xe+2
e⁻		elastic i1 i2	i1		elastic i1 i2	elastic i1 i2	i1		elastic i1	elastic i1		elastic i1	e[5d] e[6s_6p] e[7s] elastic i1 i2	i1	i1	
Ar			ch_e	ch_e												
Ar+1						ch_e										
Ar+2																
CO2																
Kr							ch_e	ch_e								
Kr+1																
Kr+2																
N2																
Ne											ch_e					
Ne+1																
O2																
Xe															che_e	ch_e
Xe[5p5_6s1]																
Xe+1																
Xe+2																

UNARY	
e⁻	specie_info.txt
Ar	specie_info.txt
CO2	specie_info.txt
Kr	specie_info.txt
N2	specie_info.txt
Ne	specie_info.txt
O2	specie_info.txt
Xe	specie_info.txt

Fig. 7.1. Database with the filled collision cross-sections and data

Concerning the written codes to complement the database, they have shown an excellent performance in retrieving the desired parameters from the database accounting for all the different requirements set in the previous chapters. To assure this performance, the results provided by these codes were checked with other environment: *MatLab* (this program was also used to perform the graphical representations provided throughout the entire document due to the handling advantages that it provides). In addition, it is noticed that the time required by these codes to achieve the results is quite low. However, it is noticed that, due to the working procedure of Python, in which the various functions used are stored in modules; the first use of the codes presents a tiny delay as all the modules and functions have to be called. Nevertheless, once all the modules have been imported, results are instantaneously provided.

All the database and complementary codes are published in the following GitHub repository:

`https://github.com/100345796/Cross-section-database-for-hybrid-PIC-fluid-plasma-codes`

7.2. Comparison between differential collision cross-sections

As explained, only the most influencing collision processes should be considered to be simulated with the purpose of reducing computational costs. The first comparison that directly provides an idea of the most relevant interactions is by means of the order of magnitude of the associated differential cross sections.

An optimum specie to start this analysis with is the current most used propellant in electric propulsion systems: Xenon. But before comparing several collision processes for any specie, it is advisable to estimate which data stored in the same space of the database are more reliable. If several cross section values were stored in the database arriving from external databases and mathematical models, a prior scrutiny should be made to conclude which data are more reliable for further applications. Figure 7.2 provides a comparison of several cross sections of electron impact ionization for Xe. These values were directly extracted from external databases or were computed from some of the models presented in Chapter 3.

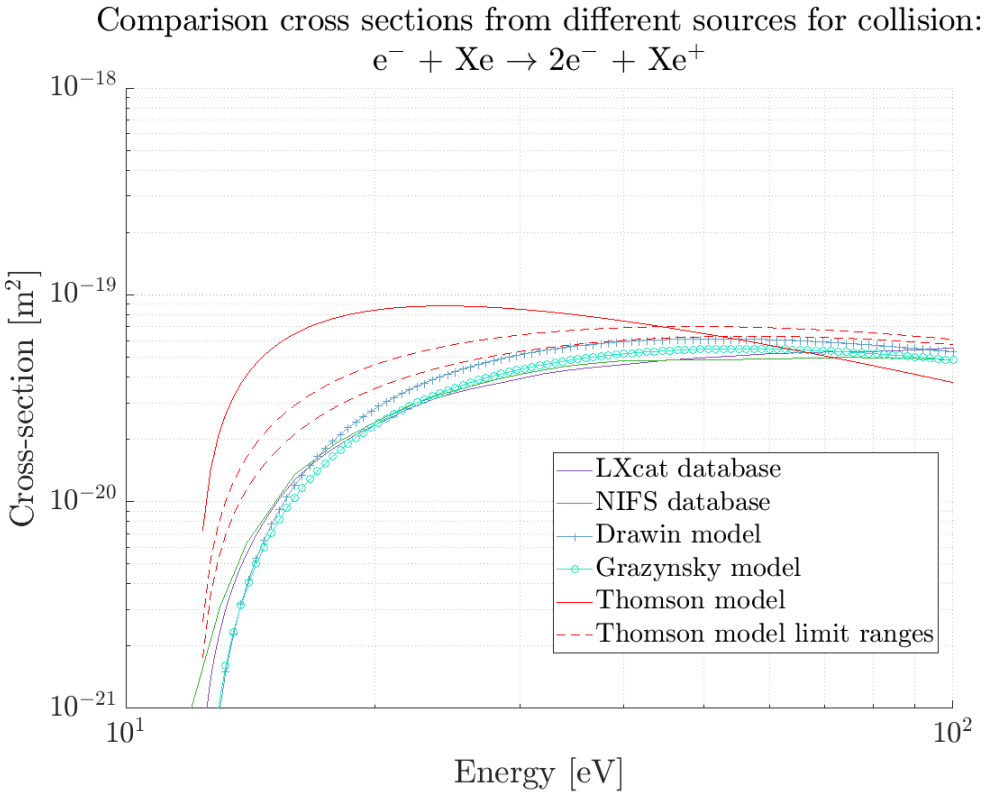

Fig. 7.2. Differential cross-section from different sources for the first ionization of Xe by electron impact

As regarded, apart from Thomson approach, the different models provide values in the same order of magnitude and converge in a clear estimation of the cross section. Gryzinski model approaches the most to the values provided by the two databases. Concerning Thomson model, despite showing values of the same order of magnitude than

his partners, the limitation ranges established for this model in Equation 3.9 invalidate the results everywhere but in a small region around 50 [eV]. Notice, however, the close values marked by this range functions and the actual measures provided by the database. It is proved, then, that Thomson values laying inside the specified range are, as explained in the model, accurate enough. Database values, on the other hand, nearly coincide. In this specific case, the data retrieved from the NIFS database was originally obtained experimentally through a crossed-beam-method (introduced in Chapter 3), while the values provided by the LXCat database where originally computed using the Magboltz program, also introduced in the same chapter. The agreement of their values provides double support, to the validity of the Magboltz program and to the validity of the values itself. It is then proved that databases provide well supported data that should be used if there is no conviction about the validity of a given model.

This convergence in all the models is not so present when studying Argon ionization, which was analyzed taking advantage of the fact the Drawing constants for this specie were also known. However, as depicted in Figure 7.3 the different values still provide an estimation of order of magnitude of the collision cross section and validate each other.

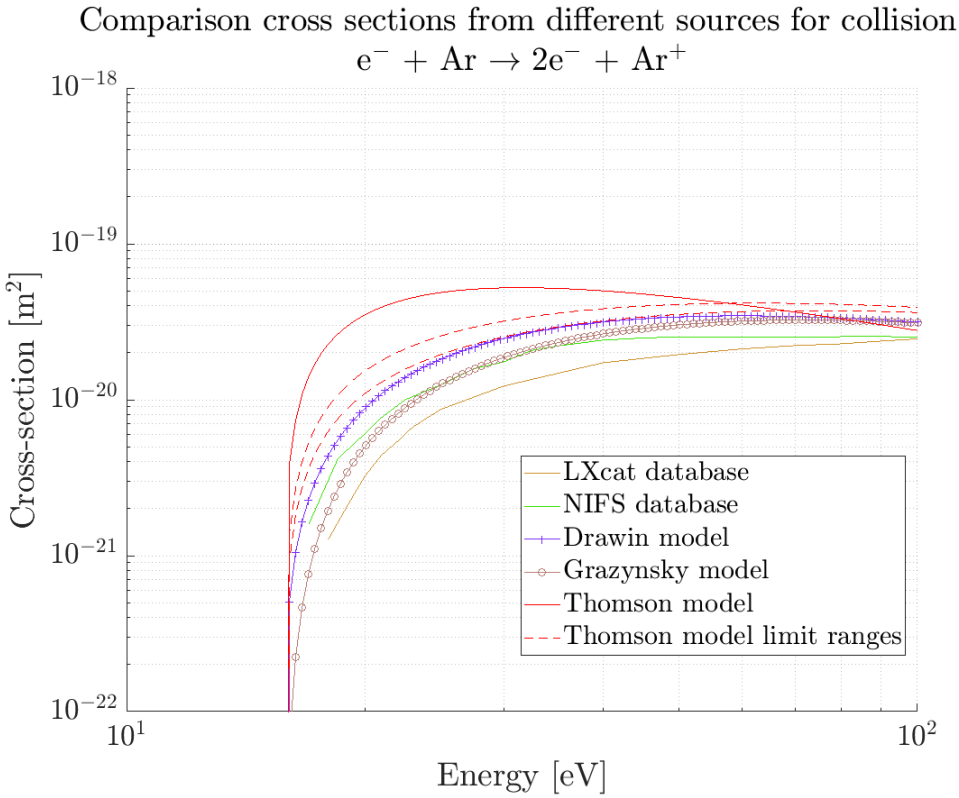

Fig. 7.3. Differential cross-section from different sources for the first ionization of Ar by electron impact

Concerning now the different types of interactions, Figure 7.4 depicts the cross sections associated with several collisions involving Xe atoms. As represented, the cross sections corresponding to electron impact excitation reactions present an order of magni-

tude (~ [$O(10^{-22})$, $O(10^{-23})$]m^2) around four times lower than charge transfer processes (~ [$O(10^{-18})$, $O(10^{-19})$] m^2) and two times lower than ionization collisions (~ [$O(10^{-20})$, $O(10^{-21})$] m^2). On the other side, elastic collisions present moderate cross section values throughout the entire scope of energies (~ [$O(10^{-19})$, $O(10^{-20})$]). Then, reactions such as charge exchange have more relevant values (meaning more influence on the evolution of a plasma volume) than others, such as excitation by electron impact, which are almost negligible.

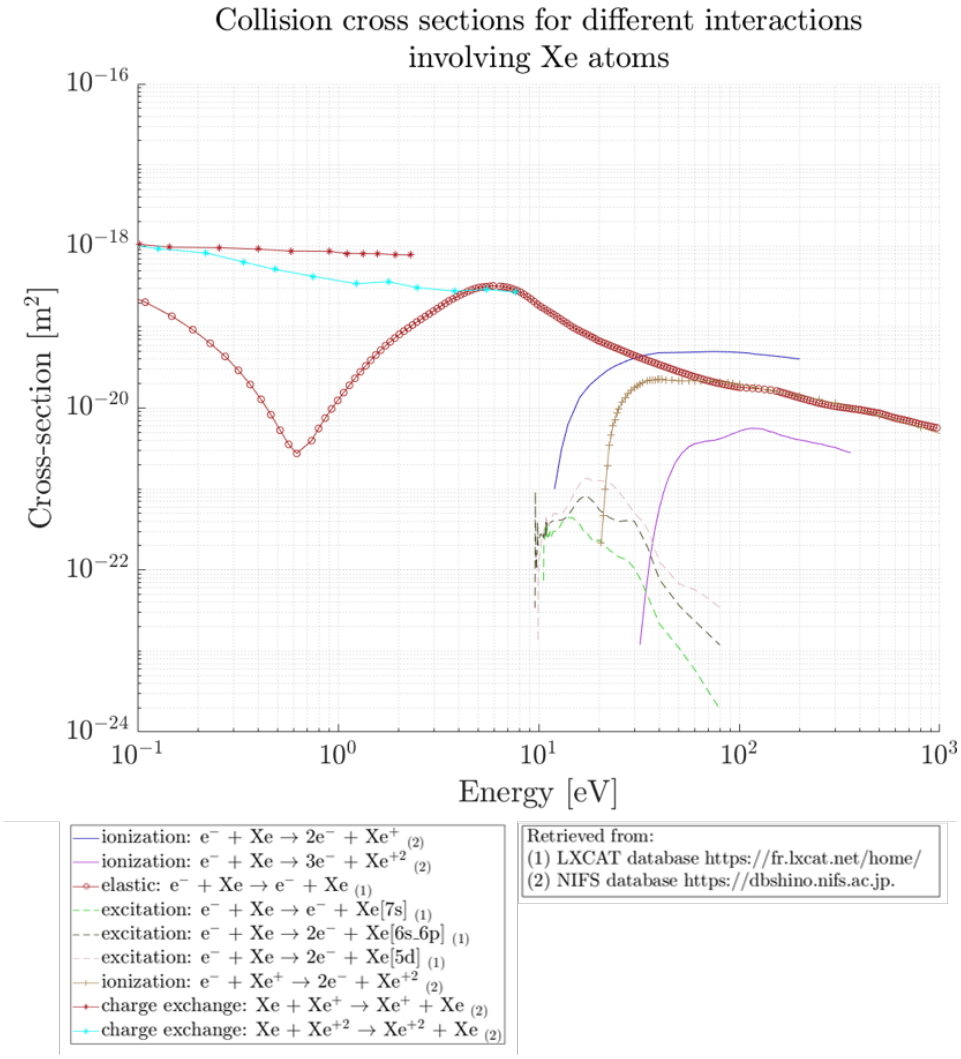

Fig. 7.4. Cross-sections for collisions involving Xe atoms [22] [23]

It is interesting to point out that the ionization reactions of neutral Xe become more relevant than elastic interactions few energies after their threshold. Similar behaviour presents the ionization of pre-ionized Xe^+, which concurs with the elastic collision cross sections. Moreover, the second ionization collisions for neutral Xe appear to be always less relevant than elastic interactions. However, all these observations, while conclusive with the provided image, should not be considered for a further selection for collisions. As repeatedly mentioned throughout the thesis, a distinction must be made between collisions with and without electrons. For those with electrons, a better approach to determine

influencing collisions is done through the results arriving from their collision rate coefficients, being computed in the following section of this chapter.

Nevertheless, before skipping to the rate coefficient results, the amount of collisions stored in the database allow to perform as well a preliminary study of other two species with potential applications in electric propulsion: Argon and Krypton. Figures 7.5 and 7.6 provide the results for several reactions with such species.

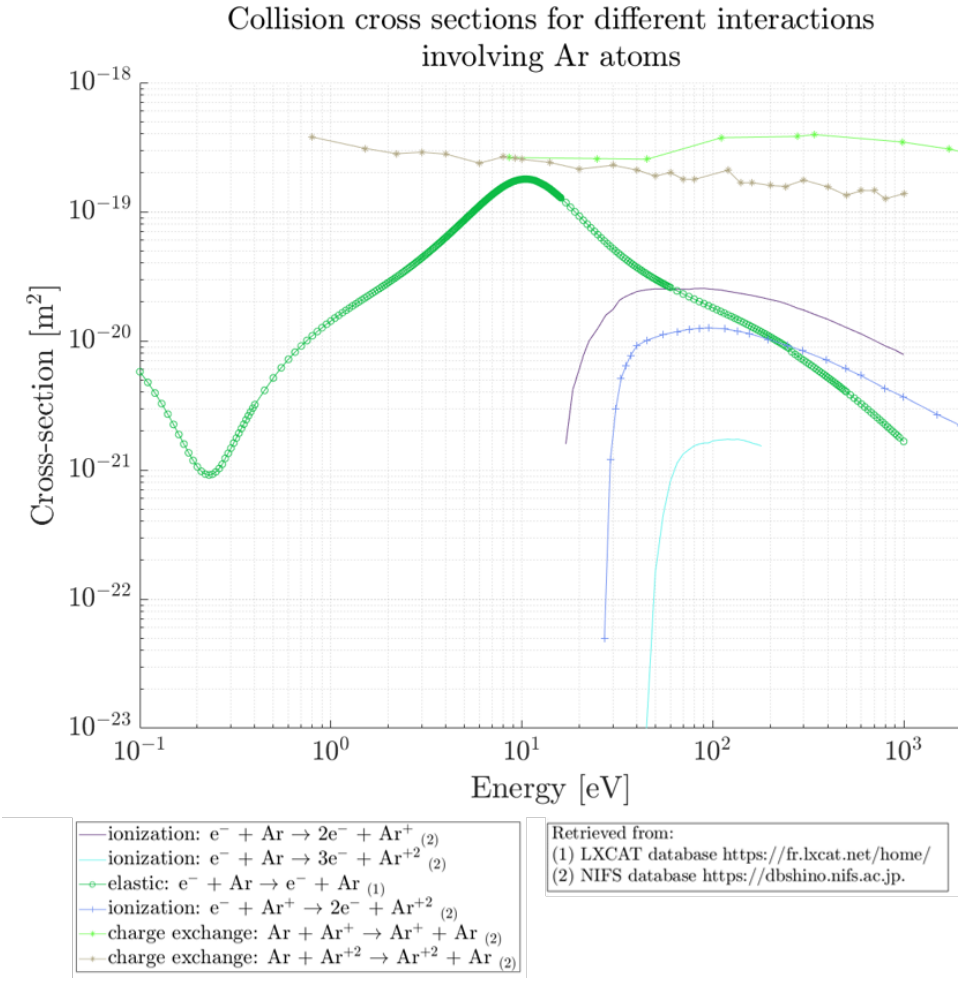

Fig. 7.5. Cross sections for collisions involving Ar atoms

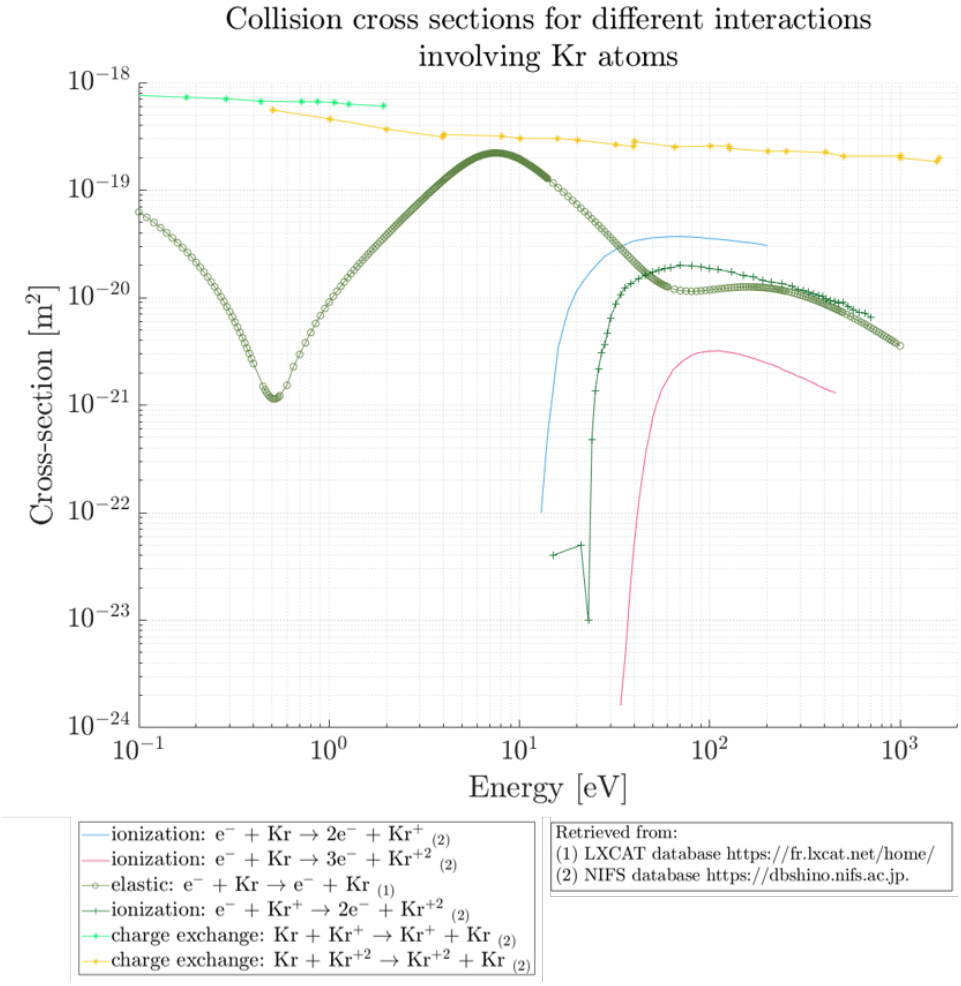

Fig. 7.6. Cross sections for collisions involving Kr atoms

Comparing these results with the Xe ones, it is observable that Argon and Krypton exhibit ionization collision cross sections of the same order and behaviour than those for Xenon. In relation with elastic collisions, Xenon atoms present slightly higher values than Argon and Krypton. Similarly, Xenon shows slightly higher values for charge transfer cross sections, although the three species display these processes in the same order of magnitude ($O(10^{-19})m^2$).

The preliminary study in terms of the differential cross sections has then exposed the high resemblance between the most widely used propellant in electric propulsion systems, Xe, and Ar and Kr, highlighting the high values of charge exchange, elastic and ionization processes.

7.3. Comparison between collision rate coefficients

The results obtained for the collision rate coefficients of collisions involving electrons are provided in the figures below. These rate coefficients have being computed through the procedures described in the theory provided in Chapter 5 and the codes of Chapter

6. Initially, due to the ease of computation and representation, isotropic systems have been considered, making use of the Maxwellian distribution function for a scope of flow energies between 1 and 10^3 eV.

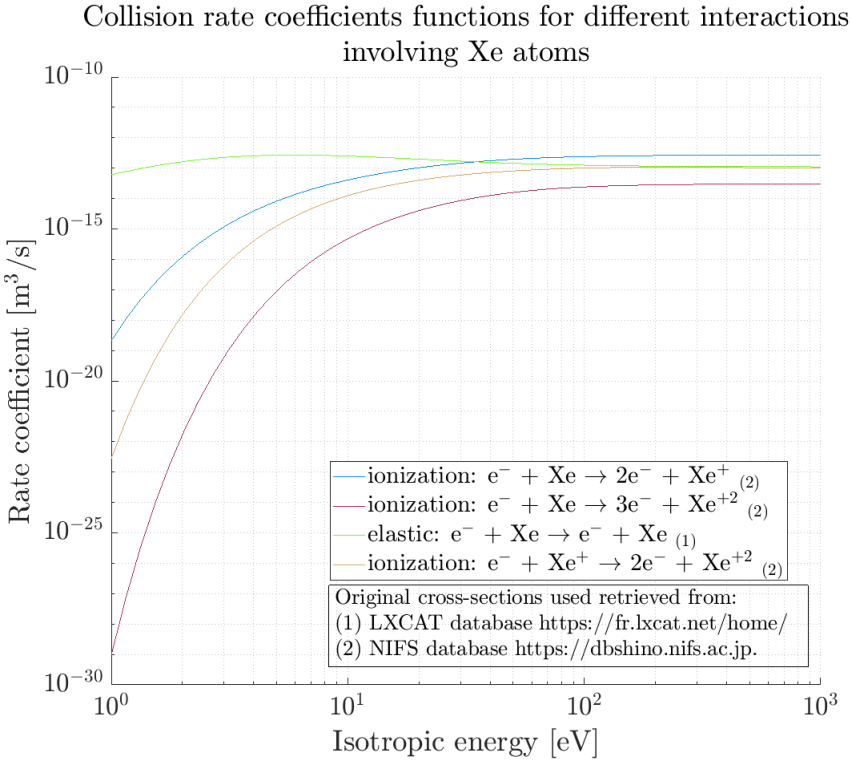

Fig. 7.7. Collision rate coefficient for several collision processes involving Xe atoms

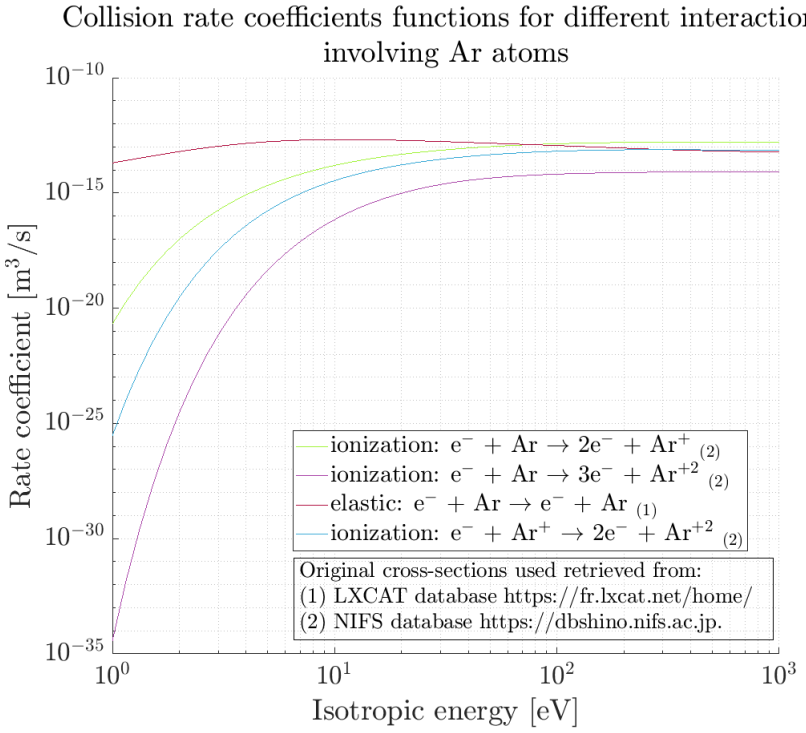

Fig. 7.8. Collision rate coefficient for several collision processes involving Ar atoms

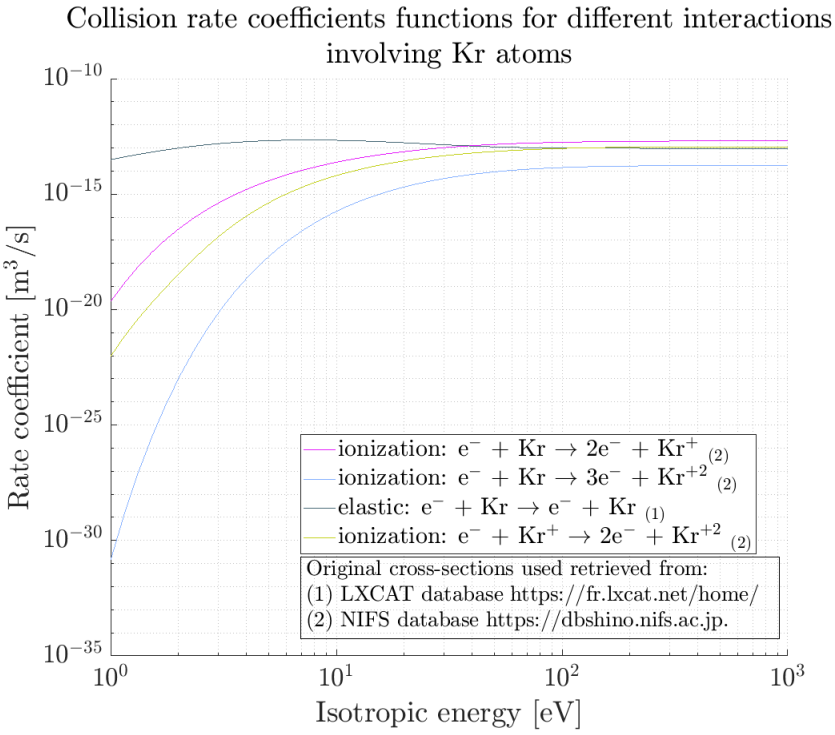

Fig. 7.9. Collision rate coefficient for several collision processes involving Kr atoms

In the same way as the figures from previous section, Figures 7.7 to 7.9 picture a high resemblance between the characteristics of Xenon, Argon and Krypton species. Concerning the ionization collisions, all of these elements exhibit higher collision rates for the ionization of the neutral state atoms, followed by the ionization of the pre-ionized atom, and double ionization present the lower rate coefficients. The rate coefficients for the elastic collisions are showed to exceed the previous values at energies up to [40, 60] eV. Over this electron flow energy, all the collisions of all the species tested tend to a constant rate: ionization reactions “0→1" and “1→2" acquire rates very close to $10^{-13} m^3/s$, ionization processes “0→2" adopt values around $10^{-14} m^3/s$, and elastic collision rates concur with those of the ionization of the pre-ionized atom, as forecast by the differential cross sections in previous section.

However, small differences are noticed when examining the cases with more detail. Xenon collision rates show slightly greater values than Argon and Krypton tests, being followed by Krypton interactions and, with the lowest rates, Argon. Although these nuances are not so perceptible at high energies, they are clearly observable at low values. Indeed, these are the regions relevant for the purpose of this thesis, as the plasma being simulated by the hybrid codes is usually a cold plasma below 30 eV. The greatest divergences between the values of the same collision process for different species are then found at the lowest energy. To make them clearly visible for the studied atoms, Table 7.1 collects the obtaiend collision rates at 1 eV.

Table 7.1. COMPARISON BETWEEN THE COLLISION RATE COEFFICIENTS FOR REACTIONS INVOLVING AR, KR, AND XE, WITH AN ISOTROPIC ELECTRON FLOW AT 1 EV (COMPUTATIONS PERFORMED WITH THE DATABASE CODES)

Specie	**Elastic collision**	**Ionization of neutral atoms**	**Ionization of pre-ionized atoms**	**Double ionization of neutral atoms**	**UNITS**
Ar	$\sim 2.2 \cdot 10^{-14}$	$\sim 2.1 \cdot 10^{-21}$	$\sim 2.9 \cdot 10^{-26}$	$\sim 2.7 \cdot 10^{-35}$	$[m^3/s]$
Kr	$\sim 3.1 \cdot 10^{-14}$	$\sim 2.2 \cdot 10^{-20}$	$\sim 9.5 \cdot 10^{-23}$	$\sim 1.4 \cdot 10^{-31}$	$[m^3/s]$
Xe	$\sim 6.1 \cdot 10^{-14}$	$\sim 2.1 \cdot 10^{-19}$	$\sim 2.8 \cdot 10^{-23}$	$\sim 9.5 \cdot 10^{-30}$	$[m^3/s]$

Xenon collisions present, in general, the highest collision rates. An exception is identified at the ionization of the pre-ionized atom between Xenon and Krypton, although Xenon rate soon overpasses the Krypton rate as the energy increases. Additionally, it is also appreciable the steps in order of magnitude from one reaction to the successive one.

Due to the outstanding order of the values of the elastic and ionization of neutral collision rates, a comparison was performed between these species more present in electric propulsion systems and those non-conventional species that are being proposed for further studies (whose cross sections are implemented in the database). Figures 7.10 and 7.11 provide these results. It is possible to appreciate that elastic rates generally share the same order of magnitude along the entire energy scope ($O(10^{-14})$). Moreover, it is observed that, although some non-conventional propellants may provide higher rates at very low energies, they soon become surpassed by those of Xenon, Argon and Krypton. Nevertheless, except for N_2, the remaining rates for CO_2, Ne and O_2 do not lay far way from those of previously studied species. Concerning the rates for ionization, differences are more visible in the range of energies relevant for this research. While Xenon still provides the highest collision rates, the majority of non-conventional species present collision rates between those characteristic of Krypton and Argon. On the other side, it is noticeable the low values provided by the noble gas Ne, of several orders of magnitude below the common ones for the entire energy scope.

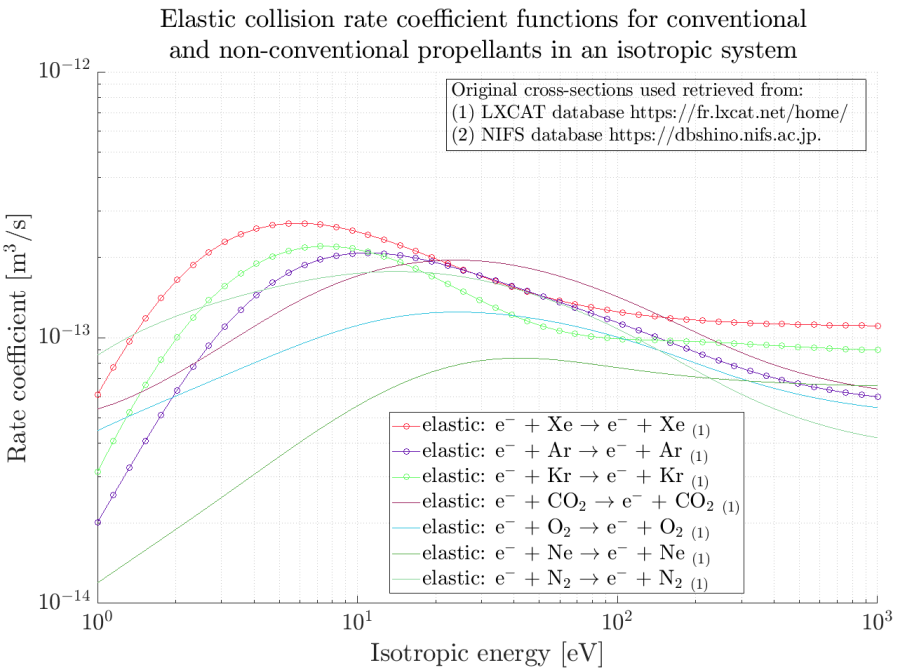

Fig. 7.10. Comparison of the elastic collision rates for conventional and non-conventional propellants modelled over a Maxwellian distribution.

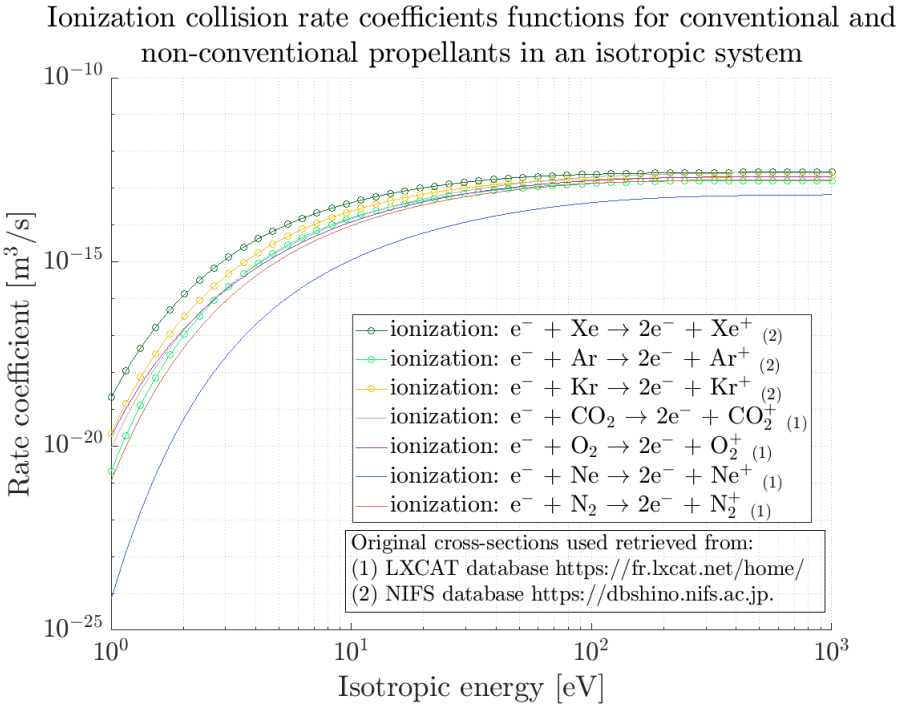

Fig. 7.11. Comparison of the ionization collision rates of neutrals for conventional and non-conventional propellants modelled over a Maxwellian distribution.

When considering an an-isotropic system, the procedure changes to evaluate the collision rate coefficient combining the parallel and perpendicular flow energies. However, the sort of rate coefficients is expected to coincide with that one predicted by the isotropic

flow. The collisions with highest collision rates are the elastic and ionization of neutrals, thus being indispensable their simulation in the hybrid codes. This is proved by the collision rate surfaces provided in Figures 7.12,7.13 and 7.14.

Figure 7.12 provides the three-dimensional expansion of the rate coefficients for the different reactions considered with Xe. It is observable how the ionization collisions hold, in the two dimensions, the behaviour anticipated by the isotropic system. Even though the elastic collision rate keeps falling under the rate of ionization of neutrals at large flow energies, at values below 30 eV is a predominant collision together with the mentioned ionization interaction. being relevant for the plasma simulation. Notice as well, the strong influence of the perpendicular flow velocity in the equation of the Bi-Maxwellian distribution (Equation 5.18): the rate of change of the collision rate coefficient is greater in the perpendicular direction. In addition, the plane at 45°, where both directional energies coincide, corresponds to the isotropic case previously analyzed.

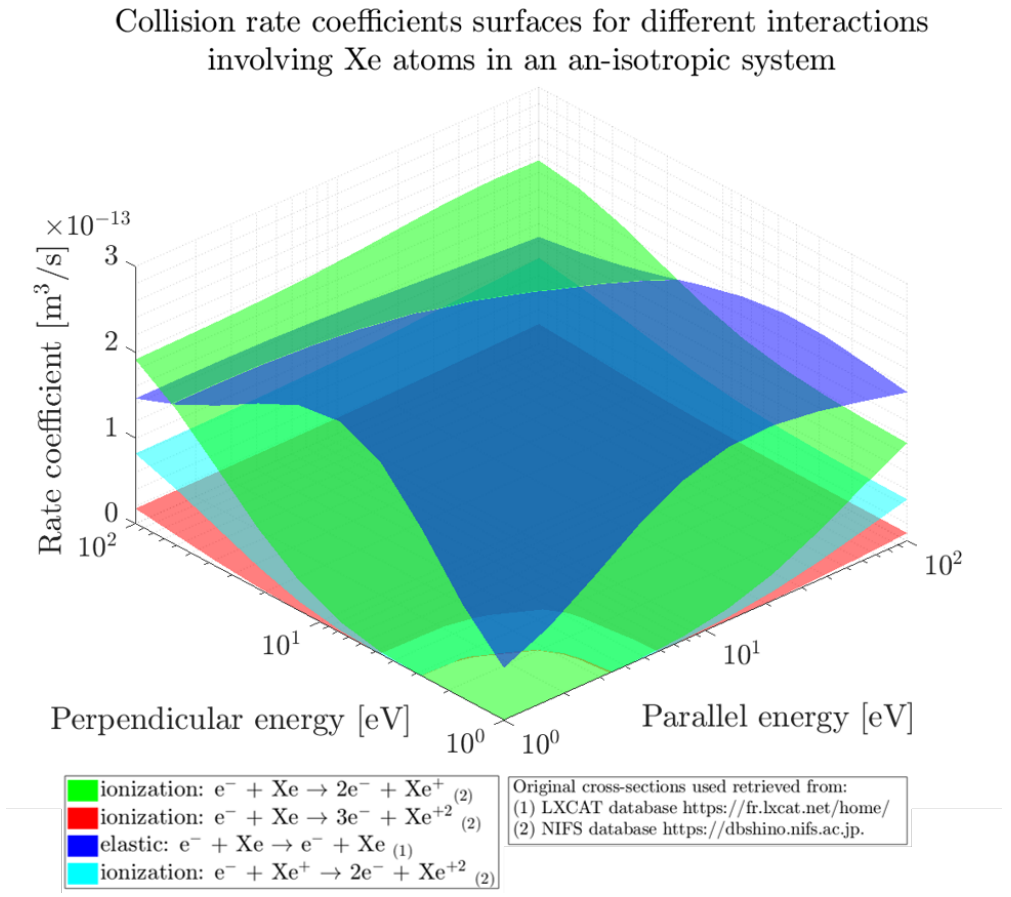

Fig. 7.12. An-isotropic collision rate coefficient surface for collisions involving Xe

The most relevant collision processes are then compared to their respective reactions with Argon and Krypton. Figure 7.13 depicts the elastic collision rate coefficient for the three species and Figure 7.14 the corresponding rate for the ionization of the three neutrals. It is visible that in the region of interest (<30eV), Krypton collision rates lay in both cases below Xenon rate coefficients and above Argon ones, in agreement with the

isotropic system results.

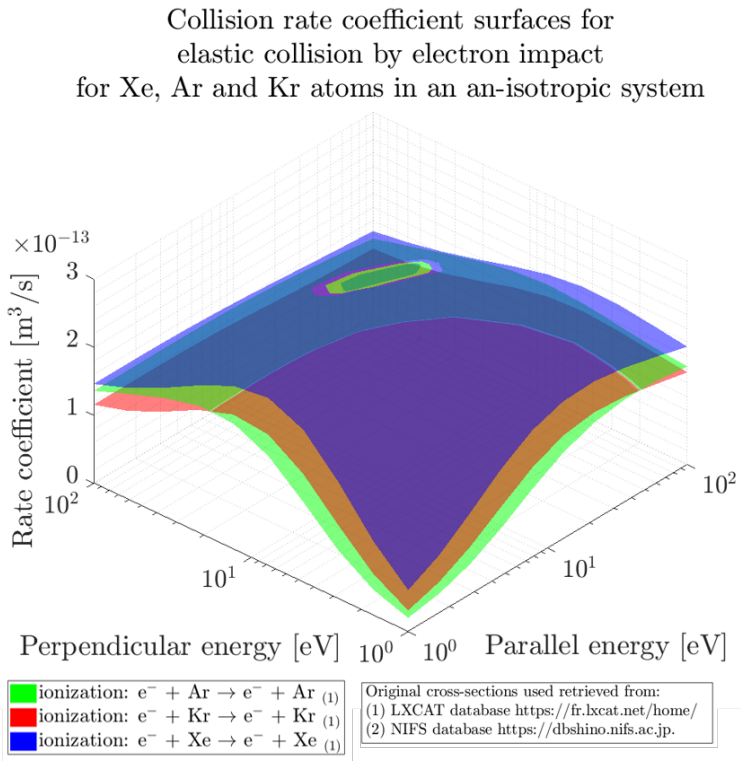

Fig. 7.13. Comparison of the an-isotropic collision rate coefficient surface for elastic collision of electron with Xe, Ar and Kr neutral atoms

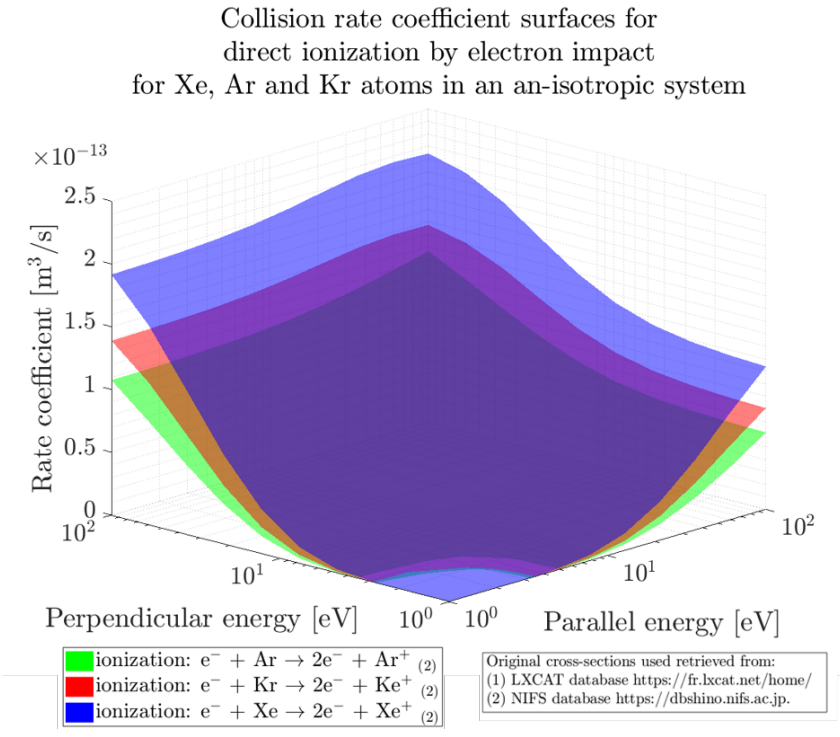

Fig. 7.14. Comparison of the an-isotropic collision rate coefficient surface for direct electron impact ionization of Xe, Ar and Kr neutral atoms

A final note that must be accounted together with the previous collision rates is the consideration of the Stepwise Ionization process. As explained in Chapter 3, if the plasma is characterized by a high density of electrons and excited neutrals, the rate coefficient of stepwise collision may be approximated with the formula expressed in Equation 3.17:

$$\frac{k_i^s(T_e)}{k_i(T_e)} \approx \left(\frac{I}{T_e}\right)^{\frac{7}{2}}$$

where $k_i^s(T_e)$ and $k_i(T_e)$ are the rate coefficient functions of the stepwise and direct ionization by electron impact respectively, I is the ionization threshold energy of the neutral specie, and T_e the velocity (expressed as energy) of the electrons flow. Regarding the high collision rates found for the direct ionization by electron impact of the neutral Xe, Ar and Kr atoms, stepwise ionization collision rate coefficients widely overpass the previous ones for flow energies below the ionization threshold of the specie. Results at 1 eV are provided in Table 7.2 to expose this effect:

Table 7.2. COMPARISON BETWEEN THE COLLISION RATE COEFFICIENTS FOR DIRECT IONIZATION AND STEPWISE IONIZATION OF NEUTRAL AR, KR, AND XE, AT 1 EV

Specie	**I [eV]**	$k_i(1[eV])$	$k_i^s(1[eV])$
Ar	~ 15.7592	$\sim 2.1 \cdot 10^{-21}$	$\sim 3.26 \cdot 10^{-17}$
Kr	~ 13.9996	$\sim 2.2 \cdot 10^{-20}$	$\sim 2.26 \cdot 10^{-16}$
Xe	~ 12.1298	$\sim 2.1 \cdot 10^{-19}$	$\sim 1.31 \cdot 10^{-15}$

8. CONCLUSIONS

Throughout chapters 2 and 3 the various collision processes were organized and presented. In addition, a brief criteria for their relevance in the simulation of plasma for electric propulsion systems was provided. As explained, there are numerous possible interaction just in the group of binary collision. In an ideal scenario where computational costs were nonexistent, all of the collision processes could be taken into account. However, in reality, computational costs are one of the main concerns and restrictions of simulations. Thus, it is essential to select from all the scope only those reactions that influence the most, and store their relevant parameters in such a way that can be retrieved and used without increasing time and computational costs.

Concerning the storage purpose of this thesis, the selection of the database organization and structure, as well as the storage file standard YAML, have proved to provide a fluid and efficient connection between the user and the data. With the easiness with which the cross sections and data are introduced into the database, and the ability to be read not only by different programming languages but also by humans without coding knowledge; the generated database is a simple and efficient tool to directly provide the hybrid codes, or any study concerning cold plasma simulations, the required differential cross section or collision rates coefficients. Additionally, it shows a potential to be expanded by future collaborators, growing a becoming more complete. For such purpose, it has been made available at the the following GitHub repository:

`https://github.com/100345796/Cross-section-database-for-hybrid-PIC-fluid-plasma-codes`

Connected to this database, the complementary codes that provide a link between the hybrid codes and the database show a good performance. The time these codes spend to retrieve the requested information is negligible once the required Python modules are already called. Only if new parameters introduced in the database require additional tasks not implemented in the codes, these will need to be modify to include them. This codes have already been uploaded to the mentioned repository to keep being used, being expanded and improved by future users.

In relation with the preliminary analysis of the different collision cross-sections stored in the database, the first conclusions arrive from the comparison of the different sources. It has been proved the agreement in collision cross sections for first ionization between the different models and external databases. The latter, specifically, provide validity to the Magboltz program and, together with the models, to the own values. It is then concluded the accuracy of models designed for specific collisions, such as Drawin model, and that databases provide well supported data that should be used if there is no conviction about the validity of a given model.

The successive results introducing differential cross-sections of several collision reactions have demonstrated the importance of charge transfer, elastic and ionization collisions as well as the high resemblance between the most widely used propellant in electric propulsion systems, Xe, Ar and Kr, reason why these last species are actively, and will continue, being studied, tested and used as propellants.

Hybrid codes, however, required the step forward of analyzing the collision rate coefficients for electron flow interactions. Higher collision rates mean faster processes (i.e. the collisions last less time) and, thus, more collisions are possible. They provide an estimation of the time that a certain specie can survive in the systems and the resulting rate of generation of charged particles. It is then deducted that for plasma systems, essential processes to account are ionization collisions, as they dictate the rate at which new charged particles will appear in the studied volume.

Results arriving from the previous results of collision rates coefficients of the different species, apart from their agreement with those rising from the collision cross-sections, also locate the spotlight over elastic collisions and ionization of already charged atoms. The characteristic high values of the latter, greater than those of double ionization of neutrals, indicate the importance of tracking the pre-existing and generated charged particles in the volume to obtain the most accurate and realistic results.

Nevertheless, the still faster rates of elastic collisions and ionization reactions of neutral atoms, compared to those of ionization of pre-ionized atoms and double ionization of neutral reactions, indicate that, not only are faster, but also more frequent in the plasma, So, their degree of influence over the plasma properties is much higher, what, nonetheless, does not exclude the necessity of considering the rest of interactions. The similar values for these collision processes provided by alternative propellants such as CO_2, O_2 and N_2 suggest that potential benefits may arrive from their use and, thus, is advisable to further test them.

Further conclusion are deducted as a consequence of the high collision rates found for the direct ionization by electron impact of the neutral Xe, Ar and Kr atoms. Stepwise ionization interactions, which many times are not even mentioned in the simulations, have shown to be of potential influence due to their large rate coefficients when conditions of high electron and excited neutral densities are reached (recall that their collision rates in such conditions are easily related with the rates of the mentioned direct ionization). If such plasma characteristics are achieved, stepwise ionization overpasses the rate of generation of charged particles of other sources and its simulation is highly required.

Moving to collisions between heavy particles, charge exchange collisions are matter of study and consideration. While they do not vary the number of charged particles in the plasma, the high cross-section values resulting in the previous studies indicate that are a potential source of changes and increases in particles momentum, which may lead to macroscopic potential hazard flows, such as the already observed back-flow in near-plume regions. With the highest differential cross sections from the tested species, charge

transfer processes dominate over the collisions between heavy particles and must not be neglected in the simulations.

As a final remark, the performed study has not involved the consideration of molecules or mixing propellants. Then, the recombination processes that could be relevant in cold, few ionized plasma (such as dissociative or ion-ion recombination) are potential interactions that should be introduced in further researches that aim to estimate the performance with these species.

9. SOCIOECONOMIC ENVIRONMENT

9.1. Budget of the performed study

The analysis referring to the budget spent in the elaboration of this thesis can be divided into costs with direct impact to the author, and costs which were assumed by third parties.

9.1.1. Costs assumed by the author

- **Computer**: The most obvious tool required for the entire purpose of the thesis. The average cost of mid-level-power computer able to support programming languages like python or MatLab without any type of memory problem or delay is around 600 €.
- **Writing tool: LaTex account**: The LaTex account used to write the thesis has been the free version, so no costs have been involved in this aspect. Cost: 0 €
- **.txt file editor program: NotePad++**: As commented, the database required a .txt file editor in order to generate the cross-section files in the appropriate standard. The used programm for such purpose has been *NotePad++*, which is freely downloadable from internetet. Cost: 0 €
- **Python program**: To coincide with the current research on hybrid codes for which this thesis is performed, the codes provided to connect the hybrid programs with the database were written in the same environment as the hybrid code, Python. Again, Python is a free commercial environment that does not need a previous investment to be downloaded and used. Cost: 0 €.

The total budget spent by the author itself in utilities used in the elaboration of the project equals then solely the cost of the computer: 600 €

9.1.2. Costs assumed by third parties

- **Books**: This thesis has been characterized by a lot of literature reading. Although all the papers used for the elaboration of this project could be found in internet, three books with essential information were obtained from the University Library. Then, the University assumed the cost of buying these books to make the available for students use. The books where:
  - Introduction to plasma physics [1]: In the current case, the soft cover version was used. Its cost in a widely spread internet store platform is approximately 67 €

  - Plasma physics and Engineering [2]: The used version available in the University library is the hard cover book, with an approximate cost in a common online store platform of 140 €.
  - Learning Python [53]: This book was used to learn all the basics about programming in Python environment. Its price in a common online store platform is around 50 €

- **MatLab**: As commented, MatLab has been used to obtain a double check of the results obtained with Python. It was also useful for the generation of the data graphs presented in the report due to the available features that this program provides to customize images. The cost of the license to use this program was assumed by the University, which provided a student licence to the author. The annual cost of student licence for Academic purposes such as the one used is around 250 €

- **Internet connection:** The research project could have not been performed without internet connection during the entire period of work. Internet has been an essential tool to consult and gather information, not only about the theoretical part of the project, but also in the retrieval of cross-sections from external databases. The average budget spent in internet during 2018, which will be assumed to be maintained constant through p to June 2019, is 53 €/month [54]. So, during the approximated 10 months during which this research took place, the internet costs have been approximately 530 €.

Then, the budget spent by third parties is approximately 1037 €., which results in a total budget spent on the project of 1637 €.

9.2. Socioeconomic impact

As exposed throughout the project, future researches must be carried to encompass as much collisions as possible and test new species and propellants. Then, on a short-term basis, no effects are expected from this study from a socioeconomic standpoint.

Nevertheless, the database generated in this thesis aims to contribute to the search of new propellant to substitute Xenon in the electric propulsion field. Current concerns with this propellant include its elevated costs of extraction and storage. The idea of a database providing vital information of a wide scope of species to be tested as new propellants could, in a long-term basis be translated in several economic savings. Two examples may be the ability of simulating new propellants with already available information, which will avoid the necessity of performing new measurements to obtain the required cross-sections; and the savings derived from the use of substitute propellants to Xenon.

In addition, an indirect impact that this work may contribute in is the environmental concern of future in-Earth propulsion. An example of this impact are the eroded materials from the structure due to plasma particle-wall collisions, which are released to the

neighbour area of the plume. A good understanding of the collision scenarios can allow the development of new material resistant to plasma wear, or even inert to react with such particles.

BIBLIOGRAPHY

[1] R. J. Golston and P. H. Rutherford, *Introduction to plasma physics*. Bristol: Institute of Physics, 1995.

[2] A. Fridman and L. A. Kennedy, *Plasma physics and engineering*. Taylor & Francis, 2004.

[3] R. S. Gutiérrez, "Código híbrido avanzado de motores de plasma de efecto Hall(Spanish)", PhD thesis, E.T.S.I Aeronáuticos (UPM), 2012.

[4] E. A. Diego, "Motores de efecto Hall de alto impulso específico(Spanish)", Trabajo de fin de carrera, E.T.S.I Aeronáuticos (UPM), 2005.

[5] D. M. Goebel and I. Katz, *Fundamentals of electric propulsion*, ser. JPL space science and technologies. Hoboken, NJ.:Wiley, 2008.

[6] D. Robert and H. Goddard, *The Green Notebooks*, ser. The Dr. Robert H. Goddard Collection at the Clark Univeristy Archives. Clark University, Worchester, vol. 1.

[7] T. M. Mel'kumov, *Pioneer of rocket technology, Selected Works*. Academy of Sciences of the USSR, Institute for the History of Natural Science and Technology, Moscow, translated from the 1964 Russian text by NASA as NASA TT F-9285, 1965.

[8] E. Y. Choueiri, *A Critical History of Electric Propulsion: The First 50 Years (1906-1956)*. Journal of Propulsion and Power, 1965, vol. 20.

[9] E. Stuhlinger, *Ion Propulsion for Space Flight*. New York: McGraw-Hill, 1964.

[10] R. G. Jahn, *Physics of Electric Propulsion*. New York: McGraw-Hill, 1968.

[11] *Introduction to Space Systems*. Universidad Carlos III de Madrid, Course 251-14169-BSc Aerospace Engineering, 2018.

[12] D. Goebel, "How do the electric thrusters on the psyche spacecraft work?", *The NASA Psyche mission: Journey to a Metal World*, 2018.

[13] C. J. Lynch, *Ion thruster sets world record*, 2009.

[14] J. Khatry, F. Aydogan, M. Ilyas, and M. Houts, "Design of a passive safety system for a nuclear thermal rocket", *Annals of Nuclear Energy*, vol. 111, pp. 536–553, 2018.

[15] W. Leahy *et al.*, "Plasma surface treatment of aerospace materials for enhanced adhesive bonding", *The Journal of Adhesion*, vol. 77, pp. 215–249, 2006.

[16] (). Plasma treatment of aerospace composite materials, [Online]. Available: `https://plasmatreatment.co.uk/industries/plasma-treatment-aerospace/` (visited on).

[17] C.-C. Wang and S. Roy, "Combustion stabilization using serpentine plasma actuators", *Appl. Phys. Lett.*, vol. 99, p. 041 502, 2011.

[18] R. Geuns, "The use of dielectric barrier discharge plasma actuators for low-speed flow control: An experimental study on plasma characteristics", MS Thesis, Faculty of Aerospace Engineering, DELFT University of Technology, 2004.

[19] (). Ecuaciones de maxwell, [Online]. Available: `https://www.lawebdefisica.com/dicc/maxwell/`. (accessed: 03.06.2016).

[20] A. Domínuez, F. Cichocki, M. Merino, P. Fajardo, and E. Ahedo, "2d and 3d hybrid pic-fluid modeling of electric thruster plumes", *35th International Electric Propulsion Conference Georgia Institute of Technology, Atlanta, Georgia, USA*, 2017.

[21] A. Lorand, O. Duchemin, S. Zurbach, D. L. Mehaute, and N. Cornu, "Alternate propellants for pps® hall-effect plasma thruster", *33rd International Electric Propulsion Conference*, 2013.

[22] (). Lxcat database: Plasma data exchange project, [Online]. Available: `https://fr.lxcat.net/home/`.

[23] (). Nifs database, [Online]. Available: `https://dbshino.nifs.ac.jp/nifsdb/`.

[24] D. L. Conde, "An introduction to plasma physics and its space applications", PhD thesis, E.T.S.I Aeronáuticos (UPM), 2014.

[25] V. L. JACOBS, "Autoionization phenomena in plasma radiation processes", *Journal of Quantitative Spectroscopy and Radiative Transfer*, vol. 54, pp. 195–205, 1995.

[26] M. Mitchner and C. H. Kruger, *Partially ionized gases*. New York: Wiley, 1973.

[27] I. Katz, R. Hofer, and D. Goebel, "Ion current in hall thrusters", *IEEE Transaction on Plasma Science*, vol. 36, no. 5, pp. 2015–2024, 2008.

[28] E. W. Bell, N. Djurć, and G. H. Dunn, "Electron-impact ionization of in^+ and xe^+", *Physical Review A*, vol. 48, no. 6, 1993.

[29] D. H. Crandall *et al.*, *Astrophys. J.*, vol. 191, no. 789, 1974.

[30] C. w. Clenshaw, *Math. Tables Comput.*, vol. 9, no. 118, 1955.

[31] D. Mathur and C. Badrinathan, "Ionization of xenon by electrons: Partial cross sections for single, double, and triple ionization", *Physics Review A*, vol. 35, no. 3, 1987.

[32] (). Nist database, [Online]. Available: `https://physics.nist.gov/PhysRefData/Ionization/atom_index.html` (visited on).

[33] B. R. Turner, M. Fineman, and R. F. Stebbings, *J. Chem. Phys.*, vol. 42, p. 4088, 1965.

[34] T. Arikawa and S. Kaneko, "Multi-crossed-beam method", *J. Appl. Phys.*, vol. 18, p. 413, 1979.

[35] (). Magboltz, [Online]. Available: http://cyclo.mit.edu/drift/www/aboutMagboltz.html.

[36] S. Biagi, "Monte carlo simulation of electron drift and diffusion in counting gases under the influence of electric and magnetic fields", *n Physics Research A*, vol. 421, pp. 234–240, 1999.

[37] A. Bovorik, "Electron-impact ionization of xenon and tin ions", PhD thesis, Justus-Liebig-Universität Gießen, Institut für Atom-und Molekülphysik, 2010.

[38] L. Biagioni, V. Kim, D. Nicolini, A. V. Semenkin, and N. Wallace, "Basic issues in electric propulsion testing and the need for international standards", *the 28th International Electric Propulsion Conference (IEPC)*, vol. 230, pp. 17–21, 2003.

[39] V. Pagonis, C. Kulp, C.-G. Chaney, and M. Tachiya, "Quantum tunneling recombination in a system of randomly distributed trapped electrons and positive ions", *Journal of Physics Condensed Matter*, 2017.

[40] *Modeling the physics of plasma thruster plumes in electric propulsion*. Universidad Carlos III de Madrid, Equipo de Propulsión Espacial y Plasmas (EP2), 2017.

[41] S. A. Maiorov, O. F. Petrov, and V. E. Fortov, "Calculation of resonant charge exchange cross-sections of ions rubidium, cesium, mercury and noble gases.", *In Proceedings of the 34th EPS Conference on Plasma Physics, Warsaw.*, 2007.

[42] B. M. Smirnov, "Tables for cross sections of the resonant charge exchange process", *Physica Scripta*, vol. 61, pp. 595–602, 2000.

[43] B. M. Smirnov, "The classical theory of resonance charge exchange", *Soviet Physics JETP*, vol. 32, no. 4, 1971.

[44] I. Kaganovich, A. Shnidman, H. Mebane, and R. Davidson, "Calculation of charge-changing cross-sections of ions or atoms colliding with fast ions using the classical trajectory method", *Nuclear Instruments and Methods in Physics Research Section A: Accelerators, Spectrometers, Detectors and Associated Equipment*, vol. 606, pp. 196–204, 2009.

[45] (2019). Yaml 1.2, [Online]. Available: https://yaml.org/ (visited on 06/08/2019).

[46] (2019). Yaml syntax, [Online]. Available: https://docs.ansible.com/ansible/latest/reference_appendices/YAMLSyntax.html (visited on 06/08/2019).

[47] H. Hernandez, "Standard maxwell-boltzmann distribution: Definition and properties", *ForsChem Research*, vol. 2, 2017.

[48] *The principles of statistical mechanics*. Courier Corporation, 1979.

[49] K. MARYNETS, "Two-point boundary problem for modeling the jet flow of the antarctic circumpolar current", *Electronic Journal of Differential Equations*, vol. 2018, no. 56, pp. 1–12, 2018.

[50] (2017). Volume of 1 hydrogen atom, [Online]. Available: https://hydrogenatomgirikosa.blogspot.com/2017/06/volume-of-1-hydrogen-atom.html (visited on 06/11/2019).

[51] (). Cylindrical polar coordinates, [Online]. Available: http://hydrogen.physik.uni-wuppertal.de/hyperphysics/hyperphysics/hbase/sphc.html (visited on 06/11/2019).

[52] (). Centroids and mass moments of inertia for homogeneous 3d volumes, [Online]. Available: http://adaptivemap.ma.psu.edu/websites/centroidtables/centroids3D/centroids3D.html (visited on 06/11/2019).

[53] M. Lutz, *Learning Python*. 5th ed., Animal Guide, 2009.

[54] C. Valero, "Los españoles pagamos por internet más que en italia, francia, reino unido y alemania", *ADSLZONE (online journal)*, 20181. [Online]. Available: https://www.adslzone.net/2018/10/18/precios-internet-espana-vs-europa-2018/ (visited on).

[55] O. Takahashi *et al.*, "Auger decay calculations with core-hole excited-state molecular-dynamics simulations of water", *The journal of Chemical Physics*, vol. 124, no. 064307, 2006.

APPENDIX A: DATABASE .txt FILES

FILE TEMPLATE

```
'TYPE': 'Model-Drawin'

'RETRIEVAL DATE': '25/03/2019' #(d/m/y)

'ORIGINAL REFERENCE': 'Robert Santos Gutierrez
                       June, 2012
                       CODIGO HIBRIDO AVANZADO DE MOTORES DE PLASMA DE EFECTO HALL
                       page 45/46
                       '
'COMMENTS': {
            'PROCESS': 'Ionization e- + Xe --> 2e- + Xe+',
            'SPECIES': 'e/Xe',
            'INITIAL STATE': 'Xe +0',
            'INITIAL # e-': 54,
            'INITIAL E.C.': '[Kr] 4d10 5s2 5p6',
            'FINAL STATE': 'Xe +1',
            'FINAL # e- ': 53,
            'FINAL E.C.': '[Kr] 4d10 5s2 5p5',
            'METHOD': 'Drawin Model for first ionization',
            'DESCRIPTION OF DATA': 'The data provided are the values of the constants needed
            for the implementation of Drawin model for the computation collision cross-sections (Beta_1 and Beta_2).
            These values have been obtained experimentally.

            Drawin Model for first ionization:

            sigma = 2.66*pi*a_0^2*Beta_1*(epsilon_i_H/epsilon_i)^2*Xi*g(u)
            where g(u) = (u-1)/u^2*ln(1.25*Beta_2*u)

            In this model:     a_0 = Bohr radius of Hydrogen atom = 5.292e-11 m
                                     epsilon_i_H = ionization energy of Hydrogen = 13.6 eV
                                     epsilon_i = ionization energy of the sample of interest
                                     Xi = Number of equivalent electrons in the external layer of the sample of
                                          interest
                                     u = dimensionless energy of the electron = [energy range of interest]/
                                          epsilon_i
                                     '
            }

'DATA': {
         'a_0': {
                    'units': 'm',
                    'values': 5.292e-11
                    },
         'epsilon_i_H': {
                          'units': 'eV',
                          'values': 13.6
                          },
         'epsilon_i': {
                        'units': 'eV',
                        'values': 12.1298
                            },
         'Xi': {
                'units': 'dimensionless',
                'values': 8
                    },
         'Beta_1': {
                    'units': 'dimensionless',
                    'values': 1.0
                    },
         'Beta_2': {
                    'units': 'dimensionless',
                    'values': 0.8
                    },
         'Final_E': {
                    'units': 'eV',
                    'values': 200
                     }
        }
```

Fig. A. Suggested .txt file for data extracted from Drawin model

APPENDIX B: MAXWELLIAN DISTRIBUTION HANDLING

Mathematical derivation of the Maxwellian distribution in terms of energies

To obtain an expression for the Maxwellian distribution in terms of energies, it will be applied the definition of the volume density. For the isotropic volume the density may be expressed by

$$n = \int_0^\infty f_M(v)dv \tag{I.1}$$

as well as by

$$n = \int_0^\infty f_M(E)dE. \tag{I.2}$$

Then it is clear that the following condition must be consistent:

$$\int_0^\infty f_M(E)dE = \int_0^\infty f_M(v)dv. \tag{I.3}$$

From which it can be deducted that

$$f_M(E) = f_M(v)\frac{dv}{dE}. \tag{I.4}$$

Substituting by their corresponding expressions:

$$f_M(v) = 4\pi n\left(\frac{m}{2\pi T}\right)^{3/2} v^2 \exp\left(-\frac{mv^2}{2T}\right) \tag{I.5}$$

$$v = \sqrt{\frac{2E}{m}} \longrightarrow \frac{dv}{dE} = \frac{1}{2}\sqrt{\frac{2}{mE}} \tag{I.6}$$

The final expression in terms of the isotropic flow energy is achieved:

$$f_M(E) = n\frac{2}{\sqrt{\pi}}\frac{\sqrt{E}}{T^{3/2}} \exp\left(-\frac{E}{T}\right) \tag{I.7}$$

Mathematical derivation of the bi-Maxwellian distribution in terms of energies

As in the isotropic distribution, the plasma density results from the integration over the velocity space of the density distribution, regardless of the dependent variable. The:

$$n = \int_{-\infty}^{\infty} \int_{0}^{\infty} f_{bM}(v_{\parallel}, v_{\perp}) dv_{\perp} dv_{\parallel} \tag{I.8}$$

and

$$n = \int_{0}^{\infty} \int_{0}^{\infty} f_{bM}(E_{\parallel}, E_{\perp}) dE_{\parallel} dE_{\perp} \tag{I.9}$$

Moreover, due to the symmetry of the cylindrical control volume, it can be said that

$$\int_{-\infty}^{\infty} \int_{0}^{\infty} f_{bM}(v_{\parallel}, v_{\perp}) dv_{\perp} dv_{\parallel} = 2 \int_{0}^{\infty} \int_{0}^{\infty} f_{bM}(v_{\parallel}, v_{\perp}) dv_{\perp} dv_{\parallel} \tag{I.10}$$

Then:

$$\int_{0}^{\infty} \int_{0}^{\infty} f_{bM}(E_{\parallel}, E_{\perp}) dE_{\parallel} dE_{\perp} = 2 \int_{0}^{\infty} \int_{0}^{\infty} f_{bM}(v_{\parallel}, v_{\perp}) dv_{\perp} dv_{\parallel} \tag{I.11}$$

leading to

$$f_{bM}(E_{\parallel}, E_{\perp}) = 2 f_{bM}(v_{\parallel}, v_{\perp}) \frac{dv_{\parallel}}{dE_{\parallel}} \frac{dv_{\perp}}{dE_{\perp}} \tag{I.12}$$

After substitution with the terms

$$f_{bM} = n \frac{m^{(3/2)}}{\sqrt{2\pi T_{\parallel}} T_{\perp}} v_{\perp} \exp\left(-\frac{m v_{\parallel}^2}{2T_{\parallel}} - \frac{m v_{\perp}^2}{2T_{\perp}} \right) \tag{I.13}$$

$$v_{\parallel} = \sqrt{\frac{2E_{\parallel}}{m}} \longrightarrow \frac{dv_{\parallel}}{dE_{\parallel}} = \frac{1}{2} \sqrt{\frac{2}{mE_{\parallel}}} \tag{I.14}$$

$$v_{\perp} = \sqrt{\frac{2E_{\perp}}{m}} \longrightarrow \frac{dv_{\perp}}{dE_{\perp}} = \frac{1}{2} \sqrt{\frac{2}{mE_{\perp}}} \tag{I.15}$$

$$\tag{I.16}$$

the final expression is obtained:

$$f_{bM}(E) = n \frac{1}{\sqrt{\pi T_{\parallel}} T_{\perp}} \frac{1}{\sqrt{E_{\parallel}}} \exp\left(-\frac{E_{\parallel}}{T_{\parallel}} - \frac{E_{\perp}}{T_{\perp}} \right) \tag{I.17}$$

APPENDIX C: DATABASE CODES CALLING EXAMPLE

FILE TEMPLATE

```
"""
CODE DESCRIPTION:

    This code exemplifies how the database would be called to compute the collision
    rate for a specific reaction at a given temperature

INPUTS REQUIRED:

    -Database_root: the root directory where the database is stored (in the
                    desktop, in a specific folder, in a USB...)
    -Type: type of the desired interaction. With the current state of the database
           this field must be one of: 'BINARY' or 'UNARY'
    -specie1: first of the species involved in the interaction
    -specie2: second specie involved in the interaction

        NOTE_1: the species are introduced with their sign an their electronic state.
                Some examples are: 'e-' for electron
                                   'Xe' for neutral Xe
                                   'Xe+2' for doble ionized Xenon-->
                                       Symbol+Charge+#charges
                                   'Xe[5s2]' for excited Xe -->
                                      Symbol[electronic state of
                                      the las valence e-]

        NOTE_2: the specied dont necessarily need to be entered in order.

        NOTE_3: If the type UNARY is introduced, the secondary specie should be left as ''

    -process: desired reaction. 'i1' for one ionization of 1 e-
                                'elastic' for elastic collision
                                'e[...]' for excitation to the [...]
                                    electronic configuration

    -file_name: name of the file that wants to be read (it must be a .txt)

```

```
32          NOTE_3: If the name of the .txt is unknown, leave it as '' and the code
33                  will automatically read the first file associated with a database or,
34                  in the case where only one file is stored, it will take read this file.
35
36      -Velocity_parallel: velocity of the flow of electrons in the parallel direction. In [eV]
37      -Velocity_perpendicular: velocity of the flow of electrons in the perpendicular direction. In [eV]
38
39  OUTPUT:
40
41      -The collision rate at the specified temperature. In [m^3/s]
42  """
43  ############ INPUTS REQUIRED ############################
44
45  Database_root = 'C:/Users/Antonio/Desktop/DATABASE'
46  Type = 'BINARY'
47  specie1 = 'e-'
48  specie2 = 'Kr'
49  process = 'i1'
50  file_name = ''
51
52  Velocity_parallel = 14.142 # [eV]
53  Velocity_perpendicular = 14.142 # [eV]
54
55  ############ CALL TO THE DATABASE  ####################
56
57  import db_codes
58  Collision_rate = db_codes.collision_rate_BiMaxwellian(Database_root, Type, specie1, specie2, process, file_name, Velocity_parallel, Velocity_perpendicular) #[m^3/s]
```